University of Southampton

Faculty of Engineering, Sciences and Mathematics
School of Ocean and Earth Science

Modelling the Speciation and Biogeochemistry of Iron in Oceanic Surface Waters at the Bermuda Atlantic Time-series Study site

by

Lisa Weber

Thesis for the degree of Doctor of Philosophy

October 2006

UNIVERSITY OF SOUTHAMPTON

ABSTRACT

Faculty of Engineering, Sciences and Mathematics
School of Ocean and Earth Science

Doctor of Philosophy

MODELLING THE SPECIATION AND BIOGEOCHEMISTRY OF IRON IN OCEANIC SURFACE WATERS AT THE BERMUDA ATLANTIC TIME -SERIES STUDY SITE

by Lisa Weber

By means of numerical modelling the cycling of iron between its various physical (dissolved, colloidal, particulate) and chemical (redox state and organic complexation) forms in the upper mixed layer of the ocean is analysed. Using the model an initial quantitative assessment is made of how this cycling influences iron uptake by phytoplankton and its loss via particulate export. The model is forced with observed dust deposition rates, mixed layer depths, and solar radiation at the site of the Bermuda Atlantic Timeseries Study (BATS). It contains an optimised ecosystem model which yields results close to the observational data from BATS.

Firstly, the results of a zero-dimensional model approach show that the mixed layer cycle strongly influences the cycling of iron between its various forms. This was mainly attributed to the light dependency of photoreductive processes and to the seasonality of primary production. The daily photochemical cycle is driven primarily by the production of superoxide and its amplitude depends on the concentration and speciation of dissolved copper. Model results are largely insensitive to the dominant form of dissolved iron introduced via dust deposition, and also to the form of iron that is taken up directly during algal growth. In the model solutions, the role of the colloidal pumping mechanism depends strongly on assumptions made regarding rates of colloid aggregation and photoreduction rate.

Secondly, a one-dimensional approach of the model is coupled with the General Ocean Turbulence Model (GOTM). The combined model was able to simulate the temporal patterns and vertical profiles of dissolved iron in the upper ocean at the BATS site reasonably well. Subsurface model profiles depended strongly on the parameter values chosen for loss processes affecting iron, colloidal aggregation and scavenging onto particles. Current estimates for these parameters result in depletion of dFe. A high stability constant of iron-binding organic ligands is required to reproduce the observed degree of organic complexation below the mixed layer. Solubility of atmospherically deposited iron higher than 2% leads to dissolved iron concentrations higher than observations. Despite neglecting ultraviolet radiation, the model produces diurnal variations and mean vertical profiles of dFe which are in good agreement with observations.

To Günther Zederbohm

Contents

List of Tables

List of Figures

Author's declaration

I, Lisa Weber, declare that the thesis entitled "Modelling the speciation and biogeochemistry of iron in oceanic surface waters at the Bermuda Atlantic Time-series Study site" and the work presented in the thesis are both my own, and have been generated by me as the result of my own original research. I confirm that:

- this work was done mainly while in candidature for a research degree at this University;
- where any part of this thesis has previously been submitted for a degree or any other qualification at this University or any other institution, this has been clearly stated;
- where I have consulted the published work of others, this is always clearly attributed;
- where I have quoted from the work of others, the source is always given. With the exception of such quotations, this thesis is entirely my own work;
- I have acknowledged all main sources of help;
- where the thesis is based on work done by myself jointly with others, I have made clear exactly what was done by others and what I have contributed myself;
- parts of this work have been published as:
  Weber, L., Völker, C., Schartau, M. and Wolf-Gladrow, D. (2005). Modeling the speciation and biogeochemistry of iron at the Bermuda Atlantic Time-series Study site. *Global Biogeochemical Cycles*, **19**, doi:10.1029/2004GB002340.

Signed: .....
Date: .....

Acknowledgements

I would like to thank

- my supervisor Andreas Oschlies for his encouragement and support with the thesis, his helpfull comments and discussions. I appreciate the efforts that he has made, to make available the resources and equipment I needed and that he gave me the oppertunity to start the thesis at the Leipnitz Institut für Meereswissenschaften in Kiel (Germany) and change to the National Oceanography Centre in Southampton for the second half of my thesis.
- my unofficial supervisor Christoph Voelker for his telephone calls, all the comments he gave and all the discussions we had. His encouragement and thoughts were always very valuable for me.
- Peter Statham, who agreed to be my co-supervisor, when I moved to Southampton and for his helpfull comments.
- Hans Burchard, for introducing me to GOTM and answering all my qustions about it.
- Markus Schartau, for providing the code of his eco-system model and also answering all my qustions about it.
- Dieter Wolf-Gladrow, who introduced me to the biogeochemical modeling of iron in the first place and to the EU project IRONAGES.
- Peter Sedwick and Jingfeng Wu, for providing me with their iron data.
- the two anonymous reviewers of my first paper, for their helpfull comments.
- David Lambkin, for proof-reading the thesis.
- Harry Bryden, the chairman of my advisory panel.

- my parents Bärbel und Frank Weber, who were always there for me and supported me.
- David Lambkin and Kai Schulz for their invaluable friendship. They always believed in me and helped me up when I felt down. They helped me not to give up.
- Ralf Schiebel and Emma Guirey, for all the laughs we had, the violins, the fruit, the cappucinos and teas. They provided me with an excellent office atmosphere for the second half of my thesis.
- many friends and collegues in Kiel, Southampton, Bochum, Berlin and elsewhere, who positively influenced my life during my PhD in so many ways. Birgit Schneider, Heike Lüger, Miriam Fischer, Toste Tanuah, Anne (Steve) Schnapp, Jens Nüchter, Charlotte Ullrich, Stella Schmid and Andreas Pflitsch are only some of the names I could mention here.

This work was partly funded by the EU project IRONAGES (Contract No. EVK2-CT1999-00031) and the DFG project OS 175/3-1.

List of abbreviations

The SI units (Système International d'Units) are used to derive units of measurement for all physical quantities and phenomena. Definitions of model-paramters and their units are listed seperatly in Tables 2.1 and 2.2 and are not included here.

0d	zero-dimensional
1d	one-dimensional
3d	three-dimensional
A	inorganic particles
BATS	Bermuda Atlantic Time-series Study
C	carbon
C:N	carbon to nitrogen ratio
CDOM	colored dissolved organic matter
CO_2	carbon dioxide
CTD	Conductivity-Temperature-Depth
Cu	copper
Cu(I)	cuprit
Cu(II)	cupric
D	detritus
dFe	dissolved iron
DIN	dissolved inorganic nitrogen
DOC	dissolved organic carbon
F_X	atmospheric deposition flux of a substance X
Fe	iron
Fe_{col}	colloidal iron
Fe_{part}	particulate iron
Fe(II)	ferrous ion
Fe(II)'	inorganic Fe(II) species
Fe(III)	ferric ion
Fe(III)'	inorganic Fe(III) hydrolysis species

FeL	organically complexed iron
GOTM	General Ocean Turbulence Model
H	mixed layer depth
h^+	entrainment
H_2O_2	hydrogen peroxide
HNLC	High Nutrient Low Chlorophyl
I	irradiance
I_{PAR}	irradiance within the photosynthetically active range
L	organic ligands
max	maximum value
min	minimum value
N	Nitrogen
NOCS	National Oceanography Centre, Southampton
NPD	Nitrogen-Phytoplankton-Detritus
NPZD	Nitrogen-Phytoplankton-Zooplankton-Detritus
M	molarity (number of moles of a solute in 1l solution)
O_2	oxygen
O_2^-	superoxide
OGCM	Oceanic General Circulation Model
OH^-	hydroxyl ion
OSP	Ocean Station Papa
P	phytoplankton
PAR	photosynthtically available radiation
PON	particulate organic nitrogen
PP	primary production
SEEDS	Subarctic pacific iron Experiment for Ecosystem Dynamics Study
SERIES	Subarctic Ecosystem Response to Iron Enrichment Study
T	temperature
t	time
UK	United Kingdom
USA	United States of America

UV	ultraviolet radiation
VIS	visible radiation
Z	zooplankton
$[X]$	molar concentration of a substance X

Chapter 1

Introduction and objectives

1.1 Background

Iron (Fe) is the fourth most abundant element in the earth's crust (around 5.6%) and was present in high concentrations in seawater during the anoxic past of the earth (Falkowski, 1997; Turner et al., 2001). Therefore, and due to its abundance and capacity to transfer electrons, Fe became a key element in many biochemical reactions. With the oxygenation of the atmosphere and oceans approximately 2 Gy ago (Holland, 1984), Fe was removed from the ocean by precipitation, resulting in the Precambrian "banded iron formations" that have been found in North America, Asia and Australia (Evans, 1980). This removal process led to a shortage of available Fe for organisms in the ocean and Fe became a "hard to get essential element" (Gran, 1931; Martin and Fitzwater, 1988).

To understand the role of iron in the present ocean and why iron is an important element in the ongoing discussion about global warming, one has to understand the theories behind (i) the biological pump, (ii) High Nutrient Low Chlorophyll (HNLC) areas and (iii) the iron hypothesis.

(i) The *biological pump* is one of several mechanisms that regulates the greenhouse gas carbon dioxide (CO_2) in the atmosphere and therefore has a

role in modulating the climate of the planet. The biological pump is the sum of a suite of biologically-mediated processes that transport carbon from the surface euphotic zone to the ocean's interior which in turn affects atmospheric CO_2 by air-sea gas exchange (Falkowski and Wilson, 1992). Basically, CO_2 fixed in photosynthesis by autotrophs in the upper ocean, is transported to deep waters by sinking organic particulate material (e.g. dead organisms or faecal pellets) and in the form of dissolved organic carbon (DOC) by physical transport processes such as downwelling. Remineralisation and decomposition processes such as bacterial respiration return the organic carbon to dissolved carbon dioxide, but as these processes are generally slower than synthesis processes, and because the particulate material is sinking, the biological pump provides net transport of carbon from the surface ocean to deep water (Raven and Falkowski, 1999). Therefore, the biological sequestration of CO_2 into the deep ocean via the sinking of particulate material may prevent CO_2 from reentering the atmosphere for long periods of time of up to centuries. The amount and duration of CO_2 storage in the deep ocean is controlled by the deep ocean circulation and the net flux of carbon deposited and buried in the seafloor (Sarmiento and Gruber, 2002).

One important and essential nutrient for phytoplankton (and therefore the biological pump) is iron. Given by its abundance and capacity to transfer electrons, it is a key element in many biogeochemical processes such as photosynthesis (Geider and La Roche, 1994), nitrogenase catalysis, nitrate reductase (Timmermans et al., 1994; de Baar and la Roche, 2003), nitrogen fixation (Mills et al., 2004) and detoxification of reactive oxygen species (Sunda and Huntsman, 1995).

Natural sources of iron in the open ocean include atmospheric deposition with dust and rain (Duce and Tindale, 1991; Piketh et al., 2000; Jickells and Spokes, 2001), upwelling and lateral transport (Martin et al., 1989; Lam et al., 2006), ice melt (Sedwick and Ditullio, 1997; Sedwick et al., 2000), volcanic eruptions (Watson, 1997; Boyd et al., 1998) and

extra-terrestrial dust (Johnson, 2001), with regional variance in the importance of each source. In coastal and shelf regions, iron from resuspended shelf sediments and upwelling is assumed to be the main source rather than riverine sources (Johnson et al., 1999).

(ii) So called *HNLC* (High Nutrients Low Chlorophyll)-areas are regions of the ocean where the biomass of phytoplankton (standing stock) is low in spite of high macro-nutrient availability (nitrate, phosphate, silicic acid) which are apparently not fully utilised by the phytoplankton. The HNLC condition has been observed in the equatorial and north-east Pacific Ocean as well as in the Southern Ocean which comprise 30% of the World Ocean (de Baar et al., 1999). There are different theories why these areas have low biological productivity. In the equatorial Pacific and the north of the Polar Front in the Southern Ocean, silicate limitation plays a role (Dugdale and Wilkerson, 1998; Hutchins and Bruland, 1998; Takeda, 1998). In the Antarctic and subarctic Pacific light limitation is important (Raven, 1990; Geider et al., 1993; Sunda and Huntsman, 1997; van Leeuwe et al., 1997). There may also be other nutrient limitations, for instance other trace metals such as zinc (Morel et al., 1994) and copper (Coale, 1991). In oceanic surface waters, the concentration of dissolved iron commonly ranges between 0.02 nM to 1 nM. However HNLC areas all have extremely low iron concentration (0.02-0.05 nM), reflecting a lack of the natural sources of iron these regions (Bruland and Rue, 2001). These concentrations are low enough for dissolved Fe to be diffusion limiting with respect to growth rates for all but the smallest phytoplankton cells (Hudson and Morel, 1990; Sunda and Huntsman, 1995).

(iii) FirstGran (1931) and then Martin and Fitzwater (1988) developed the *hypothesis of Fe limitation* of the Southern Ocean. Several in-situ iron fertilisation experiments were conducted in the three HNLC regions (Martin et al., 1994; Coale et al., 1996; Boyd et al., 2000; Gervais et al., 2002; Tsuda et al., 2003; Coale et al., 2004; Boyd et al., 2004). The important role of iron as a limiting nutrient in HNLC regions has been

repeatedly demonstrated by these experiments and has been established as one of several co-limiting factors in these regions. Similarly, analysis of ocean sediment cores suggest that a larger iron supply to the HNLC regions in glacial times could have stimulated algal photosynthesis, leading to lower concentrations of atmospheric CO_2 (Kumar et al., 1995; Petit et al., 1999).

There is commercial interest in artificial iron enrichment on a large scale as a tool for climate regulation through stimulation of the biological pump (Markels Jr. and Barber, 2001). However it is very debatable whether extensive artifical iron fertilisation is a realistic method to reduce anthropogenic carbon in the atmosphere (Chisholm et al., 2001; Buesseler and Boyd, 2003; Turner et al., 2004). The ecological consequences and possible unintended climatic feedbacks of such an interference in the complex cycle of the global climate through manipulating the marine component, which is also complex and still not well known, are still incalculable and therefore it could be seen as irresponsible.

One of the many still poorly understood links in this discussion is the biogeochemistry of iron and its availability for phytoplankton in the surface ocean itself which is the subject of this thesis.

1.2 Iron speciation

The biogeochemistry of iron in seawater is very complex and not yet fully understood. The extremely low concentration of iron in the ocean and its ubiquity as a contaminant makes it difficult to measure. Many techniques provide only indirect measurements that are only operationally defined and thus their interpretation can be argued (Bruland and Rue, 2001). The chemical *forms* of iron are usually defined by physical size fractions, separated on the basis of filtration methods. The size fractions are usually dissolved iron (dFe), which comprises soluble (smaller than 0.02 μm) and colloidal (0.02-0.4 μm) iron, and particulate iron (larger than 0.4 μm)(Wu

et al., 2001).

Iron *species* are defined as chemical constituents within a particular size fraction of the metal. Iron can exist in two different redox states, ferric ion (Fe(III)) and ferrous ion (Fe(II)), either within a variety of soluble coordination complexes with inorganic and organic ligands or in a variety of colloidal and particulate forms.

A number of processes are known to convert iron in seawater between these forms and species. The main processes include:

1. oxidation of Fe(II)' (see Section 1.2.1) by oxygen (O_2), superoxide (O_2^-) and hydrogen peroxide (H_2O_2) (Millero et al., 1987; Millero and Sotolongo, 1989; King et al., 1995).

2. photoreduction of the different iron states, both directly (Wells and Mayer, 1991; Kuma et al., 1992; Johnson et al., 1994; Barbeau and Moffett, 2000; Barbeau et al., 2001; Emmenegger et al., 2001; Barbeau et al., 2003) and indirectly by the reaction with photoproduced superoxide (Voelker and Sedlak, 1995; Miller et al., 1995).

3. complex formation and dissociation involving organic ligands (Gledhill and van den Berg, 1994; Van den Berg, 1995; Wu and Luther III, 1995; Rue and Bruland, 1995; Witter and Luther III, 1998; Witter et al., 2000; Rose and Waite, 2003b).

4. colloid formation (Johnson et al., 1994; Rose and Waite, 2003a), aggregation and disaggregation (Wells and Goldberg, 1993; Wen et al., 1997).

5. scavenging onto sinking particles (Balistieri et al., 1981; Nyffeler et al., 1984; Johnson et al., 1997).

It is assumed that iron speciation and the relative importance of each process influences scavenging and biological uptake of iron. Unlike the

macronutrients nitrate, phosphate and silicic acid, there are no analytical methods for quantifying the fraction of iron in seawater that phytoplankton can acquire (e.g. Wells et al. (1995); Sunda (2001)). Although iron uptake in synthetic culture media varies in proportion to the free ferric ion activity and is therefore suggested to be primarily a function of the free-ion concentration (Sunda and Guillard, 1976; Sunda, 1989; Anderson and Morel, 1982), inorganic iron species comprise only a small portion of dissolved iron in seawater. The bulk of iron speciation (up to more than 95%) is instead governed by complexation to organic ligands (Gledhill and van den Berg, 1994; Rue and Bruland, 1995; Wu and Luther III, 1995). Because it is still poorly understood what effect these ligands have on iron acquisition, it is still impossible to quantify the proportion of iron in given seawater that is readily accessible to all or a portion of the phytoplankton assemblage. Additionally, there are observations that a major fraction of inorganic and organically bound iron is not truly soluble but colloidal in size (Guo et al., 2000; Wells et al., 2000; Wu et al., 2001), which makes them too large to be transported intact across cell membranes (Chen and Wang, 2001). In addition, colloidal complexes might become incorporated with other aggregating colloidal matter and particles, resulting in the accelerated removal of iron from surface waters (Wells and Goldberg, 1993; Chin et al., 1998; Wu et al., 2001). Therefore a simple assumption of iron availability to organisms is not possible.

1.2.1 Redox states and the photochemistry of iron

Iron exists in oxic seawater primarily as thermodynamically stable Fe(III), which is highly reactive with respect to hydrolysis, adsorption and complex formation. Inorganic Fe(III) exists in solution as mononuclear iron hydrolysis species, such as $Fe(OH)^{2+}$, $Fe(OH)_2^+$, $Fe(OH)_3$ and $Fe(OH)_4^-$. Due to their fast exchange kinetics, they rapidly equilibrate with one another and can be viewed as a single reactive pool (Zafiriou and True,

1980; Stumm and Morgan, 1981). Therefore, the sum of all inorganic Fe(III) hydrolysis species is designated as Fe(III)'.

Similarly, Fe(II)' consists mainly of Fe^{2+}, but also includes the less abundant forms $Fe(CO_3)$, $FeCl^+$ and $FeSO_4$ (Byrne et al., 1988; Millero and Hawke, 1992).

Most of the present day ocean is oxic and has a pH around 8 which leads to the oxidation of Fe(II)' and the predominance of Fe(III)':

$$\mathrm{Fe(II)'} + \mathrm{O_2} \rightarrow \mathrm{Fe(III)'} + \mathrm{O_2^-} \tag{1.1}$$

Nevertheless, Fe(II)' may also exist in the oxic ocean, especially in surface water. The redox state of dissolved iron in the ocean is strongly influenced by the two reactive oxygen species superoxide (O_2^-), and hydrogen peroxide (H_2O_2). Both species are strong oxidants for Fe(II)' but O_2^- also acts as a strong reductant for Fe(III)' (see below, Equations 1.3 and 1.4).

The dominant source of reactive oxygen species in seawater is the photo-oxidation of coloured dissolved organic matter (CDOM) (Cooper et al., 1988) that produces superoxide, and the subsequent transformation of superoxide to hydrogen peroxide. The latter transformation can proceed directly by the reaction of two superoxide molecules to hydrogen peroxide, called dismutation (Equation 1.2) or catalyzed by the reduction and subsequent oxidation of a Fe(III) ion (Equations 1.3 and 1.4). Both processes produce one molecule of hydrogen peroxide:

$$2\mathrm{O_2^-} + 2\mathrm{H_2O} \rightarrow \mathrm{H_2O_2} + \mathrm{O_2} + 2\mathrm{OH^-} \tag{1.2}$$

$$\mathrm{Fe(III)'} + \mathrm{O_2^-} \rightarrow \mathrm{Fe(II)'} + \mathrm{O_2} \tag{1.3}$$

$$\mathrm{Fe(II)'} + 2\mathrm{O_2^-} + 2\mathrm{H_2O} \rightarrow \mathrm{Fe(III)'} + \mathrm{H_2O_2} + 2\mathrm{OH^-} \tag{1.4}$$

Significant amounts of H_2O_2 exist in atmospheric precipitation, fog and cloudwater (Gunz and Hoffmann, 1990; Sakugawa et al., 1990). Therefore, rain events can lead to increases in $[H_2O_2]$ in surface seawater (Kieber et al., 2001) and contribute to the redox reactions of inorganic iron.

Another pathway to generate Fe(II)' in oxic seawater is the direct photoreduction of the different iron states (Wells and Mayer, 1991; Kuma et al., 1992; Johnson et al., 1994; Barbeau and Moffett, 2000; Barbeau et al., 2001; Emmenegger et al., 2001; Barbeau et al., 2003). The photoreduction of Fe(III)', as shown in studies using NaCL solutions, occurs via a ligand-metal charge transfer reaction (King et al., 1993):

$$\mathrm{Fe(OH)^{2+}} \quad \rightarrow \quad \mathrm{Fe - OH^{*} \rightarrow Fe^{2+} + OH\cdot} \tag{1.5}$$

where Fe-OH* is an excited state intermediate. The direct photo-reduction of Fe(III)' decreases rapidly with pH above 6.5 as in seawater (Waite and Morel, 1984; King et al., 1993; Sulzberger and Laubscher, 1995). Nevertheless, colloidal Fe at seawater pH does appear to be photochemically reactive (Wells and Mayer, 1991; Hudson et al., 1992; Johnson et al., 1994; Miller et al., 1995). In addition, organic matter does have the potential to increase the rate of Fe(III)' photoreduction (Waite and Morel, 1984; Zuo and Holgne, 1992; Hudson et al., 1992; Kuma and Matsunaga, 1995; Rose and Waite, 2003c). Knowing that most iron in seawater is complexed or coupled to organic material (Section 1.2.2) it is assumed that most observed photoreduction reactions in marine waters are likely to be associated with absorption of light by Fe(III)-organic chromophores. These chromophores undergo ligand to metal charge transfer reactions, resulting in the production of Fe(II) and in a non-reversible decomposed organic ligand (Waite and Morel, 1984):

$$\mathrm{Fe(III) - L^{*}} \quad \rightarrow \quad \mathrm{Fe(II) + L_{ox}} \tag{1.6}$$

Furthermore, some marine siderophore-Fe(III)-complexes have shown to be photo-reactive. They produce Fe(II) in light, depending on the complexing functional group (Barbeau et al., 2001, 2003; Maldonado et al., 2005; Rijkenberg et al., 2006). For example, hydroxamate groups are photochemically resistant regardless of Fe(III) complexation. Catecholates, in contrast, are susceptible to photooxidation in the uncomplexed form but stabilised against photooxidation when ferrated. α-Hydroxy carboxylate groups are stable as the uncomplexed acid, but when coordinated to Fe(III), these moieties undergo light-induced ligand oxidation and reduction of Fe(III) to Fe(II) (Barbeau et al., 2003).
Besides the iron state and the pH of the water, the wavelength and the intensity of the irradiance is a crucial factor in terms of photoredox reactions in seawater. A strong relation has been found between irradiance level and the iron photoreduction rate (Waite et al., 1995). Rich and Morel (1990) have shown that iron is not photoreduced at light wavelengths larger than 560 nm. Correspondingly a spectral dependency of Fe(II) photoproduction was found, that generally increases with decreasing wavelength over the full solar spectrum (Wells and Mayer, 1991; Rijkenberg et al., 2005). However, the penetration of solar radiation into the upper water column depends strongly on the wavelength and degree of water colour. Ultraviolet radiation is attenuated much more rapidly than visible radiation. In moderately productive waters, visible radiation (wavelength of 500 nm) penetrates down to 50 m depth, whereas UV-B (wavelength of 310 nm) penetrates less than 10 m (Smith and Baker, 1979). Therefore, the photochemical reactions of iron are limited to surface waters.

1.2.2 Organically complexed iron

There is evidence that most of the dissolved iron in seawater is dominated by complexation with organic ligands, which regulates dissolved iron concentrations in seawater by preventing iron from adsorption to particles

and subsequent removal through sinking (Gledhill and van den Berg, 1994; Rue and Bruland, 1995; Wu and Luther III, 1995; Johnson et al., 1997; Kuma et al., 1998; Nakabayashi et al., 2001; Kuma et al., 2003). There is still a lack of knowledge about the chemical nature of these ligands, their sources, sinks and their role in Fe biogeochemistry (Bruland and Rue, 2001). Two broad categories of ligand class have been identified in seawater, a "stronger" and a somewhat "weaker" class of ligand. A provisional scenario is that the stronger ligand class, having binding strengths in seawater similar to terrestrial- and marine-derived siderophores, comprises molecules released by prokaryotic microorganisms to increase their iron acquisition, while the weaker ligands comprise intracellular molecules (e.g., porphyrin complexes) inadvertently released by grazing or cell lysis. Indeed, recent findings suggest that autotrophic eukaryotes can efficiently access iron bound only in the weaker complexes, while autotrophic prokaryotic organisms primarily acquire iron complexed by the stronger ligand class (Hutchins et al., 1999).

Siderophores are Fe-specific, low molecular weight organic ligands, which appear to be released mainly by Fe-limited bacteria to enhance Fe acquisition (Raymond et al., 1984). These complexing agents are essential for Fe acquisition by these microbes, which access the siderophore-bound Fe through a variety of dissociation mechanisms (Byers and Arceneaux, 1998). Organic Fe(III) ligands isolated from the California upwelling region have been shown to possess Fe-binding functional groups typical of siderophores (Macrellis et al., 2001), further confirming the siderophore-like nature of the strong organic Fe(III) complexes in seawater.

Many marine prokaryotes produce and excrete siderophores under Fe stress (Wilhelm and Trick, 1994; Trick and Wilhelm, 1995; Granger and Price, 1999; Reid et al., 1993; Haygood et al., 1993; Zhong et al., 2000), and acquire siderophore-bound Fe to fulfil their Fe requirements. It is believed that marine bacteria have high-affinity Fe acquisition systems specially designed to scavenge siderophore bound Fe, although the molecular

mechanisms and genetic basis for such Fe uptake systems in marine prokayotes remains unresolved (Granger and Price, 1999; Webb et al., 2001; Armstrong et al., 2004).

In contrast, only one study has thus far shown siderophore production by marine eukaryotic phytoplankton (Trick et al., 1983). Most models of Fe acquisition by eukaryotic phytoplankton emphasize the significance of inorganic Fe for uptake and growth, supporting the idea that the Fe transporters at the cell surface react with inorganic Fe species (Hudson and Morel, 1990; Sunda and Huntsman, 1995). Only recently has the importance of organically bound Fe for the nutrition of marine eukaryotic phytoplankton become apparent (Hutchins et al., 1999; Maldonado and Price, 1999). Eukaryotic phytoplankton have been shown to possess inducible reductases at the cell surface that mediate the reduction of organically bound Fe(III) and subsequent dissociation of Fe from the ligand (Maldonado and Price, 2001). Once dissociation occurs, the cells internalise the inorganic Fe via inorganic Fe transporters at the cell surface. In addition to this enzymatic reductive mechanism, light can play a role in Fe acquisition from marine siderophore-bound Fe (Barbeau et al., 2001; Maldonado et al., 2005; Rijkenberg et al., 2006) (see also Section 1.2.1).

Though it is clear that bacteria and eukaryotic phytoplankton in the open ocean are able to access Fe bound to strong organic ligands (Hutchins et al., 1999; Maldonado and Price, 1999), the relative importance of photochemical (Barbeau et al., 2001) versus biological (Maldonado and Price, 2001) reduction in mediating the release of Fe from strong organic complexes remains unresolved.

1.2.3 Colloidal iron

Recent studies about Fe forms showed that a significant fraction of the dissolved iron is colloidal (Wu et al., 2001). The name colloid (greek for glue-like) derives from Graham (1861) who studied substances that do not

diffuse through a semipermeable membrane. Today they are usually defined as a size class between soluble chemical species and sinking particles (Wells and Goldberg, 1992). However, there are no precise size boundaries between particles, colloids, or simple ionic forms. A characteristic of colloids is that they are of sufficient size to provide an interface and introduce the opportunity for other soluble or colloidal chemicals to adsorb onto the surface (Vold and Vold, 1983). It is uncertain to what extend colloidal Fe exists as colloidal-sized organic complexes or as reactive Fe(III) oxyhydroxides (Rich and Morel, 1990). In general it is believed that in the open ocean, organic forms of colloids dominate (Benner et al., 1997). In any case, the interface surface must comprise enough point charges from ionised functional groups to create an electricostatical field sufficient to stabilise the colloidal substance (Wells and Goldberg, 1992).

Tracer studies using highly active metal isotopes show that the marine colloidal phase is very dynamic, with high colloidal aggregation rates being sustained even in nutrient-poor surface waters (Moran and Buesseler, 1992; Baskaran et al., 1992; Wells and Goldberg, 1993; Wu et al., 2001). Honeyman and Santschi (1989) proposed a colloidal pumping model for metal uptake onto suspended particles, which assumed a rapid (one second or less) association of soluble metals with suspended colloids by surface complexation and subsequent aggregation of these colloids into filterable particles. This was confirmed in experimental studies by Wen et al. (1997). Colloidal pumping is also suggested to be responsible for the fast removal of iron in surface waters during iron fertilisation experiments (Nishioka et al., 2005) and it is believed to be a critical precursor for formation of marine snow (Mopper et al., 1995; Passow and Alldredge, 1995).

However, the causes of colloid production and break-up is still not very well known. Studies include, *inter alia*, production presumably through a combination of cell exudation and lysis, microbial degradation of particulate organic matter and sloppy feeding as well as excretion by zooplankton (Wells and Goldberg, 1994), and destruction by photochemical

processes (section 1.2.1) and bacterial grazers (Moffet, 2001).

1.3 Iron in models

There are several marine models which include a simple iron chemistry, treating iron mostly as a standard nutrient (Lancelot et al., 2000; Christian et al., 2002a; Moore et al., 2002; Aumont et al., 2003). This simplification complies with the incorrect assumption that all species of iron have the same bioavailability (Hutchins et al., 1999). Lefevre and Watson (1999), Archer and Johnson (2000) and Parekh et al. (2004) included very simple iron speciation equations in global models which comprise scavenging onto particles, biological consumption, remineralisation, complexation with ligands and aeolian deposition. Their models were tuned to reproduce the deep ocean Fe distribution with scavenging residence times between years and centuries. Numerical biogeochemical-physical models are now able to simulate the main patterns of total dissolved iron in the ocean (Dutkiewicz et al., 2005), but indicate that the details and, in particular, the climate sensitivity of so called HNLC areas depend on the way the iron chemistry is parameterised (Parekh et al., 2004). This simplified description of marine iron chemistry, that primarily aims to reproduce the scavenging removal of iron in the deep ocean, is not adequate to simulate the rapid disappearance of iron after pulsed deposition events or to resolve processes with short time-scales, such as photochemical cycling.

Modeling of iron cycling between its various species has recently been refined by Rose and Waite (2003c). They distinguished between five basic forms: inorganic ferrous complexes, inorganic ferric complexes, organic ferrous complexes, organic ferric complexes, and polymeric or solid ferric oxyhydroxides. The conversion between the different states is governed by eight primary kinetically driven processes. These are (1) oxidation of inorganic Fe(II), (2) hydrolysis of inorganic Fe(III), (3) oxidation of organically complexed Fe(II), (4) organic complexation of Fe(II), (5)

dissociation of organically complexed Fe(II), (6) organic complexation of Fe(III), (7) dissociation of organically complexed Fe(III) and (8) sunlight-mediated reduction of Fe(III). In addition, free radical (superoxide and hydrogen peroxide) reactions with iron were also included. The application of the model was limited to oxygen saturated, well mixed coastal waters with constant oceanic salinity and represented a limited aspect of coastal iron chemistry. However their model predictions of spatial and temporal variations in ferrous iron and hydrogen peroxide concentrations were in agreement with field measurements. These results indicate that detailed kinetic modelling of fundamental chemical processes is a useful method of estimating iron speciation at an ecosystem scale.

1.4 Rationale for the performed research

This thesis combines what is known about individual processes affecting iron speciation into a comprehensive model of the iron chemistry in the oceanic mixed layer. In contrast to Rose and Waite (2003c), who focused on the chemistry of iron in short term experiments of coastal water, this study uses a slightly less complex model for iron chemistry, but couples it to an ecosystem model to study iron biogeochemistry in the mixed layer at the Bermuda Atlantic Time-series Station (BATS) site on short (diurnal) and on longer (annual) timescales.

The BATS site is an area 85 km south east of Bermuda in the Sargasso Sea where a number of physical, chemical, and biological parameters have been measured regularly since 1988 (Steinberg et al., 2001). The site provides an ideal environment for a first assessment of a comprehensive iron-speciation model because both, the oceanographic conditions and the biogeochemistry, are well known. In addition, dust deposition rates (Kim and Church, 2001) are available. The data provide realistic boundary conditions to the model and allow some comparison of model results with observations and with data-based estimates of iron fluxes at the BATS site (Section 2.1).

Several of the modeled processes involve parameters that are either not very well known or that have been measured under conditions different from the open-ocean conditions that are considered here. This is for example true for iron scavenging and colloid aggregation rates that have both been measured at particle concentrations much higher than those usually observed at the BATS site (Nyffeler et al., 1984; Wen et al., 1997). Therefore the aim of this study is not to reproduce observations with a single model run, but rather to study the consequences that specific assumptions have for the speciation, concentration and fluxes of iron at the BATS site, and to test whether these consequences are compatible with the few available observations. At the present stage the model is primarily a tool to help in understanding the key processes of the iron cycle and their sensitivities rather than a numerically accurate reproduction of reality. Therefore the model outcomes are used to investigate some less well-known parameter values.
In the first part of the thesis, a zero-dimensional (0d) approach of the model is set up. Specific questions addressed in this part of the thesis are:

1. How strong is the daily photochemical redox-cycling of iron at the BATS site? How important is the direct photoreduction of iron species compared to the reduction by photoproduced superoxide? Do other transition metals influence the strength of the redox cycle?

2. Under which conditions can colloid aggregation lead to a significant loss of iron from the surface layer of the ocean?

3. How strong is the influence of the solubility and the chemical form of dust-deposited iron on the iron cycle in the mixed layer?

4. Does it make a difference to the iron cycle which chemical form of iron is taken up by phytoplankton? How sensitive are model results to changes in the Fe:N or Fe:C-ratio of phytoplankton uptake?

In the second part of the thesis, a one-dimensional (1d) extension of the zero-dimensional model is described. Compared to the zero-dimensional

model, that treats the surface mixed layer as a homogeneous box, the one-dimensional approach allows a better analysis of the iron processes and behaviour with depth.

The focus of this part is:

1. the concentration and fluxes of dissolved iron below the annual mixed layer and how the concentration is affected by the parameterisation of loss processes that transfer dissolved iron to sinking particles either through scavenging or through a colloid intermediate.

2. the vertical scale of the fast redox cycling within the mixed layer.

The investigation of these questions for the BATS location shall lead to a better general understanding of iron biogeochemistry and thereby also contribute to studies on much larger spatial and temporal scales (e.g. Johnson et al., 1997; Archer and Johnson, 2000; Lefevre and Watson, 1999; Christian et al., 2002b; Parekh et al., 2004). On these larger scales, the influence of detailed iron speciation can probably be parameterised using simpler models (e.g. Parekh et al., 2004). A model-based understanding of processes such as colloid aggregation might lead to improvements in these parameterisations. Iron speciation in the mixed layer might also be important in the competition between different phytoplankton groups (Hutchins et al., 1999), and therefore the study complements studies that have combined a simple iron model with increasingly complex ecosystem models (e.g. Lancelot et al., 2000; Moore et al., 2002; Aumont et al., 2003) to address the role of iron in determining phytoplankton species composition. Finally, one outcome of this study is the identification of parameters that need to be better constrained in order to improve the prediction of speciation, concentration and fluxes of iron in the world's oceans.

1.4.1 Annotation

The first part of the thesis (Chapter 2.2 and Chapter 3) is for the most part already published as: L. Weber, C. Völker, M. Schartau and D. A. Wolf-Gladrow. *Global Biogeochemical Cycles*, Vol. 19, GB1019,doi:10.1029/2004GB002340, 2005.

The modelling of the ecosystem part was mainly undertaken by Markus Schartau (Marine Sciences Research Center, SUNY Stony Brook, USA. Now at: GKSS-Forschungszentrum, Institut für Küstenforschung, Geesthacht, Germany). In the scope of the EU-Project IRONAGES, Dieter Wolf-Gladrow (Alfred-Wegener Institut für Polar und Meeresforschung, Bremerhaven, Germany) gave only the initial idea to create a detailed model of the complex processes relating to iron chemistry and was not involved in the actual development of this work. My part was the development of the biogeochemical model and the coupling with the ecosystem model as well as the interpretation of the model results. I was supervised by Christoph Völker (Alfred-Wegener Institut für Polar und Meeresforschung, Bremerhaven, Germany).

The second part deals with the one-dimensional model (Section 2.3 and Chapter 4) (to be submitted to *Global Biogeochemical Cycles* once the second author is back from traveling, early November 2006). For this part, I was supervised by Andreas Oschlies (National Oceanography Centre, Southampton, UK. Now at: Leibniz Institut für Meereswissenschaften, Kiel, Germany) for the ecosystem- and physical-model and by Christoph Völker for the biogeochemical part of the study. Hans Burchard (Institut für Ostesseforschung, Warnemünde, Germany) introduced me to the GOTM-framework. All modelling work as well as the interpretation and discussion of the results were conducted by myself.

Chapter 2

Model description

2.1 Study area

The Sargasso Sea is part of the subtropical North Atlantic, bounded in the west and northwest by the Gulf Stream. A gyre is created by the recirculation of this western boundary current. Bermuda (31°45' N, 64°10' W) lies in the northwest of the Sargasso Sea and is an isolated seamount with no significant other islands or seamounts in the region. Around Bermuda is an area of weak Gulf Stream recirculation with a net flow of less than 5 cm s^{-1} towards the southwest (Siegel and Deuser, 1997). Mesoscale eddies are observed throughout this region. These instantaneous flow rates are typically 20-50 cm s^{-1} in the near-surface waters (Siegel and Deuser, 1997). The center of the gyre is also characterised by a net Ekman downwelling (McClain and Firestone, 1993) with rates near the BATS site of 4 cm day^{-1}. A region of mode-water formation exist between 31° N latitude and the Gulf Stream (Talley, 1982). This mode-water is created each winter when convective mixing forms deep mixed layers at a temperature of around 18 °C. In summer, most of the Sargasso Sea is under the influence of a large high-pressure system. In fall and winter, this high pressure system weakens, allowing storm fronts that are typically present

over North America at approximately weekly intervals, to begin to extend down to Bermuda and further south. Strong winds and cold, dry air associated with these fronts, act to cool and homogenise the surface waters and progressively deepen the mixed layer. North of Bermuda, mixed layers up to 400 m deep occur nearly every year with temperatures around 18 °C. South of Bermuda, mixed layers rarely extend below 100-150 m, the nominal depth of the euphotic zone. The mixed layer depths near Bermuda demonstrate a large amount of interannual variability (Figure 2.1), likely because the island is at the transition between the two mixed-layer regions and thus sensitive to the interannual variations in atmospheric forcing (Michaels and Knap, 1996). The mode water advects into the main thermocline under the Sargasso Sea, forming a zone of relatively weak thermal stratification below the seasonal thermocline that is distinguishable as a minimum in the profile of potential vorticity (Talley, 1982). Near Bermuda, this "18° water thermostat" occurs between 250 and 400 m depth. This layer of near isothermal water influences the mixed-layer development at Bermuda. Years with low cooling of the surface waters result in winter mixed layer depth of 100-200 m, barely penetrating into the nutrient-rich thermocline. However, only a small amount of additional heat loss reduces the temperature of the mixed layer to 18°C. This allows mixing to the bottom of the thermostat, increasing the mixed layer depth up to 400 m and causing large nutrient inputs to the surface. Thus the depth of winter mixed layers is extremely sensitive to winter cooling. The time-series station near Bermuda is in an area of strong meridional gradients in seasonality which influence the biogeochemistry. The weak mixing to the south of Bermuda leads to a permanently stratified water column that has all the characteristics of an oligotrophic ecosystem throughout the year. Nitrate is rarely present at the surface and the ecosystem is dominated by picoplankton and the microbial foodweb (Carpenter, 1983; Olson et al., 1990b,a; Siegel, 1990). To the north of Bermuda, the deep winter mixed layers result in blooms of larger phytoplankton including diatoms and

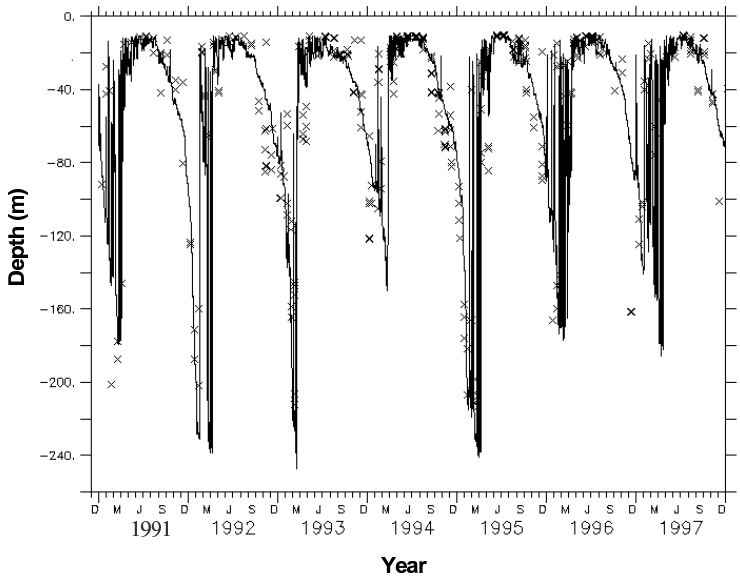

Figure 2.1: *Mixed layer depth at BATS defined by 0.1 K temperature difference to the 10 m depth temperature. Observations (crosses) (Steinberg et al., 2001) and model result with the GOTM of the present study (line).*

coccolithophores and a complex transition to oligotrophy in the summer (Siegel, 1990). Both of these seasonal patterns can occur at the BATS site depending on the intensity of winter mixing (Michaels and Knap, 1996).

2.1.1 Dust- and iron deposition at the BATS-site

The majority of dust in the water column of the Sargasso Sea is derived from Saharan dust storms and is deposited following atmospheric transport (Duce, 1986; Jickells et al., 1998). This eolian dust is the main source of iron at the BATS site (Jickells, 1999). Wet deposition of the dust is thought to be a crucial factor, determining the extent to which iron

becomes bioavailable, following chemical reactions within the rain drops. In contrast, iron from dry deposition of dust remains mostly bound to the dust and is, therefore, exported into deeper water by sinking (Jickells, 1999). Other sources of iron at the BATS site are negligible. Upwelling of iron from deeper water is unlikely due to the general Ekman downwelling in this region. Riverine sources from land are nonexistent since Bermuda is the only land in the area but without rivers. Only lateral advection, which can deliver iron through the water column, is suggested to be important for the annual nutrient budget at the BATS site (Jenkins and Doney, 2003; Gruber et al., 2002; Palter et al., 2005) and should be beared in mind. In the present study, daily values of dust deposition (both wet and dry) at the BATS site were taken from the output of a global atmospheric dust transport model (Mahowald et al., 1999). The average dust deposition between 1989 and 1998 at the nearest model grid point to the BATS location is 2.3 mg m^{-2} d^{-1}. Most of that deposition occurs in June to September (average 5.3 mg m^{-2} d^{-1} in that period), reflecting the arrival of dust blown off the Sahara, while the average deposition is low in the other months. This annual pattern and the average value agree well with observed values for dust deposition at Bermuda between September 1996 to September 1997 by Kim et al. (1999). There is considerable day-to-day variability in the dust deposition with frequent changes over two orders of magnitude from one day to the next. Annually averaged observed dust deposition varies between 1.3 (1997) and 3.4 (1985) mg m^{-2} d^{-1}.

2.1.2 Dissolved iron at the BATS-site

A number of previous studies measured dissolved iron at the BATS site (Figure 2.2) including Sedwick et al. (2005); Wu and Boyle (2002); Wu et al. (2001); Wu and Boyle (1998); Wu and Luther III (1994); Cullen et al. (2006)), whereby dFe refers to 0.4 μm-filtered samples. Wu et al. (2001) and Cullen et al. (2006) also present values where soluble (0.02 μm-filtered

samples) and colloidal iron (0.02-0.4 μm) are distinguished. Data reveal strong seasonal changes of dissolved iron (dFe) concentrations in surface waters, with high concentrations in summer (up to 2 nM) and low concentrations in spring (down to 0.1 nM) (Wu and Boyle, 2002; Sedwick et al., 2005). The dissolved iron profiles measured in summer show similar patterns with pronounced near surface maxima in dFe, a dFe minima in the 40-150 m depth range and an increase in concentration between 150 m and 500 m to concentrations around 0.4-0.6 nM. The spring dFe profiles by Wu et al. (2001) and Sedwick et al. (2005) are not in agreement but both have generally lower concentrations than the summer profiles.

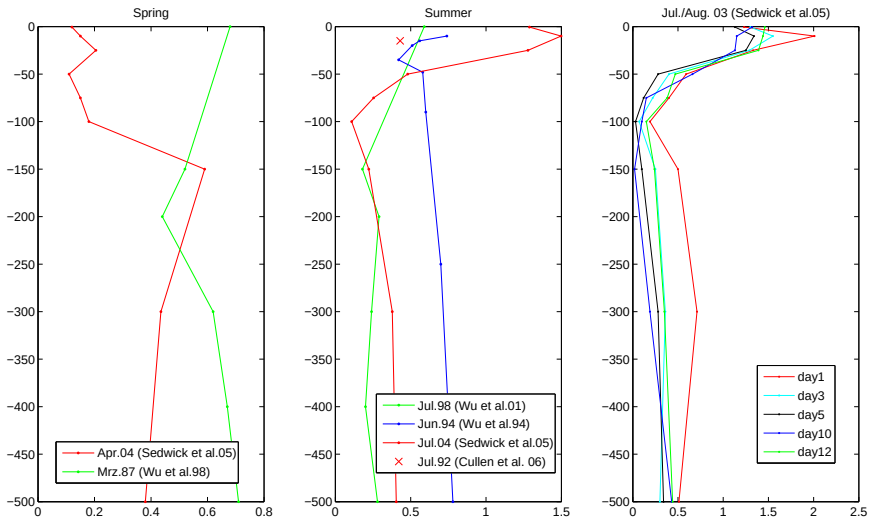

Figure 2.2: *Observed concentrations of dFe at the BATS site*

2.2 The zero-dimensional model

The model has a chemical and a biological component. The biological model only provides dynamic boundary conditions (e.g. iron uptake by phytoplankton and release during remineralisation of organic matter) for

the speciation component. Hence, in the model, phytoplankton growth is not iron limited (which is a reasonable assumption for the BATS site, see Fung et al. (2000); Watson (2001)) and the biological component remains unaffected by the speciation model part.

For simplicity it is assumed that mixing within the oceanic mixed layer acts on such a short timescale that concentrations within the layer are vertically homogeneous. Model concentrations below the mixed layer are prescribed from observations and influence the concentrations within the mixed layer by turbulent mixing and by entrainment of water during periods of mixed layer deepening.

Model runs start from arbitrary initial conditions and use a combination of observed and modeled timeseries as external forcing (section 2.2.3). The integration period is 12 years, of which the first three years are spin-up. The remaining nine years cover the period from 1989 until the end of 1997. During spin-up the model is driven with a repeated annual cycle of forcing from the year 1989. After one year of spinup the model reaches a cyclo-stationary state with repeating annual cycles in all variables. A specialised solver for stiff differential equations is used in the integrations.

2.2.1 Ecosystem model

The biological part of the model is a nitrogen-based ecosystem model with three compartments, representing (i) inorganic nitrogen, N, which includes nitrate, nitrite and ammonium, (ii) phytoplankton, P and (iii) detritus, D. The loss of phytoplankton to detritus, representing aggregation and grazing by heterotrophs is simply modeled as a quadratic function of phytoplankton concentration. A linear relationship for remineralisation and a constant sinking rate for detritus is assumed. No explicit representation of zooplankton is considered, since the zooplankton annual cycle itself is not well constrained from observations and it did not improve the data-model comparison with respect to the other variables. The main effect of this

simplification is that the maximum loss of phytoplankton through the quadratic term occurs at the time of the phytoplankton bloom instead of being somewhat delayed, as would be the case with an explicit representation of zooplankton.

The biological model formulation includes a variable carbon to nitrogen ratio (C:N) of phytoplankton primary production, depending on the availability of nitrogen and light. This new diagnostic approach greatly improves the modeled carbon uptake under nitrate depleted conditions. The parameterisation does not allow for an overall C:N decoupling of the particulate organic matter in the model, but provides a better model counterpart to observed ^{14}C-primary production rates. Models that assume a constant C:N stoichiometry in phytoplankton uptake, produce systematic errors in carbon fluxes at the BATS site (Schartau et al., 2001; Schartau and Oschlies, 2003b), and cannot reproduce the observed maximum rate of carbon uptake, which occurs shortly after the decline in chlorophyll, when nitrate becomes depleted. Light adaptation of phytoplankton is represented by a variable C:N, based on Cloern et al. (1995).

The micro-genetic algorithm of Carroll (1996) was applied to minimise the misfit between the ecosystem model and observations. The configuration of the algorithm is similar to the one chosen in Schartau and Oschlies (2003a). However, in the present study the direct misfits between model result and observation at the dates of measurement are minimised rather than the misfits of monthly averages. Particulate organic nitrogen, chlorophyll a, ^{14}C-primary production rates, and nitrate concentrations were considered for the assimilation process. Bottle data of these variables were extracted from the BATS web-site (http://www.bbsr.edu/cintoo/bats/bats.html). The data were processed in the following steps: a) linear interpolation of every bottle cast in the vertical; b) averaging of the profiles belonging to the same cruise; c) averaging this averaged cruise profile vertically over the mixed layer depth (see below for the definition of the mixed layer depth). In the data assimilation procedure, a subset of the biological model parameters

(those marked by $\star$ in Table 2.1) was optimised such that the data-model weighted least-square misfit is minimised. The full set of phytoplankton growth parameters cannot be individually constrained (e.g. Fennel et al., 2001) in a 0d-model version. Therefore, a fixed value for the maximum growth rate parameter taken from Schartau and Oschlies (2003a) was assigned. The optimisation yields one best solution of the biological model component which remains unchanged during all subsequent model runs.

The marine ecosystem influences iron chemistry in a number of ways:

1. by uptake of iron during phytoplankton growth and release of iron during remineralisation of organic matter.
2. by producing detritus onto which iron can be scavenged.
3. by introducing a source of organic ligands, either as a byproduct of remineralisation or by excretion of siderophores to enhance iron uptake.
4. by influencing the attenuation of light within the water column and thus photochemical reactions.

It is assumed here that iron is taken up by phytoplankton in constant proportion to either carbon or nitrogen, while the remineralisation of iron occurs proportionally to that of nitrogen. This is based on the general assumption that phytoplankton is not iron limited at the BATS site (Fung et al., 2000; Watson, 2001). Therefore this assumption may be justified. The iron that is released during the remineralisation of organic matter is assumed to be in organically complexed form.

2.2.2 Chemical model

Measurements of iron speciation in seawater are usually reported in terms of operationally defined categories (e.g. by filtration procedure) rather than

as chemical speciation in the true sense of the word (section 1.2). To make the model as consistent as possible with such observational data, following five iron states are differentiated in the model: (i) dissolved inorganic ferric iron Fe(III)', which includes all hydrolysed species of $Fe(OH)^{3-n}$, (ii) dissolved inorganic ferrous iron Fe(II)', (iii) organically complexed iron FeL, (iv) colloidal iron Fe_{col}, defined here by filter cutoffs 0.02 - 0.4 μm (Wu et al., 2001), and (v) iron bound to the surface of sinking particles Fe_p such as dust and organic detritus and aggregated iron (>0.4 μm). The nonreactive part of the particulate iron contained in deposited dust is also modeled, but not further considered in the present study.

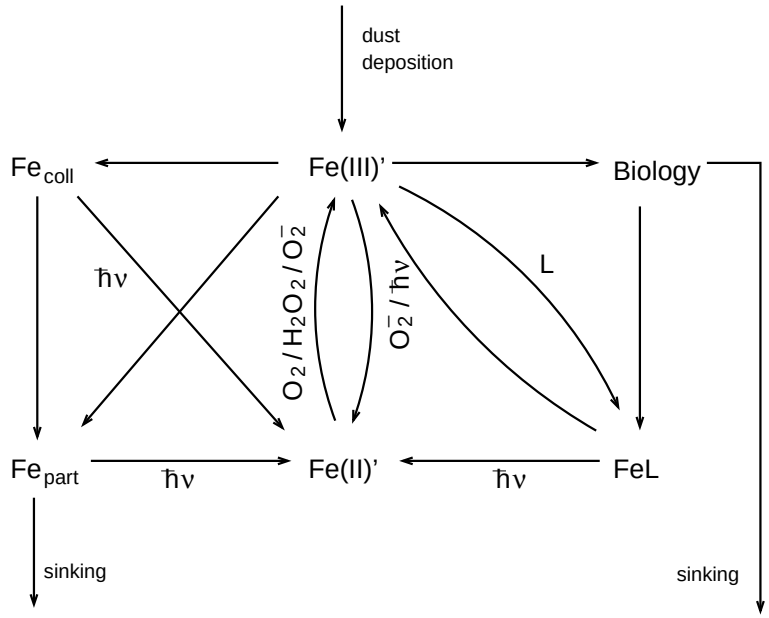

Figure 2.3: *Schematic representation of the iron pools represented in the model and the fluxes between them. Photochemically driven processes are marked with $\hbar\nu$. Fluxes due to mixing and entrainment at the base of the mixed layer are not shown.*

A number of processes are known to convert iron in seawater between these forms. The model include the processes of:

1. complex formation and dissociation involving organic ligands

(Gledhill and van den Berg, 1994; Van den Berg, 1995; Wu and Luther III, 1995; Rue and Bruland, 1995; Witter and Luther III, 1998; Witter et al., 2000; Rose and Waite, 2003b)

2. photoreduction of the different iron forms, both directly (Wells and Mayer, 1991; Kuma et al., 1992; Johnson et al., 1994; Barbeau and Moffett, 2000; Barbeau et al., 2001; Emmenegger et al., 2001; Barbeau et al., 2003) and indirectly by photoproduced superoxide (Voelker and Sedlak, 1995; Miller et al., 1995)

3. oxidation of Fe(II)' by oxygen, superoxide and hydrogen peroxide (Millero et al., 1987; Millero and Sotolongo, 1989; King et al., 1995)

4. scavenging onto sinking particles (Balistieri et al., 1981; Nyffeler et al., 1984; Johnson et al., 1997)

5. colloid formation (Johnson et al., 1994; Rose and Waite, 2003a)

6. aggregation of colloids (Wells and Goldberg, 1993; Wen et al., 1997)

Rate laws and constants for these processes were taken from the literature indicated in Table 2.2. To represent the kinetics of interconversion between the different forms of iron, the concentrations of free iron-binding organic ligands [L], of hydrogen peroxide [H_2O_2], of superoxide [O_2^-], and of sinking particles (both inorganic from dust deposition and organic detritus) were also modeled (Section 2.2.4). A schematic representation of the iron pools and fluxes between them is shown in Figure 2.3.

For each of the iron species in the model, a mass balance equation is solved that takes into account the listed reactions plus sources and sinks from atmospheric deposition, sinking, and mixing of waters at the base of the mixed layer.

2.2.3 Forcing

Several processes in the model depend on external forcing. Solar irradiance drives photochemical reactions and in combination with the depth and temperature of the oceanic mixed layer, influences the growth rate of phytoplankton. Dust deposition is a source of inorganic sinking particles and iron. Precipitation (rain water) is a source of hydrogen peroxide.

Timeseries of precipitation and daily averaged irradiance for the BATS location compiled by Doney (1996) were used. Mean daily precipitation is around 3.7 mm day^{-1} and has no pronounced annual cycle. Daily averaged irradiance varies between 80 W m^{-2} in winter and 300 W m^{-2} in summer. A daily cycle of irradiance was constructed from the daily averaged values using standard astronomical formulae for daylength and zenith angle (Brock, 1981).

Vertical profiles of temperature and salinity are available from the approximately biweekly BATS cruises since October 1988. A timeseries of mixed layer depth and temperature directly from BATS CTD data (http://www.bbsr.edu/cintoo/bats/bats.html) was constructed, whereby the lower boundary of the mixed layer is defined by the depth at which temperature is 0.1 degrees colder than at the surface. If more than one CTD cast was available within a cruise, the temperature profiles were averaged before calculating the mixed layer depth. The annual mixed layer cycle typically reaches a maximum depth between 150 and 350 m at the end of the winter, followed by a rapid shoaling towards the summer, when mixed layer depths are around 20 m. The mixed layer typically begins to deepen again in September.

To convert dust deposition to iron flux, it is assumed that the deposited dust has a composition close to that of average crustal material, with a percentage mass of 3.5% iron (Taylor, 1964; Duce and Tindale, 1991), and that a fixed fraction of that iron is dissolvable after deposition to the sea surface (Jickells, 1995). The nonreactive part of the iron contained in dust

is not further considered in the present study.

2.2.4 Model equations

Three biological model equations determine evolution of concentrations of phytoplankton P, detritus D, and dissolved inorganic nitrogen N. They are formulated in units of μM nitrogen d^{-1}.

$$\frac{d}{dt}P = (\mu - \rho_P \eta_T)\, P - \Phi_P^* P^2 - \frac{m_r + h^+}{H} P \tag{2.1}$$

$$\frac{d}{dt}D = \Phi_P^* P^2 - \gamma_D \eta_T D - \frac{m_r + h^+ + w_s}{H} D \tag{2.2}$$

$$\frac{d}{dt}N = -(\mu - \rho_P \eta_T)\, P + \gamma_D \eta_T D + \frac{m_r + h^+}{H}(N_{deep} - N). \tag{2.3}$$

The phytoplankton growth rate μ is the smaller of either a nutrient- or a light-limited growth rate $\mu = \min(\mu_N, \mu_L)$. $\mu_N = \mu^* \eta_T (N/(K_N + N))$ has the standard Michaelis-Menten dependency on nitrogen availability with K_N being the nitrate half-saturation constant, multiplied by a temperature dependency η_T of the maximum growth rate μ^*. η_T was choosen to be $\eta_T = (C_{ref})^{T[^\circ C]^{-1}}$ as in Fasham (1993). $\mu_L = \mu^* \eta_T f(\alpha, I, H, \lambda)$ is the light-limited growth function following Evans and Parslow (1985), which is a function of the slope of the photosynthesis-irradiance curve α, the daily averaged irradiance at the sea surface I, the mixed layer depth H, and the light attenuation λ. Concentrations within the mixed layer change by mixing, occuring at the base of the mixed layer at a rate m_r, and by entrainment of water during mixed layer deepening h^+, where

$$h^+ = \max\left(\frac{dH}{dt}, 0\right). \tag{2.4}$$

Detrital material is lost out of the mixed layer by sinking, for which a constant sinking velocity w_s is assumed. N_{deep} is the nitrogen concentration below the mixed layer, which is parameterized as in Schartau et al. (2001).

Although the model is formulated in nitrogen units, a variable chlorophyll:carbon ratio $r_{Chl:C}$ in phytoplankton biomass (mg Chl mg C^{-1}) following Cloern et al. (1995) is allowed:

$$\begin{aligned} r_{Chl:C} &= 0.003 + 0.0154 \exp(0.05\, T[^\circ C]^{-1}) \cdot \frac{N}{K_N + N} \cdot \\ &\quad \exp\left(\frac{-0.059\, I_{PAR}(1 - \exp(-\lambda H))}{\lambda H}\right) \end{aligned} \tag{2.5}$$

where $\lambda = k_w + \kappa Chl$ is the light attenuation by water and chlorophyll, and $I_{PAR} = f_{PAR} I$ is the irradiance within the photosynthetically active range.

A carbon:nitrogen ratio $r_{C:N}$ in phytoplankton primary production is parameterised by

$$\begin{aligned} r_{C:N} &= Q_{min} + (Q_{max} - Q_{min}) \cdot \\ &\quad \left(1 - \exp\left(\frac{-\sigma(\mu_L - \mu)}{\mu}\right)\right). \end{aligned} \tag{2.6}$$

where Q_{min} is the minimum and Q_{max} the maximum C:N ratio. This parameterisation ensures that phytoplankton grows at a ratio Q_{min} under light limitation, while nutrient limitation increases $r_{C:N}$ up to the limit Q_{max}.

The concentration of inorganic particles, A, in the mixed layer (in mg L^{-1}) is determined as the net mass balance between dust deposition and loss out of the mixed layer by mixing, entrainment and sinking, following:

$$\frac{d}{dt}A = \frac{F_{dust}}{H} - \frac{m_r + h^+ + w_s}{H}A, \tag{2.7}$$

where the same sinking speed is assumed for inorganic particles as for detritus. F_{dust} is the dust deposition flux per unit area of the sea surface.

The equations for the concentration of the three truly dissolved iron species Fe(III)', Fe(II)', and FeL (in units nM iron d^{-1}) are

$$\begin{aligned} \frac{d}{dt}\left[\mathrm{Fe(III)'}\right] &= \frac{F_{Fe}}{H} + k_{ld}\left[\mathrm{FeL}\right] + \left(k_{ox1}\left[\mathrm{O_2}\right] + \right. \\ &\quad \left. k_{ox2}[\mathrm{O_2^-}] + k_{ox3}\left[\mathrm{H_2O_2}\right]\right)\left[\mathrm{Fe(II)'}\right] - \end{aligned}$$

$$\begin{aligned} & \left(k_{col} + k_{ph3} + k_{fel}\,[\mathrm{L}] + k_{red}[\mathrm{O_2^-}] + \right. \\ & \left. k_{sca}\,(r_{m:N} D + A)\right)[\mathrm{Fe(III)'}] - \mu P R_{Fe:N} \\ & -\frac{m_r + h^+}{H}\,[\mathrm{Fe(III)'}] \end{aligned} \tag{2.8}$$

$$\begin{aligned} \frac{d}{dt}\,[\mathrm{Fe(II)'}] &= \left(k_{red}[\mathrm{O_2^-}] + k_{ph3}\right)[\mathrm{Fe(III)'}] + \\ & k_{ph4}\,[\mathrm{Fe_p}] + k_{ph1}\,[\mathrm{Fe_{col}}] + \\ & k_{ph2}\,[\mathrm{FeL}] - \left(k_{ox1}\,[\mathrm{O_2}] + k_{ox2}[\mathrm{O_2^-}] + \right. \\ & \left. k_{ox3}\,[\mathrm{H_2O_2}]\right)[\mathrm{Fe(II)'}] - \\ & \frac{m_r + h^+}{H}\,[\mathrm{Fe(II)'}] \end{aligned} \tag{2.9}$$

$$\begin{aligned} \frac{d}{dt}\,[\mathrm{FeL}] &= k_{fel}\,[\mathrm{Fe(III)'}]\,[\mathrm{L}] + r_{Fe:N}\,(\gamma_D D + \rho_P P) - \\ & (k_{ld} + k_{ph2})\,[\mathrm{FeL}] + \\ & \frac{m_r + h^+}{H}\left([\mathrm{FeL}]_{deep} - [\mathrm{FeL}]\right) \end{aligned} \tag{2.10}$$

Equations (2.8) and (2.9) are connected through the oxidation of Fe(II)' by O_2, O_2^- and H_2O_2, and by the reduction of Fe(III)' by O_2^- and by light. Equations (2.8) and (2.10) are coupled by the formation and dissociation of organic complexes, and equations (2.9) and (2.10) by the photodissociation of organic complexes. F_{Fe} is the flux of dissolved iron per unit area by dust deposition at the sea surface. Here it is assumed that dust input is a source for Fe(III)', but model experiments where dust is a source for Fe(II)', FeL or Fe_{col} are also performed as a sensitivity study (Section 3.2.3). The biological uptake if iron is $-\mu P R_{Fe:N}$, where the Fe:N-ratio is either the constant $r_{Fe:N}$ or calculated as $R_{Fe:N} = r_{Fe:C} r_{C:N}$, while the flux of iron due to remineralisation of organic matter is $r_{Fe:N}\,(\gamma_D D + \rho_P P)$. All photochemical rates k_{phN} ($N = 1$ to 4) are assumed to be proportional to the instantaneous irradiance averaged over the mixed layer depth.

Equations (2.8) to (2.10) are complemented by equations for colloidal iron and iron adsorbed onto sinking particles

$$\frac{d}{dt}\,[\mathrm{Fe_{col}}] = k_{col}\,[\mathrm{Fe(III)'}] - (k_{ph1} + k_{ag}\,(r_{m:N} D + A))\cdot$$

$$[\mathrm{Fe_{col}}] + \frac{m_r + h^+}{H}\left([\mathrm{Fe_{col}}]_{deep} - [\mathrm{Fe_{col}}]\right) \tag{2.11}$$

$$\frac{d}{dt}[\mathrm{Fe_p}] = (r_{m:N}D + A)\left(k_{sca}[\mathrm{Fe(III)'}] + k_{ag}[\mathrm{Fe_{col}}]\right) - k_{ph4}[\mathrm{Fe_p}] - \frac{m_r + h^+ + w_s}{H}[\mathrm{Fe_p}] \tag{2.12}$$

Using the method of Johnson et al. (1994), the formation of colloidal iron in (2.11) is modeled as a first-order process in [Fe(III)′]. Colloidal iron aggregates to larger sinking particles and solubelises through photoreduction. The dominant aggregation process is assumed to be due to collisions with larger particles and is modeled as a first-order process both in [$\mathrm{Fe_{col}}$] and the total particle concentration $r_{m:N}D + A$, where $r_{m:N}$ is a conversion factor from concentrations in molarity nitrogen to g L^{-1}. The scavenging of Fe(III)' onto sinking particles is modeled similarly as a first-order process in [Fe(III)′] and in $r_{m:N}D + A$.

Given the uncertainties in the source and fate of organic iron-binding ligands (Section 1.2.2), the time evolution of ligands is modeled with a simplified equation without a biological source of free ligands, but also without photochemical degradation, i.e. it is assumed that photoreduction of FeL produces free ligands, following:

$$\frac{d}{dt}[\mathrm{L}] = (k_{ld} + k_{ph2})[\mathrm{FeL}] - k_{fel}[\mathrm{Fe(III)'}][\mathrm{L}] + \frac{m_r + h^+}{H}\left([\mathrm{L}]_{deep} - [\mathrm{L}]\right) \tag{2.13}$$

This parameterisation prevents unrealistically low concentrations of [FeL] + [L] in the mixed layer to occur due to photochemical degradation.

The system of equations is completed by specifying the concentrations of oxygen, superoxide and hydrogen peroxide. At the BATS site, observed values of [$\mathrm{O_2}$] vary by about ±7% over the annual cycle. For simplicity, [$\mathrm{O_2}$] is set to a constant value in the model. The other two oxidants, however, are strongly influenced by reactions within the iron system and the daily cycle of irradiance. Their evolution is parameterised similar to Voelker and

Sedlak (1995) and Miller et al. (1995):

$$\begin{aligned}\frac{d}{dt}[\mathrm{O_2^-}] &= S_{O_2^-} + k_{ox1}\,[\mathrm{O_2}]\,[\mathrm{Fe(II)'}] - 2k_{dm}[\mathrm{O_2^-}]^2 - \\ &\quad (k_{ox2}\,[\mathrm{Fe(II)'}] + k_{red}\,[\mathrm{Fe(III)'}])\,[\mathrm{O_2^-}] - \\ &\quad \frac{m_r + h^+}{H}[\mathrm{O_2^-}] \qquad (2.14)\\ \frac{d}{dt}\,[\mathrm{H_2O_2}] &= \frac{F_{H_2O_2}}{H} + k_{dm}[\mathrm{O_2^-}]^2 + k_{ox2}[\mathrm{O_2^-}]\,[\mathrm{Fe(II)'}] - \\ &\quad k_{ox3}\,[\mathrm{H_2O_2}]\,[\mathrm{Fe(II)'}] - k_{dis}\,[\mathrm{H_2O_2}] - \\ &\quad \frac{m_r + h^+}{H}\,[\mathrm{H_2O_2}] \qquad (2.15)\end{aligned}$$

In (2.14), the rate of production of superoxide by photoreactions with coloured dissolved organic matter $S_{O_2^-}$ is assumed to be proportional to irradiance. $F_{H_2O_2}$ represent the deposition of H_2O_2 through rain. A constant concentration of H_2O_2 in rainwater (Ra) is assumed, such that $F_{H_2O_2} = [\mathrm{H_2O_2}]_{rain}\,Ra$.

Concentrations of the iron species FeL, Fe_{col}, and of free ligands L below the mixed layer are prescribed as linear functions of H using a fit to observed concentration profiles by Wu et al. (2001). All the other species are assumed to have zero concentration below the mixed layer.

2.3 The one-dimensional model

In the second part of this study a one-dimensional extension of the zero-dimensional model was made.

The processes converting iron between its different forms (see Figure 2.3) are parameterised as in the zero-dimensional model, and the same initial rate constants are adopted, the only exception being the photoreduction rate of colloidal iron (k_{ph1}). Estimates for k_{ph1} by Wells and Mayer (1991) and Barbeau and Moffett (1998) are much lower (between 0.12 and 0.43 $\mathrm{d^{-1}}$) than the value by Johnson et al. (1994) (20.16 $\mathrm{d^{-1}}$), used in the zero-dimensional model. The latter value was calculated from data obtained

Table 2.1: *Standard model parameters for the ecosystem part of the zero-dimensional (0d) model and the one-dimensional (1d) model. OD Parameters were taken from the work by Schartau et al. (2001), 1d parameters from the work by Oschlies and Schartau (2005). Parameter values optimised in the data assimilation (section 2.2.1) are marked by $\star$. The value for K_{Fe} was taken from the work by Parekh et al. (2004), the value for $r_{Fe:N}$ from Johnson et al. (1997)*

Parameter	Symbol	Unit	0d	1d
maximum growth rate	μ^*	d^{-1}	0.27	0.27
phytoplankton mortality	γ_p	d^{-1}	$0.005\star$	0.04
initial slope P-I curve	α	$m^2\ W^{-1}\ d^{-1}$	$0.159\star$	0.256
nitrate half-saturation constant	K_N	μM	$0.7\ \star$	0.7
iron half-saturation constant	K_{Fe}	nM	-	0.2
phytoplankton aggregation rate	γ_{p^2}	$\mu M^{-1}\ d^{-1}$	$0.64\ \star$	0.025
maximum grazing rate	g	d^{-1}	-	1.575
prey capture rate	ϵ	$\mu M^{-1}\ d^{-1}$	-	1.6
assimilation efficiency	γ_{za}	-	-	0.925
excretion	γ_{zb}	d^{-1}	-	0.01
quadratic mortality	γ_{z^2}	$\mu M^{-1}\ d^{-1}$	-	0.34
detritus remineralisation	γ_d	d^{-1}	$0.02\ \star$	0.048
sinking velocity	w_s	$m\ d^{-1}$	18	18
coefficient for temperature function	C_{ref}	-	1.066	1.066
PAR:short-wave irradiance ratio	f_{PAR}	-	0.43	0.43
attenuation due to chlorophyll	κ	$(mg\ Chl)^{-1}\ L\ m^{-1}$	$0.01\ \star$	0.03
attenuation due to water	k_w	m^{-1}	0.04	-
minimum C:N ratio	Q_{min}	-	5.4	-
maximum C:N ratio	Q_{max}	-	$22\star$	-
slope parameter for C:N ratio	σ	-	$0.48\star$	-
Fe:N ratio in organic matter	$r_{Fe:N}$	$nM\ \mu M^{-1}$	$3.31 \cdot 10^{-2}$	$3.31 \cdot 10^{-2}$
mass:N ratio in organic matter	$r_{m:N}$	$g\ mol^{-1}$	159	159
mixing rate	k_{mr}	$m\ d^{-1}$	$1.15\star$	-

by Waite and Morel (1984) at pH 6.5. Johnson et al. (1994) assumed that this rate was the same at pH 8, which is not a reasonable assumption (King et al., 1993; Moffet, 2001). Therefore this value is corrected here.

From the results of the zero-dimensional model, colloidal aggregation (Section 3.2.4), the influence of Cu on the concentration of reactive oxygen species and on Fe(II) (Section 3.2.5) and an excess of organic ligands (Section 3.2.6) is conciderd in the one dimensional model. To ensure an excess of ligands, a fixed concentration of free iron-binding organic ligands ($[L]$), taken from the work by (Cullen et al., 2006) is introduced.

Daily values of dust deposition were taken from the output of a global atmospheric dust transport model by Mahowald et al. (1999) as in the

zero-dimensional model.

The biological part of the model is a nitrogen-based ecosystem model by Oschlies and Schartau (2005) with four compartments, representing inorganic nitrogen (N), phytoplankton (P), zooplankton (Z) and detritus (D). Oschlies and Schartau (2005) calibrated the ecosystem model in a one-dimensional mode against observations at the BATS site and two other sites in the North Atlantic.

A decoupling between the cycling of Fe and N was allowed by reducing the uptake of iron under low concentrations, which is different to the 0d-model, for which a uniform Fe:N ratio in phytoplankton, zooplankton and detritus was assumed. This requires explicit modelling of the Fe content in the ecosystem compartments, i.e. three further model equations are introduced (Equations 2.16 - 2.18. The phytoplankton growth rate is still not dependent on the iron quota of the cells or the external iron concentration. This assumption effectively makes nitrogen cycling independent from that of iron and helps to analyse the sensitivity of the iron cycle to parameter changes without feedback through changing export production. In future studies, iron limitation of phytoplankton growth should be taken into account.

In addition to the chemical iron model by Weber et al. (2005) and the optimised NPZD ecosystem model by Oschlies and Schartau (2005) three additional biological model equations were implemented. They determine the evolution of the concentration of iron in phytoplankton (P_{Fe}), detritus (D_{Fe}), and zooplankton (Z_{Fe}) The equations are based on the NPZD model by Oschlies and Schartau (2005) and are formulated in units of nM iron d^{-1}, as follows:

$$\begin{aligned} \frac{d}{dt}[P_{Fe}] &= r_{fe:p}\rho[P] - r_{fe:p}G\left([P]\right)[Z] - \gamma_p\left(T\right)[P_{Fe}] - \\ &\quad r_{fe:p}\gamma_{p^2}[P]^2 \\ \frac{d}{dt}[Z_{Fe}] &= r_{fe:p}\gamma_{za}G\left([P]\right)[Z] - \gamma_{zb}\left(T\right)[Z_{Fe}] - \end{aligned} \tag{2.16}$$

$$r_{fe:z}\gamma_{z^2}[Z]^2 \tag{2.17}$$

$$\frac{d}{dt}[D_{Fe]} = r_{fe:p}\gamma_{p^2}[P]^2 + r_{fe:p}\left(1-\gamma_{za}\right)G\left([P]\right)[Z] + r_{fe:z}\gamma_{z^2}[Z]^2 - \gamma_d\left(T\right)[D_{Fe}] - w_s\frac{d[D_{Fe}]}{dz} \tag{2.18}$$

where $r_{fe:p} = [\mathrm{P_{Fe}}]/[\mathrm{P}]$ and $r_{fe:z} = [\mathrm{Z_{Fe}}]/[\mathrm{Z}]$. The terms on the right hand side are identical to the terms in the NPZD model except for a multiplication with either $r_{fe:p}$ or $r_{fe:z}$. One exception is the uptake of iron by phytoplankton: While the growth rate of phytoplankton μ is the smaller of either a nutrient- or a light-limited rate $\mu = \min(\mu_N, \mu_L)$, the iron uptake rate ρ also depends on iron via $\rho = \min(\mu, \mu_{Fe})$, where $\mu_{Fe} = \mu^*[\mathrm{Fe}]/(K_{Fe} + [\mathrm{sFe}])$ has the standard Michaelis-Menten dependency on iron availability, multiplied by the maximum growth rate μ^*. sFe reffers to truley dissolved iron (FeL, Fe(II)′) Fe(III)′)

The physical part of the model is the General Ocean Turbulence Model (GOTM: www.gotm.net and Burchard et al. (2006)). The GOTM was chosen because of its provision of stiff equation solvers appropriate for dealing with the very fast photochemical reaction rates in the model (order of seconds). In particular, the recently developed non-negative and conservative modified Patankar-type solver for ordinary differential equations (Burchard et al., 2005) is used. Meteorological data are derived from the ERA-40 reanalysis project (Uppala et al., 2005) to drive the physical model. The light extinction routine after Jerlov (1968) provided by GOTM is used, whereby photosynthetically available radiation is assumed to be 43% of the total incoming irradiance (Brock, 1981). Ultraviolet radiation (UV) is not separately calculated although this may be important for the iron chemistry at the surface (Kuma et al., 1992; Rijkenberg et al., 2005). As suggested by Jerlov (1968) and by adjusting the parameter for attenuation due to chlorophyll and water, the oceanic type IB was chosen. Thich gave the best model results for nutrient and chlorophyll α concentrations, with respect to observations (Section 4.2).

A timestep of $\varphi = 1$ minute was chosen for the integration. Initial studies

showed that, together with GOTM's stiff equation solver, such a timestep is short enough to deal with the fast photochemical reaction rates. The short timesteps allow analysis of iron biogeochemistry over the course of a day. A total period of 9 years (covering the period from the beginning of 1988 until the end of 1997) was integrated, of which the first two years are spin-up time. The vertical grid consists of 100 layers over 600 m, with layer thickness increasing non-linearly from 0.9 m in the upper layer to 12.45 m at 600 meters depth. All sinking biogenic matter is instantaneously remineralised in the lowermost model box. As only the upper 250 m of the water column are considered in this study, this assumption does not affect model results within the timescale of the experiments.

Table 2.2: *Standard parameters of the chemical model for the zero-dimensional (0d) model and changed parameters in the one-dimensional (1d) model.*

Parameter	Symbol	Unit	0d	1d	Source
		Chemistry			
Fe(II)′ oxidation rate by O_2	k_{ox1}	$\mu M^{-1}\ d^{-1}$	0.864	-	Millero et al. (1987)
oxygen concentration	$[O_2]$	μM	214	-	Millero et al. (1987)
Fe(II)′ oxidation rate by O_2^-	k_{ox2}	$nM^{-1}\ d^{-1}$	864	-	Voelker and Sedlak (1995)
Fe(II)′ oxidation rate by H_2O_2	k_{ox3}	$nM^{-1}\ d^{-1}$	6.24	-	Johnson et al. (1994)
Fe_{col} photoreduction rate at 30 $\mu E\ m^{-3}\ s^{-1}$	k_{ph1}	d^{-1}	20.16	1.32	Johnson et al. (1994)
FeL photoreduction rate at 30 $\mu E\ m^{-3}\ s^{-1}$	k_{ph2}	d^{-1}	86.4	-	Emmenegger et al. (2001)
Fe(III)′ photoreduction rate at 30 $\mu E\ m^{-3}\ s^{-1}$	k_{ph3}	d^{-1}	1.32	-	Johnson et al. (1994)
Fe_p photoreduction rate at 30 $\mu E\ m^{-3}\ s^{-1}$	k_{ph4}	d^{-1}	20.2	-	Johnson et al. (1994)
Fe_{col} formation rate	k_{col}	d^{-1}	2.4	-	Johnson et al. (1994)
FeL formation rate	k_{fel}	$nM^{-1}\ d^{-1}$	172.8	-	Hudson and Morel (1993)
FeL conditional stability constant	k_{ld}	M^{-1}	$10^{20.3}$	10^{22}	Wu and Luther III (1995)
free organic ligand concentration	$[Lig]$	nM	-	2.4	Cullen et al. (2006)
Fe(III)′ reduction rate by O_2^-	k_{red}	$nM^{-1}\ d^{-1}$	$1.3 \cdot 10^4$	-	Voelker and Sedlak (1995)
Fe(III)′ scavenging rate	k_{sca}	$kg^{-1}\ l\ d^{-1}$	$2.5 \cdot 10^4$	$2.5 \cdot 10^3$	Nyffeler et al. (1984)
Fe_{col} aggregation rate	k_{ag}	$kg^{-1}\ l\ d^{-1}$	$1.224 \cdot 10^6$	$1.224 \cdot 10^1$	Wen et al. (1997)
O_2^- dismutation rate	k_{dm}	$nM^{-1}\ d^{-1}$	2.64	-	Voelker and Sedlak (1995)
O_2^- production rate at 30 $\mu E\ m^{-3}\ s^{-1}$	$S_{O_2^-}$	$nM\ d^{-1}$	1037	-	Voelker and Sedlak (1995)
H_2O_2 decay rate	k_{dis}	d^{-1}	0.24	-	Johnson et al. (1994)
solubility of atmospheric iron	k_{sol}	%	1	10	Jickells and Spokes (2001)
Total Cu concentration	$[Cu_T]$	nM	1	-	Voelker and Sedlak (1995)
Cu(I) oxidation rate by O_2^-	k_{cuox}	$nM^{-1}\ d^{-1}$	$8.1 \cdot 10^5$	-	Voelker and Sedlak (1995)
Cu(II) reduction rate by O_2^-	k_{cured}	$nM^{-1}\ d^{-1}$	$1.4 \cdot 10^3$	-	Voelker and Sedlak (1995)

Chapter 3

The zero-dimensional model approach: Results, disscussion and sensitivity studies

This chapter is adapted from the publication:
L. Weber, C. Völker, M. Schartau and D. A. Wolf-Gladrow. *Global Biogeochemical Cycles*, Vol. 19, GB1019,doi:10.1029/2004GB002340, 2005 (see also Section 1.4.1).

3.1 Results and discussion

3.1.1 Ecosystem model

The optimized ecosystem model yields the best results for chlorophyll *a* concentration (Figure 3.1c) and carbon-based primary production (PP) (Figure 3.1d). Limitations in modeled PON dynamics (Figure 3.1b) are detectable and may result from the simplifications of the NPD model, for example the neglect of zooplankton and bacterial biomass. Focusing on the simulated concentrations of dissolved inorganic nitrogen (DIN, representing

nitrate, nitrite, and ammonium) reveals winter values close to observations with some distinct interannual variations (Figure 3.1a). The modeled summer DIN concentrations are somewhat higher than the observed nitrate concentrations by about 0.1 mmol N m^{-3}. However, this deficit falls within the range of the analytical detection limit and the data-model intercomparison uncertainty, since ammonium observations were not explicitly included. The few available ammonium measurements are close to this summer deficit.

Simple nitrogen-based ecosystem models generally underestimate primary production shortly after the bloom period and during summer (Schartau et al., 2001; Schartau and Oschlies, 2003b). The model used here uses a very simple parameterization of the C:N uptake ratio of phytoplankton that increases under nitrogen limitation and therefore emulates some of the dynamics as expressed in more complex models where C and N utilization are fully decoupled (e.g. Geider et al., 1998; Bissett et al., 1999; Mongin et al., 2003). Since the C:N decoupling is so important under oligotrophic conditions, this particular parameterization allows the model to capture the annual cycle and interannual variability of primary production (PP) very well, in spite of the fact that it is only nitrogen based. The modeled carbon uptake rate provides an important link to the chemical iron speciation component, especially when a constant Fe:C ratio is assumed rather than a fixed Fe:N uptake rate.

Estimates of the annual export production or new production at the BATS site range from 0.7 mol C m^{-2} to 4.4 mol C m^{-2}, depending on the method used (Carlson et al., 1994). The model predicts an annual export of 3.4 mol C m^{-2} out of the mixed layer by mixing, detrainment and sinking of particulate organic matter, assuming a constant Redfield N:C ratio in particulate organic matter. Using the sinking and remineralization rate from the model, a scaling of the export to a depth of 150 m results in 2.5 mol C m^{-2}, somewhat higher than the trap-based estimates at that depth (0.7 mol C m^{-2}) cited in Carlson et al. (1994). Part of this discrepancy

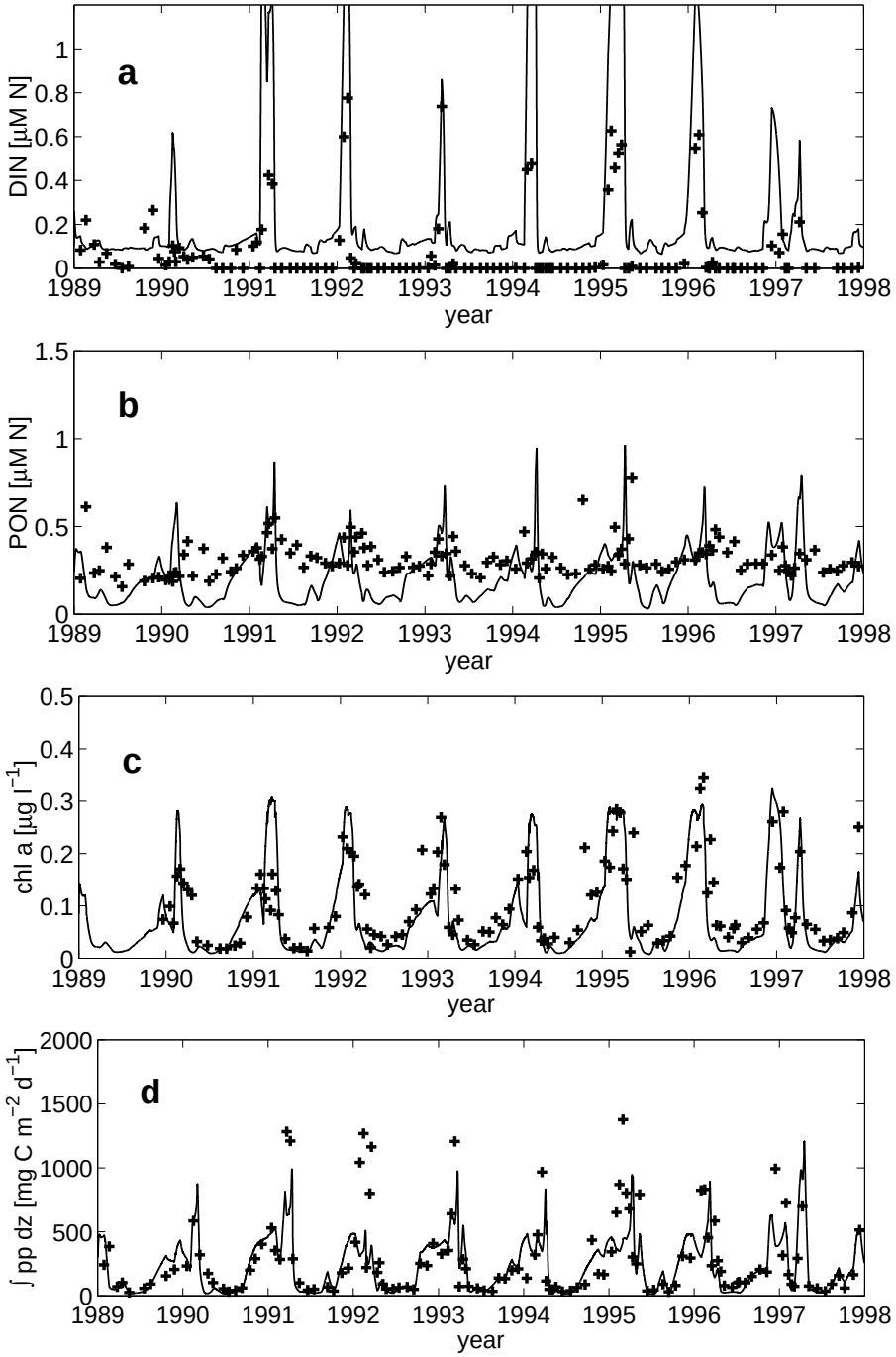

Figure 3.1: *Observed (crosses) and modeled (line) concentrations of (a) nitrate+nitrite, (b) particulate organic nitrogen, and (c) chlorophyll, and (d) vertically integrated primary productivity at the BATS site. Observations have been averaged for each cruise and over the mixed layer depth, as described in Section 2.2.3.*

might be explained by the absence of a dissolved organic matter pool in the model.

In general, the model results demonstrate a reasonable fit to the observations, comparable to results of more complex models such as the models by Hurtt and Armstrong (1996) and Spitz et al. (2001), although it does not include an explicit representation of zooplankton, bacteria, ammonia, or dissolved inorganic carbon. Further improvement in the biological model would probably require making the C:N ratio not only in the uptake, but also in the particulate biomass variable. A second improvement would be the resolution of the depth-dependency to avoid the unphysical prescription of deep nitrate concentration.

3.1.2 Particulate material

In the open ocean, most of the particles within the surface mixed layer are typically of biological origin. Jickells et al. (1990) showed that at the BATS site more than 60% of the particulate matter in the upper 200 m of the water column are organic, while less than 5% are terrigeneous clays. The rest is presumably mainly calcite and silicate shells of planktonic organisms. However, episodic dust deposition events might increase the concentration of terrigeneous particles temporarily, leading to enhanced scavenging and thus loss of iron. In the model, sinking particles are therefore split into two classes, one representing detritus, the other deposited terrigeneous material. For simplicity, an equal sinking rate for both is assumed. The concentration of detritus (in kg L^{-1}) is calculated from the nitrogen-based ecosystem model, assuming a fixed Redfield C:N stoichiometry and that half of the mass of detritus is carbon. Scavenging of iron depends on particle surface area rather than mass. To keep the model simple it is assumed that the two are proportional, i.e. that the particle size spectrum is invariant.

Applying these assumptions, model results show a strong dominance of biological over terrigeneous particles during most of the year. Only in late

summer, when dust deposition reaches its peak, are inorganic particles more abundant than organic detritus. On average, the concentration of biogenic particles is about two orders of magnitude larger than that of inorganic particles. The average composition and annual cycle of particles are broadly consistent with Jickells et al. (1990). The modeled total concentration of particles is significantly lower (12 mg m^{-3}) than the value by Jickells et al. (1990) (55 mg m^{-3}). This difference is due to (i) silicate and calcite shells which are not represented in the model and (ii) to the underestimation of particulate organic nitrogen by the model (Figure 3.1b). One conclusion is therefore that the model is likely to underestimate scavenging of iron onto sinking particles, although a larger source of uncertainty is contained in the scavenging rate.

3.1.3 Reactive oxygen species

The redox state of dissolved iron in the ocean is strongly influenced by the two reactive oxygen species superoxide, O_2^-, and hydrogen peroxide, H_2O_2. Both species are strong oxidants for Fe(II)', but O_2^- also acts as a strong reductant for Fe(III)' (Section 1.2.1).

Since the model does not include an explicit pool of coloured dissolved organic matter (CDOM), the photoproduction rate of superoxide is assumed to be proportional to light intensity. Voelker and Sedlak (1995) give a range of O_2^- photoproduction rates in midday sunlight between 3 and 300 pmol L^{-1} s^{-1} in oligotrophic and productive surface waters, respectively. In the model solutions, $[H_2O_2]$ varies approximately linearly with the photoproduction rate. A rate of 12 pmol L^{-1} s^{-1} in the standard experiment is chosen, because with that rate the model produces summer mixed layer $[H_2O_2]$ values around 50 nmol L^{-1}, close to observations in the subtropical Atlantic (Obernosterer et al., 2001).

Rain events can lead to significant increases in $[H_2O_2]$ in seawater (Kieber et al., 2001). Here, monthly averaged precipitation rates are used and

therefore, such singular events are not reproduced. Over longer timescales, rainfall and uncatalyzed dismutation (Equation 1.2) are of minor importance as sources of H_2O_2 compared to the iron-mediated conversion of superoxide (Equations 1.3 and 1.4).

The modeled concentrations of H_2O_2 and O_2^- are shown in Figure 3.2. The life-time of superoxide is extremely short, so that its concentration during the night is essentially zero. The maximum concentration reached at noon follows an annual cycle that reflects the annual cycle of irradiance (see discussion in Section 2.2.3). The model produces maximum values of up to 0.7 nM in summer, when the mixed layer is shallow and irradiance at the sea surface is highest, and around 0.2 nM in late winter.

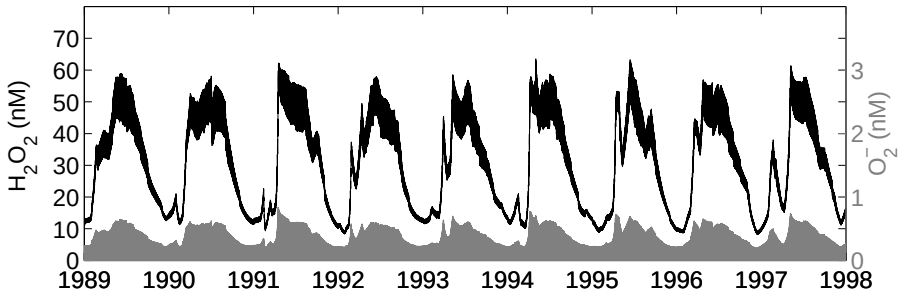

Figure 3.2: *Modeled concentrations of hydrogen peroxide (black), and of superoxide (gray). Note the different scale for the two concentrations.*

The mixed-layer averaged concentration of H_2O_2 in the model shows a strong annual cycle, varying between about 10 nM in winter and around 60 nM in summer. Within this annual cycle is also a regular diurnal cycle of amplitude 1 nM in winter and around 10 nM in summer. The amplitude of the daily cycle in summer is similar to observed amplitudes in waters of the open tropical and subtropical Atlantic (Yuan and Shiller, 2001; Obernosterer et al., 2001).

The time-scale for concentration changes of the reactive oxygen species is similar to that of vertical mixing, so that vertical gradients in these species might persist for some time within the mixed layer (Doney et al., 1995),

contrary to the assumptions in the model. Due to nonlinearities in the chemical reaction equations, this might lead to a daily cycle of the vertically averaged concentrations that differs slightly from the predictions of the vertically averaged model of this study. Mainly in winter, when the mixed layer is deep, a stronger daily cycle at the surface could be expected than the one predicted with the zero-dimensional model of this study. However, the deviations should not be very large since the timescales are similar.

3.1.4 Diurnal variability of iron speciation

The modeled iron speciation shows a strong diurnal variability, especially in summer (Figure 3.3). During the night, FeL and Fe_{col} are the dominant forms of iron. After sunrise their concentrations decrease quickly while that of Fe(II)′ increases. A few hours after noon [Fe(II)′] reaches its maximum, subsequently it decreases while [Fe(III)′] increases.

Because of its short lifetime in oxygenated seawater, there must be a sustained source of Fe(II)′ throughout the day. Fe(II)′ is produced by direct photoreduction of ferric iron species, and by the reduction of Fe(III)′ by photoproduced superoxide. Model results show, that the latter operates at a rate that is up to more than one hundred times the maximum rate of all direct photoreductive processes taken together. The dominance of reduction by superoxide over direct photoreduction has already been proposed for a more simple laboratory system by Voelker and Sedlak (1995).

The Fe(II)′ produced is subsequently oxidized again to Fe(III)′ by O_2, O_2^- and H_2O_2. The strong diurnal cycle of [H_2O_2] and [O_2^-] (Figure 3.2) leads to a corresponding cycle of the redox-reactions. Until midday, iron reduction outweighs the oxidation, leading to an increase of [Fe(II)′], and also of [Fe(III)′] at the expense of [Fe_{col}] and [FeL]. In the afternoon, the balance between reduction and oxidation is reversed because [H_2O_2] reaches its maximum and [Fe(II)′] decreases. During the night, all photochemical reactions stop so that all Fe(II)′ is oxidized to Fe(III)′. Parts of Fe(III)′ are

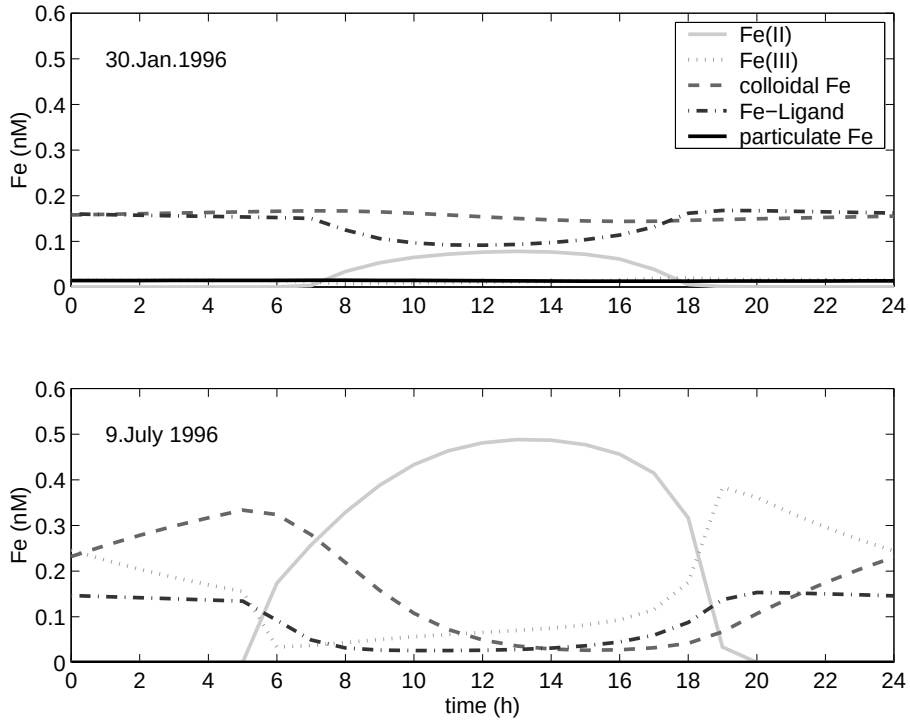

Figure 3.3: *Modeled concentrations of iron species. Upper picture: diurnal variability in winter. Lower picture: dirinal variability in summer.*

quickly complexed by free organic ligands, with rates up to 5.3 nM day^{-1}. The formation of colloidal iron is a much slower process (up to 1.1 nM day^{-1}) compared to organic complexation and oxidation, so that [Fe_{col}] increases slowly at the cost of [Fe(III)$'$] during the night.

In summer, the modeled total iron concentration becomes larger than the complexation capacity by organic ligands (Figure 3.5), leading to enhanced formation of colloidal iron during the night. See Sections 3.1.5 and 3.2.6 for discussion.

The diurnal cycle of iron speciation at the BATS site is much weaker in winter than in summer (Figure 3.3 and 3.4). This is due to a combination of less sea surface irradiance, deeper mixed layers and higher attenuation by chlorophyll that all reduce the vertically averaged irradiance within the mixed layer during winter.

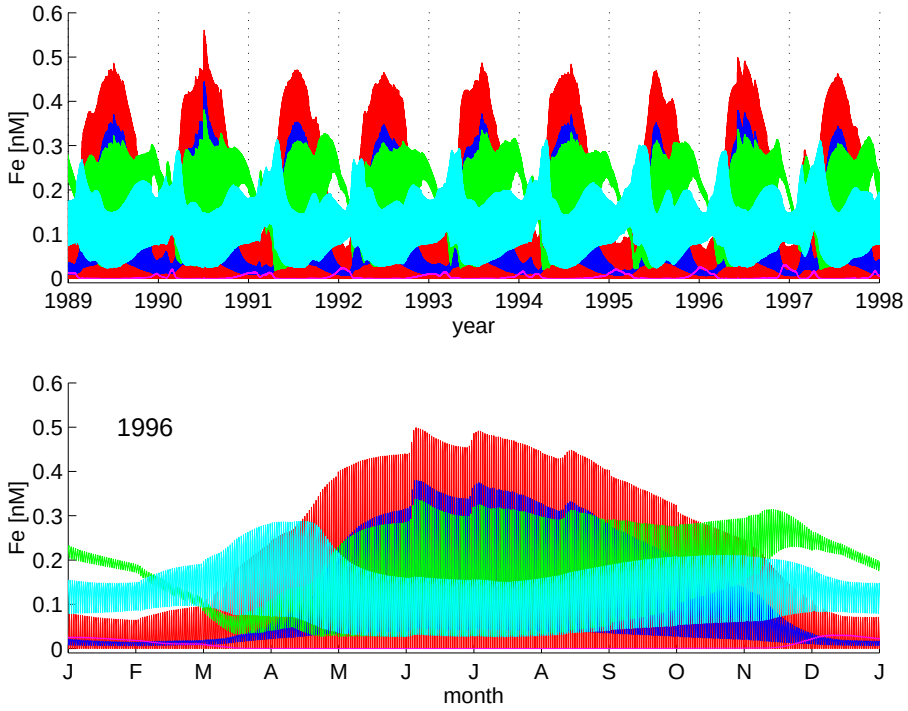

Figure 3.4: *Modeled iron speciation (*[Fe(III)′] - *red,* [Fe(II)′] - *blue,* [Fe_{col}] - *green,* [FeL] - *cyan,* [Fe_p] - *purple). Upper figure: interannual variability. Lower figure: annual variability (year 1996).*

There is only limited data available to validate the modeled daily cycle in iron speciation. Measurements of the organic complexation of iron (Wu and Luther III, 1995; Wu et al., 2001; Witter and Luther III, 1998) and of colloidal iron (Wu et al., 2001) take substantial time after sampling. They therefore most likely reflect near-equilibrium conditions with no or little photochemical production of Fe(II)′ that can best be compared with model results of the night. The modeled average nighttime concentration of colloidal iron in July is 0.24 nM, which is somewhat smaller than the observation at the BATS site (0.47 nM) by Wu et al. (2001).

Mesurements of [Fe(II)′] in the ocean are still relatively rare (O'Sullivan et al., 1991; Kuma et al., 1992; Waite et al., 1995; Croot et al., 2001), but have generally shown nonvanishing values of [Fe(II)′]. Waite et al. (1995)

observed a speciation cycle of comparable strength to the model results in Australian shelf waters, a system with much higher concentrations of organics and total iron than for open ocean conditions. The concentrations observed in the Southern Ocean by Croot et al. (2001) are of a similar order of magnitude as the model results. Boye et al. (2003) stated that [Fe(II)′] becomes especially important at higher iron concentrations across the continental shelf with up to 80% of dFe. Their data suggest that [Fe(II)′] in shelf waters is stabilized by organic complexation. Hopkins and Barbeau (2006) detected [Fe(II)′] just below the oxic-suboxic interface, suggesting production in-situ by normal cellular processes. Biomediate reduction is unlikely to be as efficient as photoreduction and further laboratory and in-situ studies are required to confirm whether this process produce Fe(II)' at rates that are rapid enough to maintain significant steady-state concentrations of Fe(II)' in oxic seawater (Ussher et al., 2004). Measurements of [Fe(II)′] at the BATS location are not forthcoming. In the absence of more speciation data, it is not possible to come to a final conclusion as to whether the strength of the modeled daily cycle of [Fe(II)′] is realistic, but it is possible to discuss its dependency on assumptions in the model:

The main factor that influences values of [Fe(II)′] is its production rate either by direct photoreduction of ferric iron species, especially of FeL, or by reaction with O_2^-. Although the direct photoreactivity of ferric iron species may be lower than assumed here (Barbeau et al., 2003), this is unlikely to affect [Fe(II)′] significantly. The reduction of Fe(III)′ by O_2^- dominates. The main uncertainty is therefore the value of $[O_2^-]$ that has not yet been measured at the BATS site.

The photoproduction rate of O_2^- was constrained by demanding the modeled values of $[H_2O_2]$ to be close to observed values. Constraining $[O_2^-]$ with $[H_2O_2]$, however, works only if the model includes all significant sinks of O_2^-. Voelker and Sedlak (1995) have shown that the reaction described in Equations 1.3 and 1.4 can also be catalyzed by copper, a reaction that has

not been included in the present model run. The possible influence of copper is considered further in Section 3.2.5.

In reality, one might also expect that the speciation cycle is somewhat stronger close to the surface and weaker at the base of the mixed layer (Section 3.1.3).

3.1.5 Annual cycle and interannual variability of dissolved iron

The modeled total concentration of dissolved and colloidal iron ($[Fe_T] = [Fe(III)'] + [Fe(II)'] + [FeL] + [Fe_{col}]$) ranges between 0.3 nM in spring and 0.7 nM in summer (Figure 3.5). Our results are close to observed values in summer (0.6 nM in July 1992, (Wu and Luther III, 1994) and 0.58 nM in July 1998 (Wu and Boyle, 2002)) but higher than observations in spring (0.2 in March 1998 (Wu and Boyle, 2002)) and in autumn (0.2 nM in October 1991, Wu and Luther III (1994)). Two mechanisms that could explain the difference are considered in Sections 3.2.2 and 3.2.4. However, Wu and Boyle (1998) also measured around 0.5 nM Fe in March 1987 in surface water near Bermuda.

The total concentration of organic ligands ($[L_T] = [L] + [FeL]$) varies between 0.15 nM in summer and about 0.5 nM to 0.85 nM in late winter/early spring (Figure 3.5). This annual cycle results from the annual cycles of mixed layer depth and from the concentration of total organic ligands below the mixed layer. The latter was prescribed using a linear fit to observations of soluble ligands in the eastern North Atlantic from Wu et al. (2001). The annual variation is somewhat greater than the range of observations by Wu and Luther III (1995) (0.3 nM to 0.6 nM) which, however, do not necessarily cover the complete seasonal variability. The modeled excess of iron over total ligands in summer has no counterpart in observations at the BATS location. This is clearly an indication that the model is too simplistic with respect to organic ligands and suggests that a

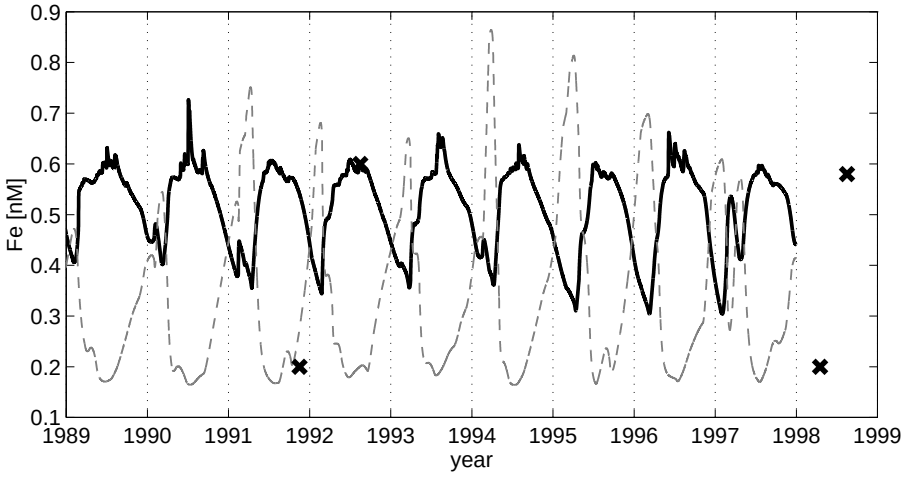

Figure 3.5: *Modeled total Fe-(black) and total ligand concentration (dash) as well as observed iron concentration by Wu and Luther III (1994); Wu and Boyle (2002) (crosses)*

production of ligand by the biota should be included in future models. However, this work is restricted to studying the effect of a persistent ligand excess on the cycling of iron (Section 3.2.6).

The temporal variation of $[Fe_T]$ in the mixed layer is caused by several factors, including seasonal variations in biological uptake and remineralisation, scavenging, dust deposition, and exchange with deeper water (Figure 3.6a).

The spring phytoplankton bloom leads to a strong uptake of iron. Only part of the iron taken up is remineralized, so that a significant drawdown of iron is observed. During spring, the drawdown of iron is further enhanced by the formation of detritus that leads to increased scavenging of iron on particles. Most of the scavenging flux (99.7% of the annual mean) occurs through colloid aggregation, only 0.3% occurs through direct scavenging from the dissolved phase.

In summer, the dust deposition reaches its annual maximum. At the same time the mixed layer is very shallow so that the incoming iron is distributed

over a lower depth than during the rest of the year. Since biological productivity is low, the dust deposition results in an elevated iron concentration.

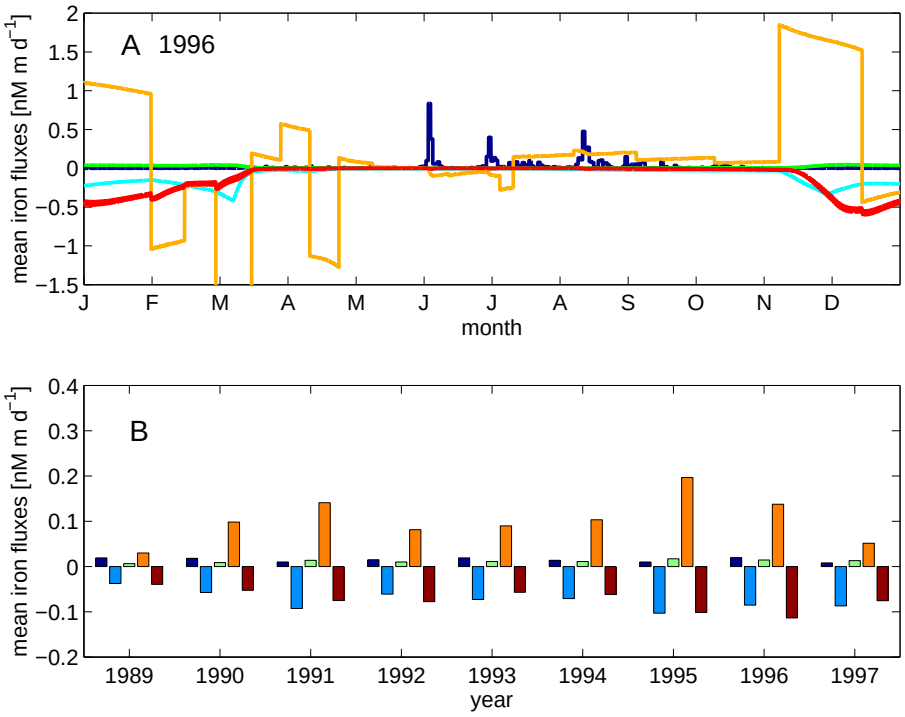

Figure 3.6: *Modeled iron fluxes (dust deposition - blue, biological uptake - light blue, remineralisation of biological matter - green, exchange with deeper water - orange and scavenging - brown)*

The flux of iron due to the exchange with water from below the mixed layer changes direction during the year (Figure 3.6a). The main export and import processes through water exchange are caused by the annual cycle of the mixed layer depth. During the deepening of the mixed layer at the end of the year water from below is mixed in and delivers new iron. Due to the mixed layer shoaling in spring, iron is lost to deeper water. The annual input by entrainment of water during mixed layer deepening is higher than the export during mixed layer shoaling, because the strongest annual mixed layer shoaling takes place during the plankton bloom when iron

concentrations within the mixed layer are low.

A further process of water exchange is ambient turbulent mixing at the base of the mixed layer. As the total concentration of dissolved and colloidal iron is mostly lower within the mixed layer than below, this leads to a net upward transport of iron, albeit only half as strongly as the annual mixed layer cycle.

The different iron fluxes are also variable on interannual scales (Figure 3.6b). Lower iron input and/or higher biological export during certain years are compensated by water mass mixing. In years with low atmospheric deposition or high biological export, less iron can be exported by mixing with deeper water so that the nett import due to water mixing is relatively high. This ensures that the interannual cycle of the iron concentration is stable and barely dependent on the strength of the biological activity and atmospheric deposition.

Jickells (1999) estimated a budget for the various iron fluxes at the BATS site from available observations. A comparison of his estimate with the average budget of the present study (Table 3.1) displays some similarities but also some differences. Jickells (1999) estimates of dissolved iron input from dust is approximatley seven times higher than in the present study, due to a combination of a higher estimate of total iron input (4.2 μmol m^{-2} d^{-1}, vs. 1.4 μmol m^{-2} d^{-1}) and higher average solubility (2.4% vs. 1%). Both flux values are possible (see Section 3.2.1). The average net biological iron uptake predicted by the present study, falls within the (fairly broad) range given by Jickells (1999). However, a much stronger vertical flux from mixed layer dynamics is obtained than Jickells estimate of the vertical diffusion. This can be explained by the fact that the fluxes of the model used in the present study involve the temporal correlation of mixed layer depth and iron concentration. This is an effect that cannot be captured by estimating the flux from vertical diffusivity and an average concentration profile. In fact, the vertical flux from turbulent mixing at the base of the mixed layer is within the range given by Jickells (1999). In the budget of

this study, the large upward flux of iron from mixed layer dynamics is compensated to a large extend by the sinking of iron scavenged onto particles, a process that Jickells (1999) did not attempted to estimate. It is important to emphasize here that the model does not consider its budget in any way more realistic than the one by Jickells (1999), given the large uncertainty in the parameter values that were used. However, it demonstrates the importance of mixed layer dynamics when considering the balance of fluxes at the BATS site.

Table 3.1: *Comparison of iron flux estimates at the BATS site (Jickells, 1999) with average fluxes from the model. All fluxes are given in 10^{-3} μmol m^2 d^{-1}, positive values are fluxes into the mixed layer. Here n.a. denotes 'not applicable'*

Iron flux	Jickells (1999)	Model average (1989 – 1998)
Dissolved atmospheric input	100	15
Biological export	-4 – -105	-51
'Upwelling' flux	3 – 40	106
Scavenging loss	n.a.	-72

3.2 Sensitivity studies

Current research is bringing the iron biogeochemistry into sharper focus but uncertainties remain in critical parts of the iron system. To date, the aim of the iron model used in this study is not so much to give accurate numerical predictions of iron fluxes and concentrations, but to provide a numerical modeling environment, which allows better investigation of the complex relationship between iron inputs, speciation, and bioavailability in oceanic surface waters. The differentiation between the various forms of iron allows to have a closer look at individual processes within the complex biogeochemistry of the iron cycle and enables statements about the sensitivity of model results to changes in still less-well constrained parameter values.

3.2.1 Solubility of atmospheric iron

The solubility of iron in aeolian deposited dust depends on the form of deposition (wet or dry), the composition and the atmospheric history (e.g. the number and duration of times the dust particle underwent entrapment in water droplets and subsequent drying) of the dust particle (Spokes and Jickells, 1996; Jickells and Spokes, 2001; Arimoto, 2001) and of their size (Baker and Jickells, 2006). Observed solubilities vary between 0.1% and 10%, with earlier measurements or estimates (Zhuang et al., 1990; Duce and Tindale, 1991) generally tending towards higher values than more recent ones (Spokes and Jickells, 1996; Jickells and Spokes, 2001). This large range of solubilities means that iron fluxes, that are calculated from model- (Mahowald et al., 1999) or observation- (Kim et al., 1999; Kim and Church, 2001) based dust deposition rates, have an uncertainty of at worst two orders of magnitude. It is therefore crucial to study the sensitivity of the modeled iron concentrations and fluxes to variations in this parameter.

Several model runs were conducted which differed only in the solubility (between 0.1 and 10%) of iron from dust. Results show that the variation of solubility over two orders of magnitude does not lead to a proportional variation of the concentration of total dissolved iron within the mixed layer (Figure 3.7). On average, the concentration in the model run with 10% solubility is 1.2 times (maximally 3 times) higher than the run with 1% solubility. Most affected are the summer concentrations, when the stable and shallow mixed layer prevents exchange with deeper waters. Increasing the solubility above 2.5% leads to summer values of $[Fe_T]$ over 1 nM which are incompatible with most observations (Wu and Boyle, 1998; Cullen et al., 2006).

This raises the question, why are the mixed layer concentrations so insensitive to the value of the solubility? Over annual timescales, the input of iron from dust deposition must be balanced by other fluxes of iron into or out of the mixed layer. These include: (i) net biological uptake, (ii) loss

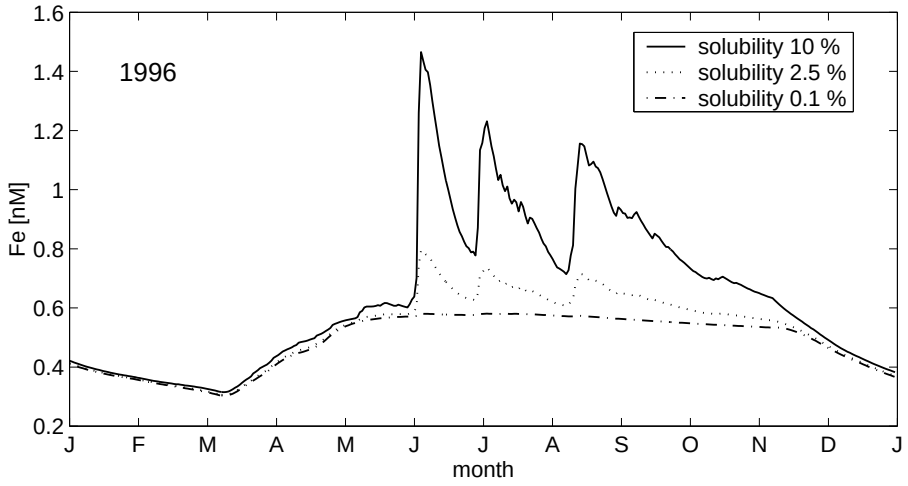

Figure 3.7: *Total Fe concentration of model runs with varying solubility of deposited dust (year 1996).*

of iron adsorbed to the surface of sinking particles, and (iii) exchange with water below the mixed layer by turbulent mixing, entrainment and detrainment. The biological uptake (i) is fixed, since a fixed phytoplankton Fe:N ratio and a growth rate independent of Fe concentrations is assumed.

Compensation by sinking of iron adsorbed on particles (ii) is possible if more iron is adsorbed per particle. The two pathways of adsorption are scavenging and aggregation of colloids. Both pathways involve a step whose rate is proportional to [Fe(III)′]. A ten times higher loss by (ii) would thus imply a ten times higher concentration of [Fe(III)′] with unchanged concentration of particles. This is not found in the model results.

The main process that damps changes of [Fe_T] with varying iron input is mixing with deeper water (iii). The mean annual flux of iron due to exchange with deeper water is the difference between the strong positive flux during mixed layer deepening and the negative flux during mixed layer shoaling (Figure 3.6 and Section 3.1.5). The import flux is proportional to [Fe_T] below the mixed layer, while the export flux is proportional to [Fe_T] within the layer. Because the net flux is the difference between two large

opposite fluxes, a small change in [Fe_T] within the mixed layer can lead to a large change in the export flux and hence in the net flux.

The weak sensitivity of iron concentrations to the solubility is therefore caused by the strong vertical mixing mainly associated with the annual mixed layer cycle at the BATS site. Similar behavior would be expected at other locations with strong vertical mixing, but not at more stratified oceanic regions, e.g. in the tropics.

3.2.2 Fe:N and Fe:C ratio of the phytoplankton uptake

The uptake of iron is modeled assuming either a constant Fe:N ratio or a constant Fe:C ratio in phytoplankton primary production. Observed Fe:N- or Fe:C-ratios of different phytoplankton species vary by up to two orders of magnitude: Sunda and Huntsman (1995, 1997) reported Fe:C-ratios between 2 and 13 μmol mol^{-1} (Fe:N 13-86 μmol mol^{-1}, assuming Redfield stoichiometry) for open ocean phytoplankton, and much higher values for coastal species, while Muggli et al. (1996) measured a comparatively high Fe:N ratio of 250 μmol mol^{-1} in an open ocean diatom. Moreover, phytoplankton cells seem to possess the physiological plasticity to adapt their Fe:C-ratio to environmental conditions, such as iron limitation (Sunda and Huntsman, 1995).

In the standard model run, an Fe:N-ratio of 33 μmol mol^{-1} is assumed (corresponding to a Fe:C-ratio of 5 μmol mol^{-1}, assuming Redfield stoichiometry). Using this ratio, Johnson et al. (1997) were able to reproduce a variety of different deep vertical iron profiles with a one-dimensional diffusion-remineralization-scavenging model. This should therefore be close to an average Fe:N-ratio in the remineralization of organic matter and possibly also to an average uptake ratio. Nevertheless, the Fe:N-ratio in phytoplankton uptake at the BATS site might deviate from such an average, e.g. due to the presence of nitrogen fixers at the BATS site.

A number of model runs were performed, varying the value for the Fe:N-ratio (10, 20, 33, 50, 100 and 200 μmol mol^{-1}) or the Fe:C ratio (2, 5 and 13 μmol mol^{-1}). Surprisingly, the difference between model runs that assume a constant Fe:C ratio is small (Figure 3.8, lower panel), when compared to the difference between runs assuming a constant Fe:N ratio (Figure 3.8, upper panel). This is in spite of the fact that the C:N ratio in primary production in the model reaches values more than double the Redfield value in summer. However, this happens during a time where the biological iron uptake is relatively small compared to the iron source from dust deposition.

In summer, therefore, the variation of the Fe:N or Fe:C ratio causes only a small change in the concentration of dissolved iron (Figure 3.8). Only during the spring phytoplankton bloom period does the concentration of dissolved iron decreases with increasing biological uptake. Fe:N-ratios up to 100 μmol mol^{-1} lead to concentrations of dissolved iron that are in the range of observed concentrations. In contrast, Fe:N-ratios above 150 μmol mol^{-1} lead to iron concentrations tending to zero during the phytoplankton bloom and therefore to iron-limited conditions. The subtropical Atlantic is not thought to experience regular iron limitation (Fung et al., 2000), due to ample supply of iron from dust deposition from the surrounding land masses. Therefore it was assumed the mean Fe:N-ratio at the BATS site does not exceed a value of 150 μmol mol^{-1}.

The balances of the annually averaged fluxes of the model are strongly affected by the elemental ratio. The more iron is taken up, the more iron is entrained by mixing with deeper water and the less iron is scavenged. For example, a 10 times higher Fe:N ratio leads on average to entrainment fluxes 2.6 times higher and to scavenging fluxes 0.8 times lower. The exchange with deeper water and the reduced scavenging compensate the higher uptake so that the iron concentration remains relatively stable.

The main compensation is again caused by the mixing with deeper water. Due to the strong seasonal mixed layer cycle small changes in iron

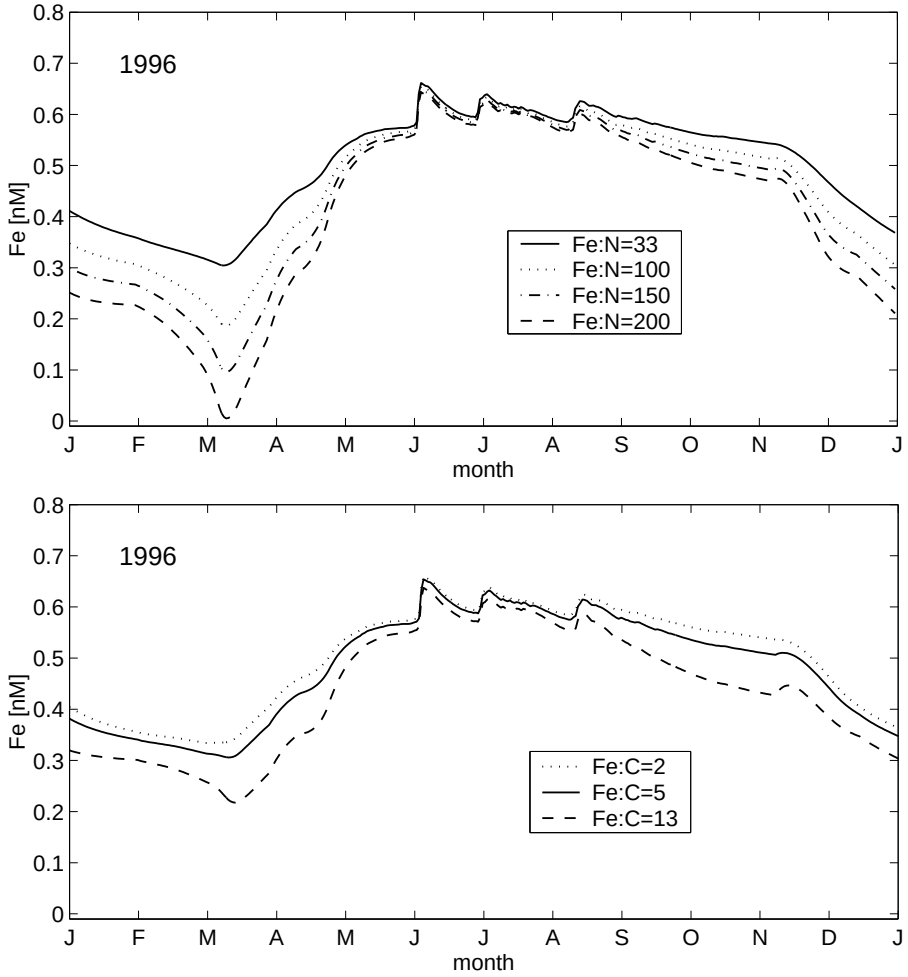

Figure 3.8: *Total Fe concentration (year 1996) of model runs with varying Fe:N-ratio ($\mu mol\ mol^{-1}$) in phytoplankton (upper panel) or with varying Fe:C-ratio ($\mu mol\ mol^{-1}$) (lower panel)*

concentration lead to strong changes in vertical iron fluxes (Section 3.2.1). A decrease in scavenging with increasing Fe:N-ratio is caused by the lower values of [Fe(III)′] during the spring bloom, the time when most of the scavenging takes place because of high particle concentrations.

3.2.3 The form of bioavailable and atmospheric iron

It is generally assumed that phytoplankton only assimilates dissolved iron. Dissolved iron concentrations in seawater are low because of the low solubility of $Fe(III)'$ in oxygenated seawater (Byrne and Kester, 1976), so the availability of iron can limit phytoplankton productivity (Bruland et al., 1991). Furthermore, not all forms of iron in seawater are equally available for uptake by phytoplankton. Experiments in artificial or UV-digested seawater (Anderson and Morel, 1982; Hudson and Morel, 1990) have shown a dependency of iron uptake on ferric dissolved inorganic $Fe(III)'$. However, complexation by strong organic ligands (e.g. Gledhill and van den Berg, 1994; Van den Berg, 1995; Rue and Bruland, 1995; Wu and Luther III, 1995) results in $Fe(III)'$ concentrations in seawater that are too low to support growth. Uptake of iron bound to organic complexes has been demonstrated (Soria-Dengg and Horstmann, 1995; Maldonado and Price, 1999, 2001), but cyanobacteria and eukariotes differ in the classes of organic complexes they can access (Hutchins et al., 1999), probably because of different uptake mechanisms. Uptake by eukariotes often involves extracellular iron reductases, a theoretically very efficient iron uptake mechanism (Völker and Wolf-Gladrow, 1999). Barbeau et al. (1996) suggested that microbial protozoan grazers can solubilize colloidal iron. Results by Nodwell and Price (2001) and Chen et al. (2003) demonstrate a direct uptake of colloidal iron.

Therefore, sensitivity runs were conducted, with varying form of iron ($Fe(III)'$, $Fe(II)'$, FeL, or Fe_{col}) that is actually taken up by phytoplankton during its growth. This allows to study whether this has an effect on the

iron biogeochemistry in the mixed layer. The model results demonstrated no significant effect caused by this change. The differences in concentration between model runs are maximally 0.01 nM and are therefore far from causing iron limiting conditions. The reason for that result is that the biological iron uptake rate reaches maximally 0.01 nM d^{-1} during the bloom, while the photochemical rates of cycling between different iron forms are 1 to 4 orders of magnitude higher (Figure 3.9). Uptake is a relatively slow process compared to the rapid iron cycling between its different forms, so that cycling ensures enough supply of iron whichever form of iron is taken up.

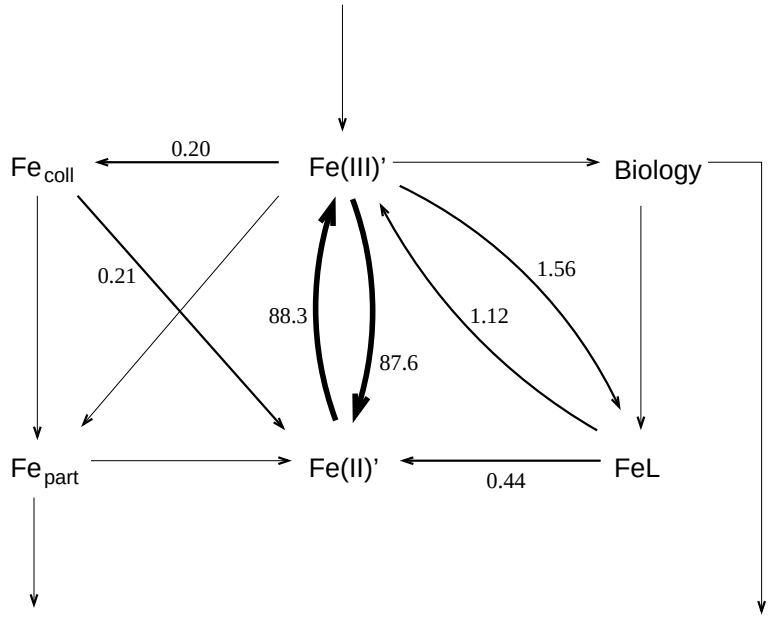

Figure 3.9: *Flux diagram showing the annually averaged rate of change of iron concentrations associated with individual processes (in nM d^{-1}). Arrows without number correspond to an average rate of change smaller than 0.01 nM d^{-1}.*

The model has a similarly weak sensitivity to the form of atmospheric iron. Zhuang et al. (1992) suggested that up to 50% of iron in rainwater is dissolved Fe(II) due to low pH-values and photoreduction in atmospheric

water. In contrast to that, Zhu et al. (1997) assumed that only 1-2% of the iron is reduced to Fe(II) during the atmospheric transport. Jickells and Spokes (2001) concluded that the form of iron that dominates in atmospheric iron depends on the source of dust, the duration of transport and the intensity of the atmospheric processes.

Model runs were conducted with varying form of the deposited iron ([Fe(III)′], [Fe(II)′], [FeL] or [Fe_{col}]) to investigate whether this has an effect on the iron biogeochemistry in the mixed layer. The model results are only slightly affected by which form of iron is deposited and only at times of high iron input. The concentration difference of total dissolved iron in the mixed layer is maximally 1 pM depending on which form of iron is deposited. The annual mean rate of change of the iron concentration in the mixed layer due to atmospheric deposition varies between 0.0007 and 0.0013 nM per day (maximal rate 0.08 nM d^{-1} during dust deposition events in summer), which is much smaller than the cycling rates (see above) between the iron forms. Hence, whatever form of iron is deposited, the fast cycling of iron between its different forms ensures that neither the concentration and speciation of iron nor the iron fluxes are significantly affected.

3.2.4 Aggregation of colloids

Colloids are a size class between soluble chemical species and sinking particles (Wells and Goldberg, 1992). In the present study, colloidal iron is defined by the filter cutoffs 0.02 - 0.4 μm used by Wu et al. (2001). The aggregation of marine colloidal matter is an important mechanism for transferring dissolved substances into the macro-particle size range (Farley and Morel, 1986; Honeyman and Santschi, 1989). The stability of colloids is mainly influenced by chemical interactions with particle surfaces (Stumm, 1992). In spite of low particle concentrations in the open ocean it is suggested that marine colloids are very dynamic with high colloidal aggregation rates (Moran and Buesseler, 1992; Baskaran et al., 1992).

Colloid aggregation and scavenging have been suggested by Wu and Boyle (2002) to explain part of the gradient in total dissolved iron concentration between Bermuda and the Bahamas.

To investigate the role of colloidal aggregation on the transfer of iron to sinking particles, model runs were conducted with and without colloidal aggregation. A further uncertainty is, that the photoreactivity of iron on marine particles (and therefore of the newly formed aggregates) is to the best of our knowledge not very well constrained. Iron tends to build strong inner-sphere surface complexes with particles (Stumm, 1992) that are probably not very photoreactive. Therefore both model runs (with and without aggregation) were performed twice, varying the photoreduction rate of iron on particles, k_{ph4}, between that of colloidal iron, k_{ph1} and zero.

Without colloidal aggregation the modeled total iron concentrations do not differ between the runs with and without photoreduction of particle-bound iron (Figure 3.10). The particle concentration at the BATS site is so low that, without colloid aggregation, the scavenging of iron becomes negligible compared to the fluxes by atmospheric input, biological uptake and exchange with deeper water.

With colloidal aggregation the modeled total iron concentration during the spring bloom is significantly lower (on average 26% lower with photochemical reduction of particle-bound iron, and 57% lower without) than without (Figure 3.10). With colloidal aggregation, the average total loss of iron by adsorption onto sinking particles is -72 $\times$ 10^{-3} μmol m^2 d^{-1} with photochemical reduction of particle-bound iron, and 171 $\times$ $10^{-3}\mu$mol m^2 d^{-1} without. In both cases around two orders of magnitude larger than without aggregation. This increased loss through aggregation is compensated by exchange fluxes from below. The exchange flux increases because of the lowered iron concentration during the spring bloom, which leads to a smaller loss of iron during the mixed layer shoaling in late spring.

It is obvious that we need to know more about aggregation rates and the

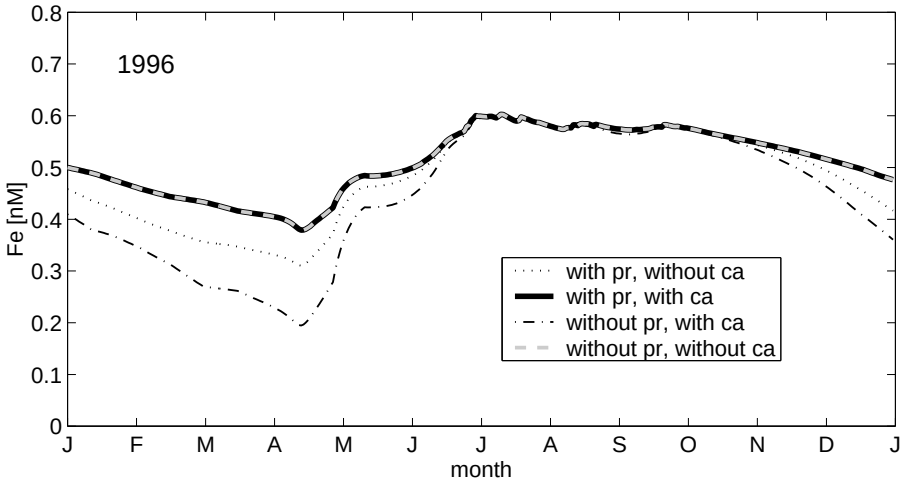

Figure 3.10: *Total Fe concentration (year 1996) of model runs with and without colloidal aggregation (ca) and with and without photoreduction of particles (pr).*

photoreactivity of iron bound to particulate surfaces to determine the role of colloid aggregation in the cycling of iron. Nevertheless, the sensitivity study suggests that the fate of dissolved organic matter exuded by phytoplankton and its role in colloidal aggregation is expected to strongly influence the iron speciation process and thus iron availability for algal growth.

3.2.5 Influence of Cu on the concentration of reactive oxygen species and Fe(II)

The strong daily cycle of iron speciation and the high concentrations of Fe(II)' reached during the day are mostly a consequence of the photochemical production of superoxide. The necessary rate of photochemical superoxide production from observed concentrations of hydrogen peroxide was inferred. Superoxide itself has a very short lifetime and has yet not been measured at the BATS site. However, there is a possible flaw in the indirect constraint of superoxide concentration by

observations of hydrogen peroxide: The reaction from superoxide to hydrogen peroxide can be catalyzed by several other transition metals besides iron. In seawater this is primarily done by copper via the two coupled reactions

$$O_2^- + \mathrm{Cu(II)} \rightarrow O_2 + \mathrm{Cu(I)} \tag{3.1}$$

$$O_2^- + \mathrm{Cu(I)} + 2H_2O \rightarrow H_2O_2 + \mathrm{Cu(II)} + 2OH^- \tag{3.2}$$

(Voelker and Sedlak, 1995).

To investigate the influence of copper on the strength of the daily cycle of superoxide concentration and iron speciation, rate expressions corresponding to reaction equations (3.1) and (3.2) were added to the evolution equations for hydrogen peroxide (2.15) and superoxide (2.14), with reaction rates taken from Voelker and Sedlak (1995) (Table 3.2). The concentrations of Cu(I) and Cu(II) were determined from the total Cu concentration, assuming the two reactions (3.1) and (3.2) to be in steady state.

Total copper concentrations at the BATS site are about 1 nM, with somewhat higher concentrations in summer. Most of that copper is bound to strong organic ligands, but in summer there is a weak excess of copper over ligand concentrations (Moffett, 1995). Voelker and Sedlak (1995) have shown that reaction rates of organically complexed Cu(II) with O_2^- are orders of magnitude lower than for free cupric ion Cu^{2+}. Therefore, two sensitivity experiments **Cu1** and **Cu2** were performed, the first assuming that all copper is complexed by organic ligands, the other assuming that all

Table 3.2: *Additional or changed model parameters in experiments* **Cu1** *and* **Cu2**.

Parameter	Symbol	Unit	**Cu1**	**Cu2**
total Cu concentration	Cu_T	nM	1	1
Cu(I) oxidation rate by O_2^-	k_{cuox}	$nM^{-1}\ d^{-1}$	$8.1 \cdot 10^5$	$8.1 \cdot 10^5$
Cu(II) reduction rate by O_2^-	k_{cured}	$nM^{-1}\ d^{-1}$	$1.4 \cdot 10^3$	$6.9 \cdot 10^5$
$[O_2^-]$ production rate at 30 μE $m^{-3}\ s^{-1}$	$S_{O_2^-}$	$nM\ d^{-1}$	778	173

Cu(II) is present as the free cupric ion Cu^{2+}. The photochemical production rate of O_2^- ($S_{O_2^-}$) in these experiments were re-adjusted, in order to compensate for the increase in $[H_2O_2]$ due to reactions (3.1) and (3.2).

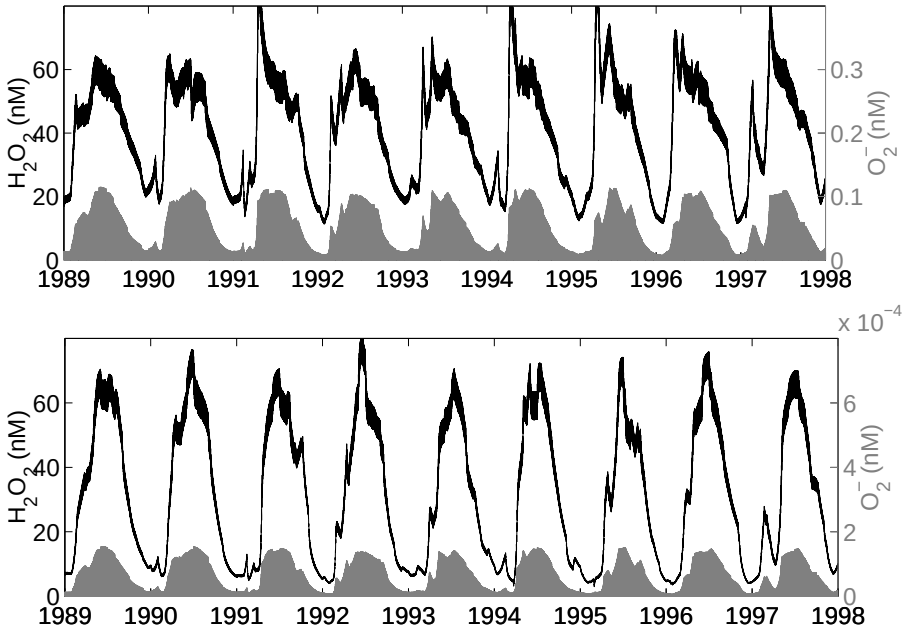

Figure 3.11: *Modeled concentrations of hydrogen peroxide (black), and of superoxide (gray) with catalytic superoxide dismutation by Cu. Upper picture: experiment* **Cu1**. *Lower picture: experiment* **Cu2**. *Note the different scale for the two concentrations.*

The additional catalytic pathway for O_2^- dismutation lowers the maximum mid-day summer $[O_2^-]$ values from 0.7 nM in the reference experiment to 0.1 nM in **Cu1** and even $1.5 \cdot 10^{-4}$ nM in **Cu2** (Figure 3.11. This decrease in $[O_2^-]$ causes a similar, but weaker decrease in maximum mid-day summer $[Fe(II)']$ values from 0.45 nM for the reference experiment to 0.3 nM in **Cu1** and 0.013 nM in **Cu2**.

In spite of this drastic reduction in $[Fe(II)']$ both experiments show a strong diurnal cycling of Fe between its different dissolved forms (Figure 3.12), albeit somewhat smaller than in the reference experiment.

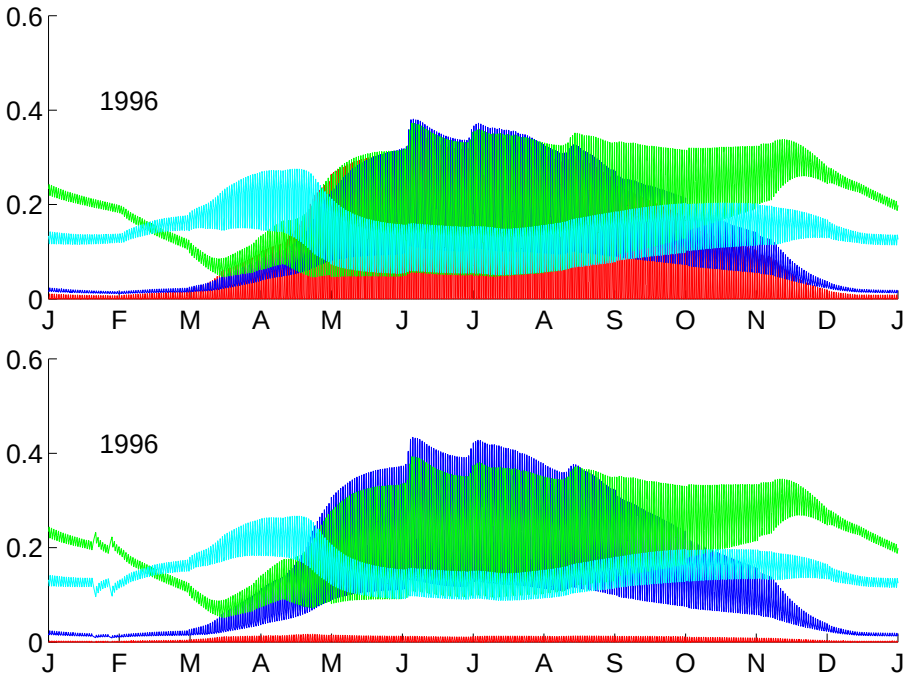

Figure 3.12: *Modeled concentrations of Fe(III)' (blue), of Fe(II)' (red), of* Fe_{coll} *(green), and of FeL (cyan) with catalytic superoxide dismutation by Cu. Upper picture: experiment* **Cu1**. *Lower picture: experiment* **Cu2**.

3.2.6 The role of excess ligands

Most determinations of organic complexation of iron in seawater have shown an excess of dissolved organic ligands over total dissolved iron (e.g. Rue and Bruland, 1995; Van den Berg, 1995; Wu and Luther III, 1995; Witter and Luther III, 1998), leading to picomolar concentrations of Fe(III)′. In the eastern Atlantic, however, Wu et al. (2001) have also shown the opposite can occur. The question therefore is how model results would change under a permanent excess of $[L_T]$ over $[Fe_T]$. Potentially, a permanent ligand excess might change model results significantly, because [Fe(III)′] determines the rates of scavenging, of colloid formation, and of the reduction of iron by superoxide.

The sensitivity of the model results to a permanent ligand excess is tested

here by changing the prescribed vertical profile of [L] such that [L_T] below the mixed layer is always at 2 nM. As expected, this change drastically reduces [Fe(III)′] and changes the daily speciation cycle in summer: While the speciation at night in summer was dominated by [Fe(III)′] and [Fe_{col}] in the standard model run (Figure 3.3), it is dominated by [FeL] in the sensitivity study (Figure 3.13), followed by [Fe_{col}]. During the day, [Fe(II)′] increases until shortly after noon, and decreases afterwards. Although the increase in [Fe(II)′] is accompanied by a corresponding decrease in [FeL], it is not principally caused by direct photoreduction of FeL, but by reduction of Fe(III)′ by O_2^-. Fe(III)′ is then replenished by dissociation of the FeL-complex. The amplitude of the daily [Fe(II)′]-cycle is somewhat smaller (about 25% smaller for the specific day chosen in Figure 3.13) than in the reference run. One may therefore conclude that a change from an excess of iron over ligands to an excess of ligands over iron affects which iron species are most involved in the daily speciation cycle. The overall strength of the cycle itself is hardly altered. The reduced concentration of Fe_{col} and Fe(III)′, compared to the situation with excess iron, decreases the rate at which iron is lost from the mixed layer by the aggregation of colloids and the scavenging of iron onto sinking particles. The total loss of iron via these pathways is 46% lower in the sensitivity run than in the standard model run. However, since the fluxes of iron at the BATS site are dominated by water mass mixing, dust deposition and net biological consumption, this does not influence the modeled total iron concentration and its annual cycle significantly.

3.3 Summary and conclusions of Chapter 3

A zero-dimensional model was constructed that describes the cycling of iron between its various physical (dissolved, colloidal, particulate) and chemical (redox state and organic complexation) forms in the oceanic mixed layer. The model is coupled to a simple ecosystem model and is driven by

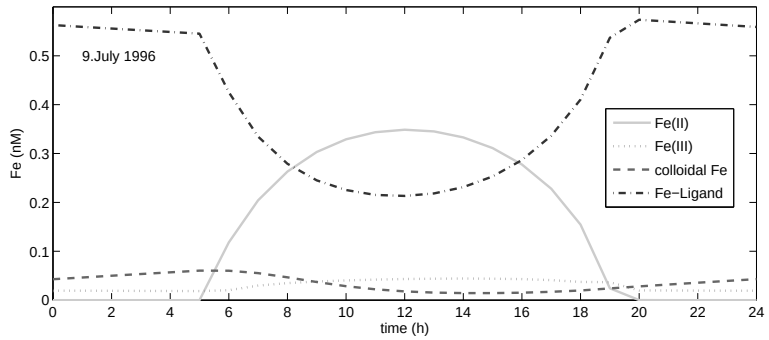

Figure 3.13: *Diurnal cycle of iron speciation for July 9, 1996 (compare to Figure 3.3) with permanent excess of organic ligands ($[L_T] \approx 2$ nM) over dissolved iron concentrations.*

observed or modeled values of dust deposition, mixed layer depth, temperature, and solar irradiation from the Bermuda Atlantic Timeseries Study (BATS).

Despite its simplicity, the ecosystem model performed well in reproducing chlorophyll *a* concentrations and primary production data from BATS. This was achieved by applying an optimization algorithm to determine a best parameter set for the ecosystem model and by using a parameterization for variable C:N phytoplankton nutrient utilization rates, which becomes important as soon as phytoplankton experiences nitrogen limitation. The annual export production is somewhat on the high side of the available data-based estimates. The model underestimates the concentration of particulate organic nitrogen in summer, probably due to the absence of an explicitly modeled microbial loop.

Model results show total dissolved iron concentrations that are in good agreement with observed values (Wu and Luther III, 1995; Wu and Boyle, 2002). Modeled annual average fluxes of iron are also within the (still broad) limits of data-based estimates (Jickells, 1999), but depend strongly on relatively uncertain parameter values. The model results of the present study, however, show that an important role in the vertical flux of iron

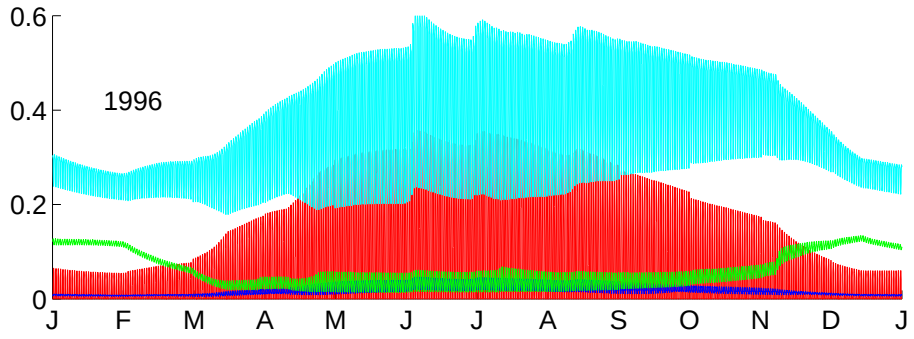

Figure 3.14: *Modeled concentrations of Fe(III)' (dark blue), of Fe(II)' (red), of Fe_{coll} (green), and of FeL (cyan) with permanent excess of organic ligands ($[L_T] \approx 2$ nM) over dissolved iron concentrations.*

plays the entrainment and detrainment of water during the annual cycle of mixed layer deepening and shoaling. This flux is dominant in the sense that it balances the other fluxes in such a way that the total dissolved iron concentration in the mixed layer at the BATS site does not depend strongly on the size of e.g. dust input, but remains tightly coupled to the concentration below the mixed layer. This result clearly depends on the strength of the annual mixed layer cycle and cannot be generalized to other more quiescent oceanic regions.

The primary aim of the present study was to achieve a better qualitative understanding of the role of iron speciation and the processes influencing it as part of the biogeochemical cycling of iron. Since there is little data on iron speciation and its temporal evolution at the BATS site, the conclusions here are made on the basis of sensitivity studies using the model and are of a more qualitative nature. Using these results, the original questions posed in the introduction (Section 1.4) are re-stated and answered below:

1. How strong is the daily photochemical redox-cycling of iron at the BATS site? How important is the direct photoreduction of iron species compared to the reduction by photoproduced superoxide? Is there an influence of other transition metals on the strength of the

redox cycle?

Regardless of the details of the chemical model, the daily irradiance cycle drives a strong cycle of iron speciation. This cycle is characterized by concentrations of Fe(II)′ that closely follow the irradiance cycle (with maximum values attained soon after noon). During the night, speciation is dominated by ferric iron species. The increase of [Fe(II)′] during the day is primarily driven by the reduction of Fe(III)′ by photoproduced superoxide, with direct photoreduction of organically complexed Fe(III) or other ferric iron species being much weaker. A strong diurnal cycling of Fe between its different dissolved forms was found in all model experiments. The maximum value of [Fe(II)′] reached during the day depends strongly on the chemical environment (mainly on the concentration and degree of organic complexation of copper, and on the rate of photochemical production of superoxide, less on the presence of organic ligands for iron). The model results therefore suggest that daylight concentrations of Fe(II)′ in the surface ocean will depend on local conditions such as presence of copper and colored dissolved organic matter. Nevertheless, the photochemically driven cycling of iron between its various chemical forms is generally rapid. The photochemical reactivity of organic complexes of iron seems to be of little importance for this cycling.

2. Under which conditions can colloid aggregation lead to a significant loss of iron from the surface layer of the ocean?

   This study does not include a full model of colloid formation and aggregation, but implies the formation of inorganic iron-containing colloids and their aggregation onto larger sinking particles. Bearing that in mind, and that the aggregation rate has been extrapolated from measurements made at much higher particle concentrations, the model results suggest that aggregation of colloids is an important

process even in the open ocean, which can lead to significant iron removal from the mixed layer. Whether the iron that adsorbs on sinking particles by aggregation of colloids is exported out of the mixed layer, however, also depends on the photochemical lability of the adsorbed iron, which is not analysed in field or laboratory yet.

3. How strong is the influence of the solubility and the chemical form of dust-deposited iron?

   Model results show that increasing the percentage of dissolvable iron in dust increases the concentration of iron in the mixed layer mainly in summer, when the mixed layer is shallow. The annual mean concentration of iron is much less sensitive to the solubility. In an annual average the variation of iron input by variation of the solubility of iron in dust is compensated by the the iron flux via exchange with deeper waters, especially during the strong vertical mixing in winter. However, solubilities of atmospheric iron greater than 2.5% lead to dissolved iron concentrations in summer that are incompatible with observations. The small sensitivity of the average dissolved iron concentration at the BATS site to the value of the solubility is caused by the very strong vertical exchange associated with the mixed layer cycle at the BATS site and cannot be generalized to more stratified oceanic regimes. There has been some debate over which chemical species of iron is prevalent in dust deposition, especially in wet deposition. However, the speciation of deposited iron makes no significant difference to the model results. Whatever form of iron is deposited, the rapid daily cycling of iron between its different forms assures that neither the concentration and speciation of iron nor the iron fluxes are significantly affected.

4. Does it make a difference to the iron cycle, which chemical form of iron is taken up by phytoplankton? How sensitive are model results to changes in the Fe:N or Fe:C-ratio of phytoplankton uptake?

Changes in the Fe:N ratio in organic matter do not strongly affect modeled total dissolved Fe concentrations. They lead to corresponding changes in the vertical biologically mediated flux of iron, but these changes are compensated by the same mechanism as changes in dust iron solubility, namely by exchange with water masses from below the mixed layer. Only Fe:N ratios above 150 μmol mol^{-1} lead to iron concentrations during the phytoplankton bloom that would limit phytoplankton growth. This is generally not assumed to happen at the BATS site. The insensitivity of modeled iron concentrations to the Fe:N ratio is again not valid for the ocean generally, but due to the strong vertical exchange at the BATS site. However, a more general conclusion is that from the point of view of the dissolved iron chemistry, it makes no significant difference whether phytoplankton cells take up Fe(III)$'$, Fe(II)$'$ or FeL. The rapid cycling of iron between its different dissolved forms ensures that any pool that is depleted by biological uptake gets replenished quickly. This is mainly due to the redox-reactivity of iron with respect to superoxide and on the daily concentration cycle of superoxide. It does not mean, on the other hand, that the preference of phytoplankton for the one or the other form of dissolved iron cannot have biogeochemical consequences: it is assumed here that phytoplankton growth is unlimited by iron availability, but in reality, the uptake rate of any chemical species depends on its concentration in the medium, which would be different for individual iron species. This is likely to be of importance in iron-limited ocean regimes.

Many of the still qualitative statements above could be made more quantitative if more data to validate the model predictions would become available. A dataset of time-resolved iron speciation, including measurements of Fe(II)$'$, H_2O_2, and also some information on the concentration and organic complexation of copper would be useful in this respect.

One should expect that modeling oceanic regions which are more stratified than the BATS site, would yield modeled iron concentrations that are much more sensitive to parameters such as the solubility of iron in dust or the colloid aggregation rate. Therefore, validating such model results at different sites in the ocean has more potential to constrain these parameters.

Further model development is required to address:
(i) the simplistic assumption of uniform nutrient concentrations within the mixed layer. The short timescale of photochemical processes can lead to vertical concentration differences within the mixed layer that can only be represented with a depth-dependent physical model. The next step is therefore to set up a one-dimensional extension of this model (Section 2.3 and Chapter 4).
(ii) the simplistic representation of photochemical reactions, assumed to vary with irradiance over the visible band. In reality, ultraviolet radiation is probably also important, but much more attenuated with depth.
(iii) the still very simple representation of the cycling of organic iron ligands and colloids.
The points (ii) and (iii), however, require further information from laboratory and field experiments with regards to the quantum yield of the different photochemical processes, and to the origin and fate of organic ligands for iron present in seawater.

Chapter 4

The one-dimensional model approach: results, disscussion and sensitivity studies

4.1 Results of the physical model (GOTM)

The annual cycle of the physical properties in the model is driven primarily by seasonal changes in surface heat flux and wind stress. Strong thermal stratification is present in summer, largely due to higher heat fluxes and lower wind stresses. The modelled temperature and salinity profiles (Figure 4.1 and 4.2) as well as the mixed layer depth (Figure 2.1) are in good agreement with observations (Steinberg et al., 2001): In summer, the mixed-layer has temperatures around 24 °C, and is generally of reduced salinity compared to the rest of the year. There is a subsurface salinity maximum, and strong density gradients in the upper 100m. Temperature fluctuation of the surface layer (top 1-2m), associated with the diurnal thermal cycle, ranges from 0.2 to 2.5 °C depending on the net daytime surface heat flux (controlled by cloud cover and wind stress) and mixed-layer depth. In winter, the mixed layer is more saline and mean

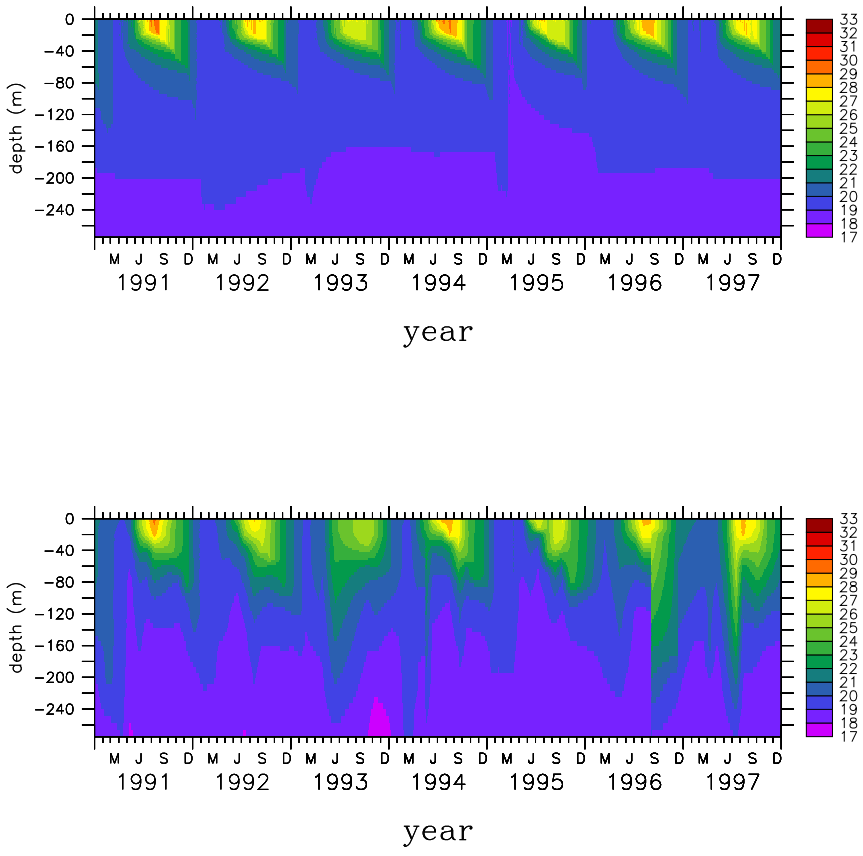

Figure 4.1: *Temperature profile at the BATS site in °C. Top: Model results with the GOTM of the present study. Bottom: Observed data (Steinberg et al., 2001).*

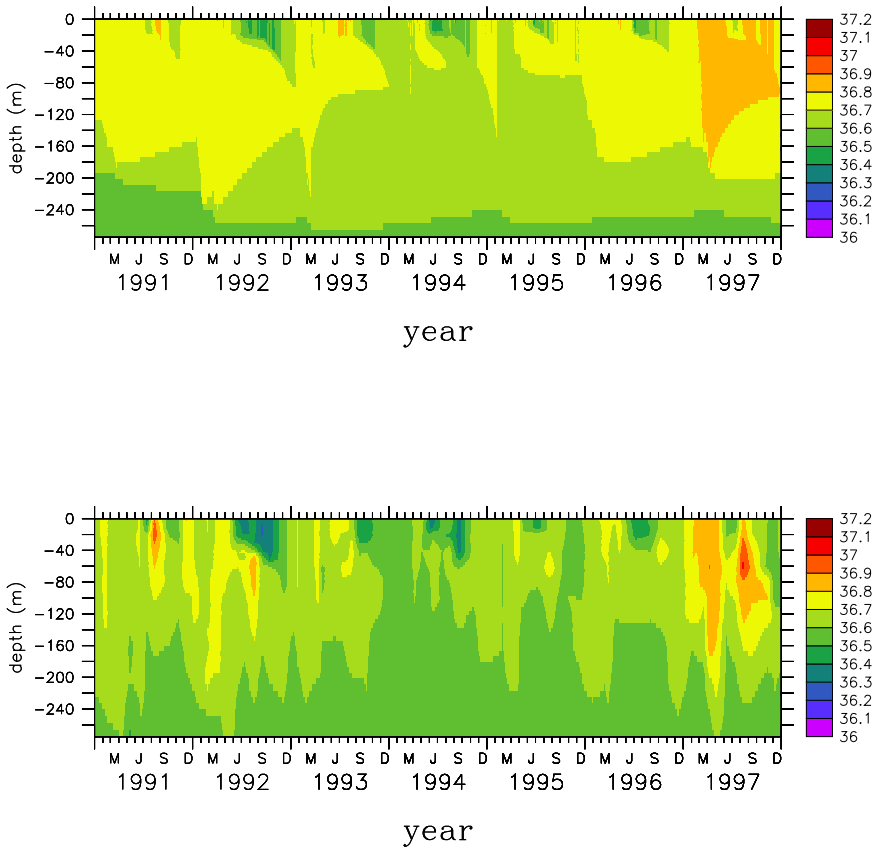

Figure 4.2: *Salinity profile at the BATS site in ppm. Top: Model results with the GOTM of the present study. Bottom: Observed data (Steinberg et al., 2001).*

temperatures are around 19 °C, while mixed-layer depths vary from 150 to 250m. In general, the GOTM results show a passable fit to the observations (compare also with Section 2.1) which meets the requirements of the present study.

4.2 Results of the ecosystem model

The ecosystem model has already been used to study the nitrogen cycle at the BATS site with good results (Oschlies and Schartau, 2005). However, the present study used a different physical model and different forcing fields. Therefore, the main features of the biological model solution are presented here briefly.

The biological part of the model produces dissolved inorganic nitrogen (DIN) and chlorophyll a (Chl α) concentrations, that are close to observations (Figure 4.3).

DIN concentrations at the BATS site are low in the upper ocean (lower than 1 μM N), reflecting the oligotrophic conditions in the North Atlantic subtropical gyre. In late winter, the deepening of the mixed layer leads to a peak in DIN concentrations. The model reproduces this annual cycle quite well, with slightly overestimation of DIN concentrations (by around 1 μM N) at the spring maximum. The modelled vertical DIN gradients are also close to those observed, with slight underestimation (by around 1 μM N) in seasonal variability of DIN below 120 m.

The distribution of Chl α at the BATS site is characterised by a spring bloom that is initiated by the increasing irradiance during the annual shoaling of the mixed layer, and later by the development of a deep chlorophyll maximum below the shallow summer mixed layer. The modelled timing of the spring bloom is in good agreement with observations. During late spring and summer the modelled concentrations reveal a deep Chl α maximum just like in the observations. Chl α

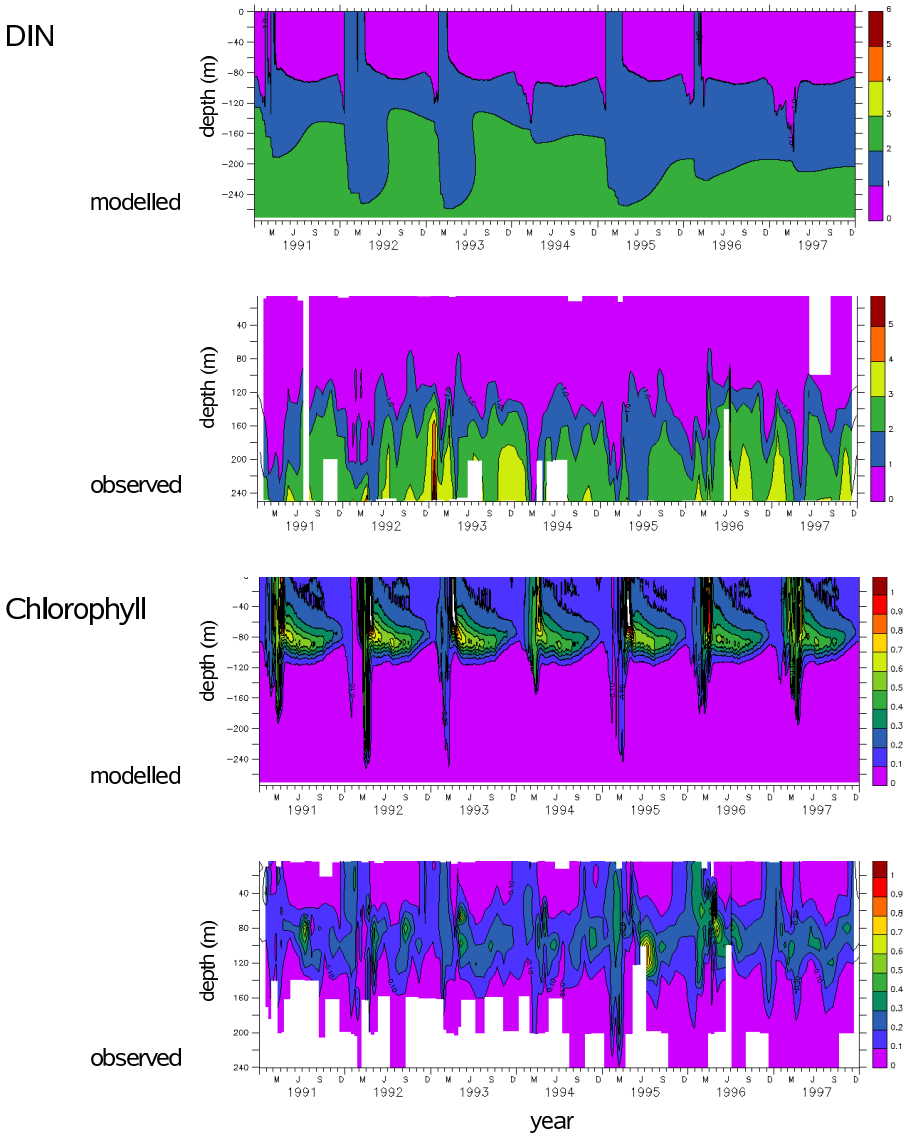

Figure 4.3: *Modelled and observed concentrations of DIN (Nitrate + Nitrite) in μM (top) and chlorophyll α in $\mu g\ l^{-}1$ (bottom)*

concentrations are slightly overestimated in the model, especially in the upper 60 m (by around 0.1 μg l^{-1}). Lower concentrations in Chl α were observed in years 1990 and 1991 which are not reproduced by the model.

The annually averaged vertical sinking flux of detritus at 100 m depth varies between 0.67 and 0.83 mol C m^{-2} a^{-1}, which is within the range of published estimates of export production at the BATS site (0.7 to 4.4 mol C m^{-2} a^{-1}, Carlson et al. (1994)), albeit at the lower end. Both the assumption of a constant C:N ratio of 6.625 in organic matter and the lack of a dissolved organic carbon pool might cause the export production of the model to be biased somewhat downward.

In general, the ecosystem model results demonstrate a reasonable fit to the observations which meet the demands of the present study.

Model solutions for P_{Fe}, Z_{Fe} and D_{Fe}, i.e. the iron content in the ecosystem model, depend on the dissolved iron concentrations in the water column and will be discussed in the following sections.

4.3 Iron fluxes below the mixed layer

4.3.1 Initial state

For the initial model run (Run I) of the 1d model, the same parameter set for the iron chemistry is used as in the 0d model (Table 2.2; apart from the photoreduction rate of colloidal iron discussed as in Section 2.3). Run I does not generate results close to observations (Figure 4.4, top). Modelled iron concentrations within the mixed layer varies between 0.2 nM in summer and 1 pM in spring. Because of the very low [dFe] values in the mixed layer, uptake of iron by phytoplankton is strongly limited, leading to Fe:N quotas in the ecosystem model far below the maximum. Below the mixed layer, concentrations are lower than 1 pM. This result is independent of the chosen bottom boundary condition. In contrast, observations at the

BATS site show annual variations between 0.1 nM and 2.0 nM at the surface, a subsurface minimum around 0.1 nM near 100 m depth, and values between 0.4 - 0.6 nM below (Wu and Boyle, 2002; Sedwick et al., 2005). These unrealistic model results can be traced back to the basic model structure as follows:

Unlike the earlier zero-dimensional model approach, the iron profile below the mixed layer is not prescribed in the one-dimensional model. In consequence, the source of iron from deeper water has to be generated by the model itself. The lack of iron at depth may result either from an underestimated iron source or from overestimated iron sinks. From observations of dissolved iron it has been estimated that the scavenging residence time of iron in the deep ocean is around 200 years (Johnson et al., 1997; Bergquist and Boyle, 2006). Close to the surface however, residence times for dissolved iron concentrations are estimated to be in the order of 1 to 5 months (Bergquist and Boyle, 2006). Even faster removal processes (second or less) of iron at the surface are observed during iron fertilisation experiments (Nishioka et al., 2005). These are associated with the association of dFe with suspended colloids by surface complexation and subsequent aggregation of these colloids with filterable particles. Hence, the one-dimensional model suffers from the necessity to reconcile slow iron loss processes at depth with fast timescales in the mixed layer.

Vertical diffusion, providing a source of iron and compensation for loss processes, is rather low in the model (< 1 cm^2 s^{-1}), in agreement with observational estimates by Musgrave et al. (1988) and Ono et al. (2001). One missing process in a one-dimensional model is lateral advection which might import or export iron throughout the water column.

Note, hereafter, “deep water” will be referred to as water at z= 250 m unless otherwise specified since for the present study only concentrations directly below the mixed layer are relevant.

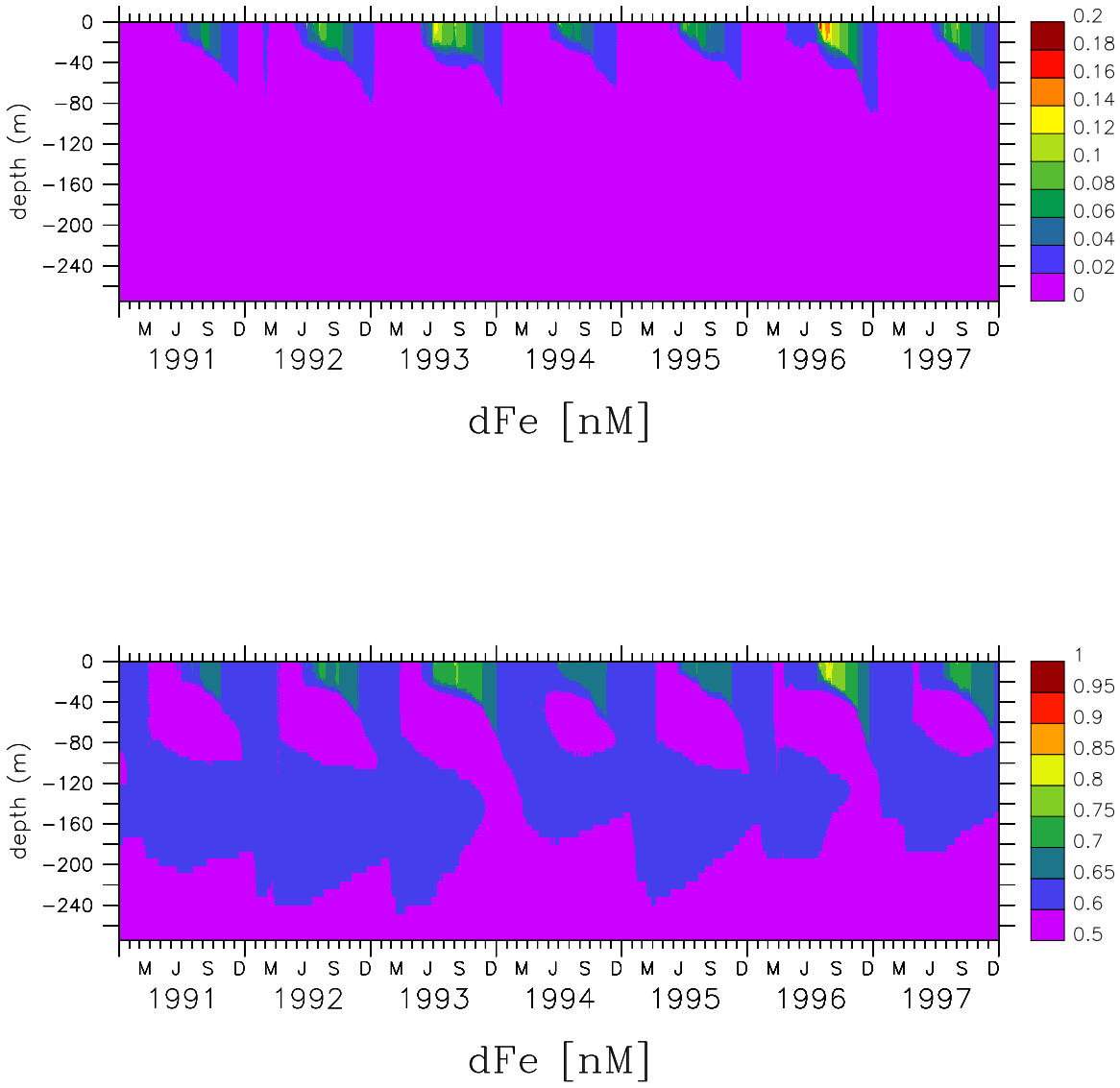

Figure 4.4: *Modelled concentrations of dFe in nM: Model Run I (top) and Model Run A (bottom). Note the different scales for the two plots.*

4.3.2 Reconciling slow iron loss processes at depth with short timescales in the mixed layer

While the zero-dimensional model has its focus on fast removal processes in surface waters, the parameter setting of the one-dimensional approach of this study needs to handle the slower processes below the mixed layer as well.

After running the model with the parameter values chosen for the 0d model, the lack of iron below the mixed layer is a result of export fluxes (through colloidal aggregation and scavenging) being bigger than the supply through remineralisation of detritus which, in the model, is the only large source of iron below the mixed layer.

The imbalance between the different fluxes can have three explanations: (i) the assumed rates for colloidal aggregation and/or scavenging are too large and/or (ii) organic complexation processes, that increase the residence time of iron, are not strong enough and/or (iii) the assumed sources of iron are not sufficient.

Point (iii) will be discussed in Section 4.6. To examine (i) and (ii) the following simple calculation can be made. Below the mixed layer the photochemistry can be safely ignored. For simplicity, vertical diffusion will be neglected here as well. Averaging over a time interval long enough to neglect time derivatives, the following balances are obtained:

- balance equation for colloidal iron Fe_{col}: colloid formation equals aggregation loss,

$$0 \quad = \quad k_c \mathrm{Fe(III)}' - k_a \mathrm{Fe}_{col} \tag{4.1}$$

  where $k_a = k_{ag}(P + r_{m:N} D)$ is the effective aggregation rate for a given concentration of inorganic particles P and detritus D

- balance equation for $\mathrm{Fe(III)}'$: dissociation of iron complex equals

formation of ligands + scavenging + colloid formation

$$0 \quad = \quad k_{ld}\mathrm{FeL} - k_{fel}\mathrm{Fe(III)}'L - k_s\mathrm{Fe(III)}' - k_c\mathrm{Fe(III)}' \qquad (4.2)$$

where $k_s = k_{sca}(P + r_{m:N}D)$ is the effective scavenging rate for a given concentration of inorganic particles and detritus

- balance equation for complexed iron FeL: remineralisation of iron from decay of organic matter + complex formation equals complex dissociation,

$$0 \quad = \quad R + k_{fel}\mathrm{Fe(III)}'L - k_{ld}\mathrm{FeL} \qquad (4.3)$$

where R is the iron remineralisation rate $R = r_{Fe:N}\gamma_d D$

These equations are simple enough to be solved analytically, as follows:

$$\mathrm{Fe(III)}' \quad = \quad \frac{R}{k_c + k_s} \qquad (4.4)$$

$$\mathrm{Fe}_{col} \quad = \quad \frac{k_c}{k_a}\frac{R}{k_c + k_s} \qquad (4.5)$$

$$\mathrm{FeL} \quad = \quad \frac{R + k_{fel}\mathrm{Fe(III)}'L}{k_{ld}} \qquad (4.6)$$

Average modelled values of detritus and inorganic particle concentrations at 250 m depth are $D = 0.0086\,\mu$M and $P = 1.3\,\mathrm{kg\,l^{-1}}$. The average temperature is $T = 18.5^\circ$ C. At these concentrations of particulates, k_s is much lower than k_c. To first order $\mathrm{Fe}_{col} = R/k_a$ and $\mathrm{Fe(III)}' = R/k_c$, i.e. the colloidal iron concentration is inversely proportional to the colloid aggregation rate, and the inorganic iron concentration is inversely proportional to the colloid formation rate. However, during the spring bloom, detritus concentrations in the model at 250 m depth can reach D = 0.07 μM, which makes it a crucial factor at this time of the year which needs to be taken into consideration. Calculating R from the models temperature and detritus concentration and by inserting the parameter values of the 0d-model, results in $\mathrm{Fe}_{col} = 0.3$pM and FeL = 0.9pM. These

Table 4.1: *Conditional stability constant of organic complexes (k_{ld} [M^{-1}]).*

Reference	k_{FeL}	Location
Observations		
Gledhill et al. 1994 (min)	$10^{18.8}$	North East Atlantic
Wu et al. 1995	$10^{20.6}$	North West Atlantic
Rijkenberg et al. 2006	$10^{21.75}$	Southern Ocean
van den Berg et al. 1995	$10^{21.8}$	North West Atlantic
Cullen et al. 2006	$10^{22.01}$	Sargasso Sea
Witter et al. 2000	$10^{22.4}$	Southern Ocean
Gledhill et al. 1994 (max)	$10^{22.5}$	North East Atlantic
Model		
Run I	$10^{20.3}$	BATS site
Run A	10^{22}	BATS site

values are orders of magnitude lower than observations. From Eq. 4.5 it is obvious that the only way to have Fe_{col} closer to observations is to decrease the colloid aggregation rate k_{ag}. FeL can be increased by either increasing ligand strength (i.e. decreasing k_{ld}) or by increasing Fe(III)′ through decreasing k_c, or by a combination of both. Observed conditional stability constants for iron binding ligands (e.g. Table 4.1) range between $10^{18}M^{-1}$ to $10^{22.5}M^{-1}$.

The rate constant for the formation of colloidal iron, k_c, appears to be somewhat better constrained, e.g. by Johnson et al. (1994) who determined k_c by measuring the change in dissolved Fe(III) concentrations during dark periods after addition of 10 nM Fe(III). Under the assumption that k_c is already of the correct order of magnitude, a pragmatic increase of k_{ld} by a factor of 50 as well as a decrease of k_{ag} by a factor of 1000 yields the concentrations in the right order of magnitude Fe_{col} = 0.3 nM and FeL = 0.1 nM. Results of the 1d model with parameters modified (Run A) accordingly to k_{ag} = 1224 and $k_{ld} = 10^{22}$ (see Table 2.2) are close to observations and will be discussed in more detail in Section 4.4. Run A will be referred as the standard model run of the present study.

4.3.3 Is the parameter modification justified in terms of observations?

Colloidal aggregation

The colloidal aggregation rate needs to be three orders of magnitude lower than in the zero-dimensional model to achieve model results close to observations. In spite of low particle concentrations in the open ocean it is suggested that marine colloids are very dynamic with high colloidal aggregation rates (Moran and Buesseler, 1992; Baskaran et al., 1992). So far, there are no methods to measure colloids directly in situ in seawater at typical oceanic concentrations. Detailed processes that lead to changes in particle size are not fully understood (Wells, 2002). This makes it difficult to represent colloidal processes in a model adequately. Wen et al. (1997) performed some radiotracer experiments to study the interactions between ionic, colloidal and natural particulate forms of iron. The initial colloidal aggregation rate (Run I) was derived from this work, proportional to the concentration of particles and colloids. However, Wen et al. (1997) preformed the experiments with particle-rich waters (10 mg/L) from the Galveston Bay, at the coastline of Texas, USA. For the particle poor region at the BATS site (around 0.01 mg/L), conditions which lead to aggregations are different.

Strong ligands

In the 0d-model a conditional stability constant of Fe-organic complexes of $10^{20.3}\mathrm{M}^{-1}$ was used, as was measured by Wu and Luther III (1995). However, the range of the measured conditional stability constants by different authors is wide (e.g. Table 4.1) and reaches from $10^{18}\mathrm{M}^{-1}$ to $10^{22.5}\mathrm{M}^{-1}$. Therefore, a large window of opportunity exists for the choice of the model's conditional stability constant, bearing in mind that in the ocean different classes of ligands with different binding strength exist (Gledhill

and van den Berg, 1994; Cullen et al., 2006) and that the relatively simple representation of this model approach only allows for one "typical" class. The value $10^{22}M^{-1}$ that is used is within this admittedly large range of variation and agrees with the observed value for iron binding ligands in the Sargasso Sea by Cullen et al. (2006). However, different from Gledhill and van den Berg (1994) who found strong binding ligands throughout the water column, Cullen et al. (2006) suggested that in surface waters in the Sargasso Sea, strong ligands with a conditional stability constant of $10^{22.01}$ relative to total inorganic Fe appeared to dominate while in deep water ligands have stability constant 12-15 times smaller. The model cannot confirm these observations, since stronger ligands with a stability constant of around 10^{22} are required, especially below the mixed layer, to reproduce a realistic iron profile. Further model development in terms of different ligand classes is required. Since this will add new parameters to the model, such an approach will also need further information (qualitatively and quantitatively) from laboratory and field experiments with regard to the origin, strength and fate of organic ligands for iron in the seawater.

4.4 Temporal dynamics in the mixed layer

4.4.1 Diurnal variability of iron speciation

The modelled iron and reactive oxygen speciation show a strong diurnal variablity in the upper water column (Figures 4.5), just like the model results of the 0d-model.

The hydrogen peroxide ($[H_2O_2]$) concentration follows a distinct diurnal pattern, with highest values during mid- to late afternoon and lowest concentration in the morning. The depth limit of diurnal variations in H_2O_2 concentration is variable, ranging from 20 m in winter to around 40 m in summer. The mixed-layer averaged concentration of hydrogen peroxide in the model demonstrate a strong annual cycle, varying between 25 nM in

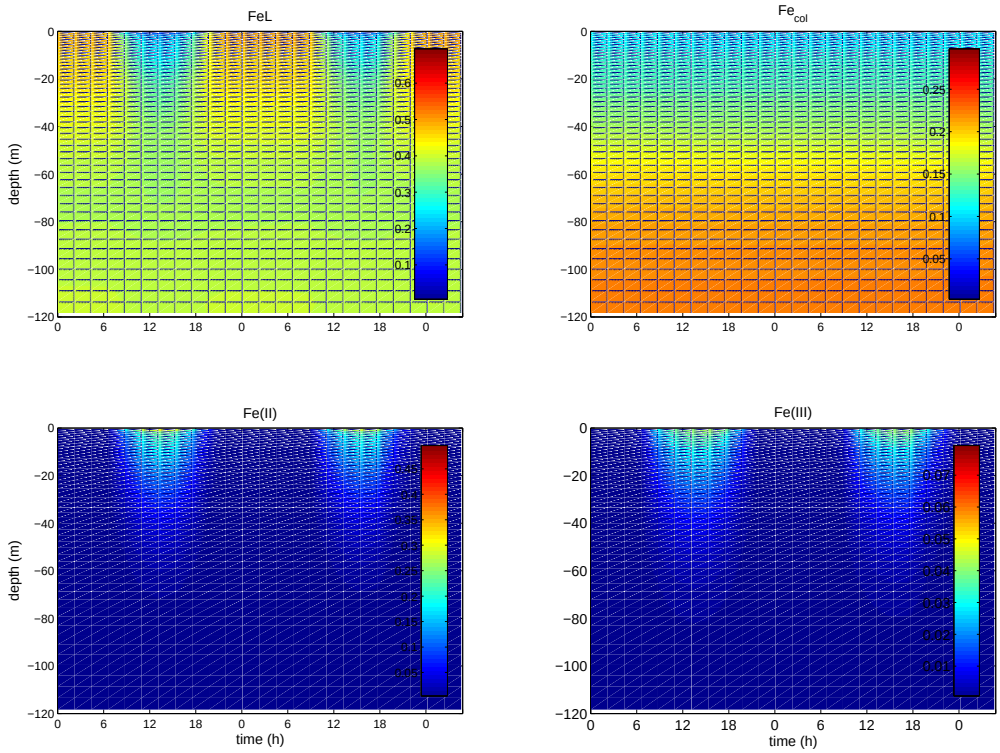

Figure 4.5: *Diurnal variability of modelled iron concentrations (nM)*

Table 4.2: *Maximum redox rates in nM d^{-1} at noon in August*

Rate	1 m depth	40 m depth	100 m depth
k_{ox1}	70.52	10.84	0.40
k_{ox2}	424.10	14.84	0.05
k_{ox3}	454.10	21.44	0.06
k_{red}	871.80	41.37	0.24
k_{ph1}	0.44	0.04	0.00
k_{ph2}	40.37	5.51	0.34
k_{ph3}	0.19	0.00	0.00
k_{ph4}	0.01	0.00	0.00

winter and around 65 nM in summer. These results are in good agreement with observations in the subtropical Atlantic by Obernosterer et al. (2001). They detected H_2O_2 concentrations of, on average, 42 nM both in surface waters and in profiles up to 50 m depth. This followed a distinct diurnal pattern, with highest concentrations during mid- to late afternoon and lowest concentrations during the morning. The lifetime of superoxide is extremely short (order of seconds) so that its modelled concentration correlates strongly to irradiance with maximum concentration at noon and zero values at nighttime. FeL and Fe_{col} are the dominant forms of iron during the night. During daytime the concentrations of Fe(II)', Fe(III)' become significant due to photochemical reactions. At the surface Fe(II)' is produced by direct photoreduction of ferric iron species but mainly by the reduction of Fe(III)' by photoreduced superoxide (Table 4.2).

Consistent with the rates estimated by Voelker and Sedlak (1995), iron reduction by superoxide occurs at a rate that is up to more than a hundred times the maximum rate of all direct photoreductive processes taken together. Photoproduction of superoxide and its subsequent transformation to hydrogen peroxide leads to a corresponding cycle of iron redox-reactions and to an increase in [Fe(II)′] and [Fe(III)′] in the daytime at the expense of [FeL]. Variation in [FeL] between day and night is up to 60% at the surface. The Fe(II)′ produced is subsequently oxidised again to Fe(III)′ by O_2, O_2^-

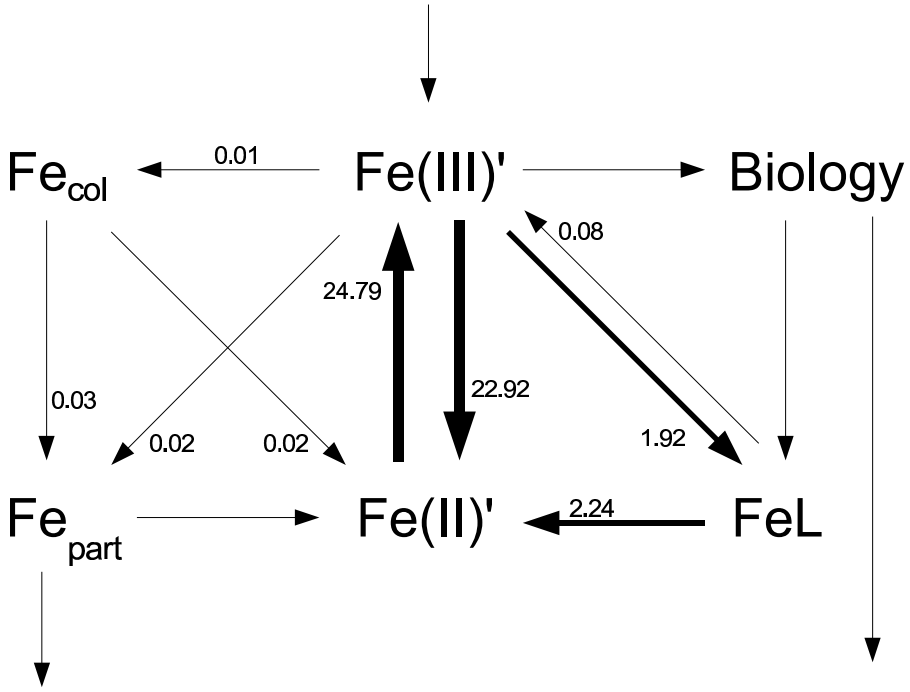

Figure 4.6: *Annually averaged rates of change of modelled iron concentrations [nM d^{-1}] at 0-40 m depth. Arrows without number are smaller than 0.01*

and H_2O_2. Until midday, iron reduction outweighs oxidation, leading to an increase of [Fe(II)′], but also of [Fe(III)′] at the expense of [FeL]. In the afternoon, the balance between reduction and oxidation is reversed because [H_2O_2] reaches its maximum and [Fe(II)′] decreases. During the night all photochemical reactions stop so that all Fe(II)′ is oxidised to Fe(III)′, some which is rapidily complexed by free organic ligands. The formation and photoreduction of colloidal iron in the model is a much slower process (one to two orders of magnitude) compared to organic complexation, oxidation and photoreduction (Figure 4.6). Variations in [Fe_{col}] between day and night are therefore in the order of a few percent (around 1% at the surface).

Light as the driving force behind photochemical cycling decays strongly with depth. Compared to the surface, modelled photoreduction and oxidation rates are about one order of magnitude lower at 40 m depth and about four orders of magnitude lower at 100 m depth (Table 4.2). On the other hand, the strong vertical mixing within the mixed layer acts to oppose the creation of concentration gradients within the mixed layer. The vertical distribution of (directly or indirectly) photoproduced species, such as Fe(II)′ therefore depends on the equilibrium between mixing and production which is strongly affected by the life-time of the species. The shorter the life-time of a species is, compared to the time-scale of vertical mixing, the stronger its vertical distribution is coupled to that of its production (Doney et al., 1995). Model results clearly show strong vertical gradients in the amplitude of the diurnal cycle of all photoproduced species (superoxide, Fe(II)', Fe(III)' and hydrogen peroxide) within the mixed layer. The different life-times of the different photochemically produced species are reflected in different depth dependencies of their daily cycle (Figure 4.7).

The concentration of the shortest-lived species, superoxide, decreases strongest with depth, while the daily cycle of hydrogen peroxide is less directly related to the exponential decrease of light intensity. The creation of vertical gradients within the mixed layer is enhanced by the stabilisation of the water column during the day by solar warming. The redox-reactions of inorganic Fe and organic complexation determine the residence time of dissolved iron in the euphotic zone by keeping iron in solution (Fe(II)', Fe(III)' and FeL) and therefore preventing it from scavenging or building colloids and subsequently aggregating. Therefore, a distinct profile of [dFe] develops with higher concentrations of iron at the surface, strongly decreasing then over the upper 40 m with decreasing light availability. Additional to the decrease in photochemical activity with depth, a [dFe] minimum develops between 40 and 100 m due to increased biological activity at this depth (Section 4.2). Below the deep chlorophyll maximum [dFe] increases back to a concentration of approximately 0.6 nM due to

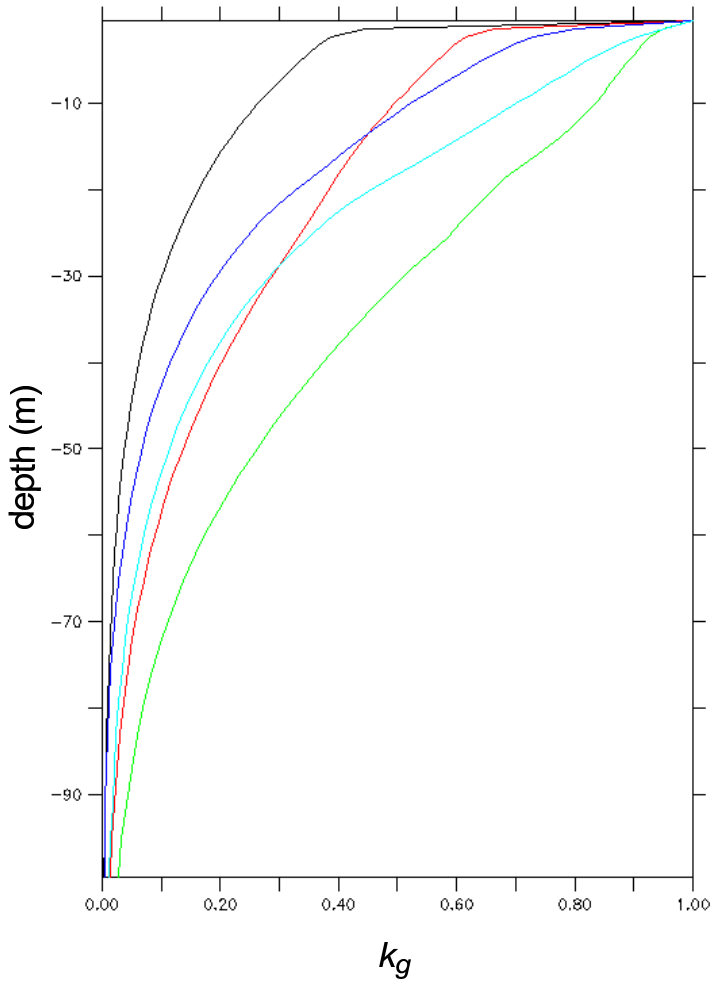

Figure 4.7: *Vertical gradients of irradiation (black) and the photoproduced species* O_2^- *(red), Fe(II)' (blue), Fe(III)' (magenta) and* H_2O_2 *(green) at noon in summer (1. June - 31. August).*

remineralisation of organic detritus.

The model results agree well in summer with observations by Wu and Luther III (1994) (Figure 4.8). A similar vertical pattern is also observed by Sedwick et al. (2005) but with a greater range between maximum and minimum concentrations of the profile. The iron profile concentrations in spring are simular to the observations by Wu and Boyle (1998), with smaller differences between minimum and maximum concentrations in spring than in summer.

4.4.2 Annual cycle and interannual variability of dissolved iron

The modelled concentration of dissolved iron in the mixed layer ranges from 0.56 nM in spring to 0.85 nM in summer (Figure 4.4, bottom), which is a little higher than observations by Wu and Boyle (2002) (0.2-0.6 nM) and within the range of observations by Sedwick et al. (2005) (0.1-2 nM). These iron concentrations are never limiting for phytoplankton uptake. Therefore the Fe:N quota in phytoplankton, zooplankton and detritus are always close to the prescribed maximum quota $r_{Fe:N}$, justifying *a posteriori* the neglection of iron limitation for phytoplankton growth in the present study. The model seems to overestimate the minimum [dFe] concentrations, possible because of the low value required for colloidal aggregation (see also Section 4.6).

The range of iron concentration over the year is subject to a strong seasonal cycle of [dFe], caused by the annual mixed layer cycle, spring phytoplankton bloom and dust deposition.

Strong winter deepening of the mixed layer leads to dilution of [dFe]. Increased detritus concentrations in March and April, caused by the spring phytoplankton bloom, supports colloidal aggregation and scavenging, which lead to a further drawdown in [dFe]. Additionally, the uptake of iron by

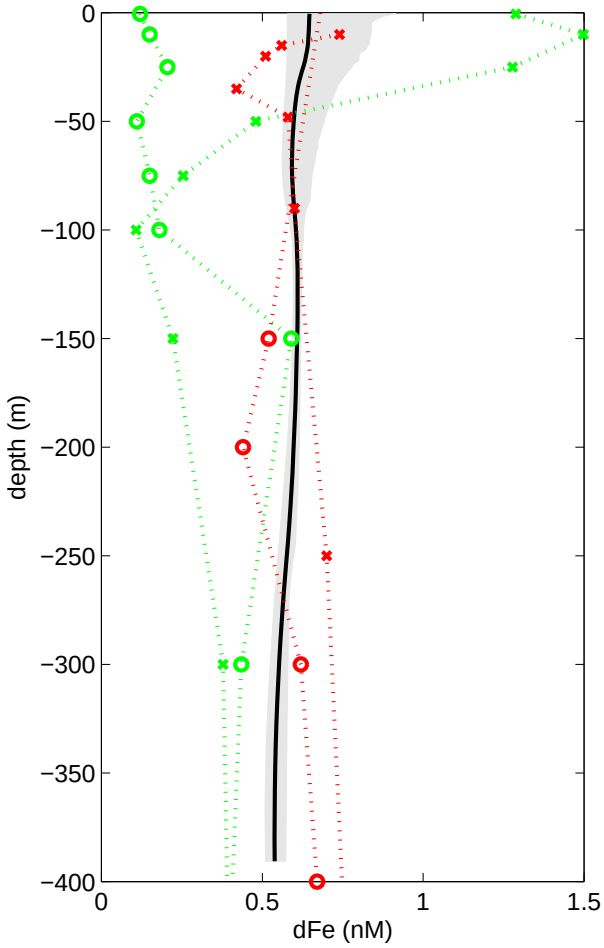

Figure 4.8: *Annual mean profile of modelled dFe concentration (black line) with maximum (summer) and minimum (spring) values (area in light gray). Measured dFe concentration at BATS in spring (circle) and summer (cross) by Wu and Luther III (1994); Wu and Boyle (1998) (red) and Sedwick et al. (2005) (green)*

phytoplankton is increased at this time. The main import of iron occurs in summer when dust storms from the Sahara arrive. At this time the mixed layer is shallow and phytoplankton activity is low. The import of atmospheric iron increases [dFe] in the surface water until the winter deepening of the mixed layer starts again.

The annual cycle of modelled Fe has no significant interannual changes in dFe concentration and speciation. In contrast to that, the dust deposition has a interanual variability, with changes by a factor of more than 2.5. Changes in iron input due to increased dust deposition are buffered by a change in the residence time of dFe (Section 4.4.3) due to associated increase in particle concentration and therefore increased colloidal aggregation and scavenging.

4.4.3 Residence time of iron

The residence time of dissolved iron is usually defined as the ratio between the total dissolved iron concentration (in nmol/l) and the rate at which dissolved iron is lost (in nmol/l/d). Typically a constant scavenging residence time, i.e. a proportionality between dissolved iron concentration and scavenging loss is assumed. However, iron speciation, and nonlinearities in the dependency of loss on concentrations may make this assumption invalid. In the present model these processes are at least partially resolved. It is therefore interesting to investigate how the effective residence time in the model varies over time and depth, as the colloid aggregation rate had to be changed in such a way that the model results are consistent with subsurface observations (Section 4.3.2).

The focus here is on the residence time with respect to scavenging and colloid aggregation, i.e. the two processes that transfer iron from the colloidal and dissolved phase to filterable particles. This rate is formally

defined by

$$\tau = \frac{[\mathrm{Fe(III)}'] + [\mathrm{Fe(II)}'] + [Fe_{col}] + [\mathrm{FeL}]}{(k_{ag}[Fe_{col}] + k_{sca}[\mathrm{Fe(III)}'])\,([A] + [D_{Fe}])} \tag{4.7}$$

where $[A]$ is the concentration of inorganic particles.

The annual cycle of τ at the surface shows values up to 30000 days in winter when neither organic nor inorganic particles are present in great numbers. This is of the same order of magnitude as estimates for the deep ocean (see Section 4.3.1). The residence time is reduced markedly to approximatley one hour in late spring following the phytoplankton spring bloom. The phytoplankton bloom influences the residence time negatively by uptake of dFe directly but also vicariously by producing detritus. A second reduction in the residence time occurs in summer as a consequence of dust deposition events (Figure 4.9). In winter, the smaller deposition of atmospheric iron remains within the mixed layer longer, while in summer the higher deposition leads to a stronger source, but also to a faster loss because of the increased particle density.

4.5 Parameter sensitivity

As for all numerical models, the particular solution depends on the choice of biogeochemical parameters. Some of the model parameterisations, e.g. for colloid aggregation, attempt to describe a complex process in a simple way. Estimation of the corresponding parameters therefore remains a major challenge. Even though some of the parameters of this study are based upon measurements taken in the laboratory and the ocean, most are based on approximations and also often on pragmatic assumptions. It is therefore necessary to investigate the sensitivity of the model results to changes in the parameter values that are most uncertain.

Because of the large number of parameters involved, the sensitivity tests are limited to variation in one parameter at a time, leaving all other

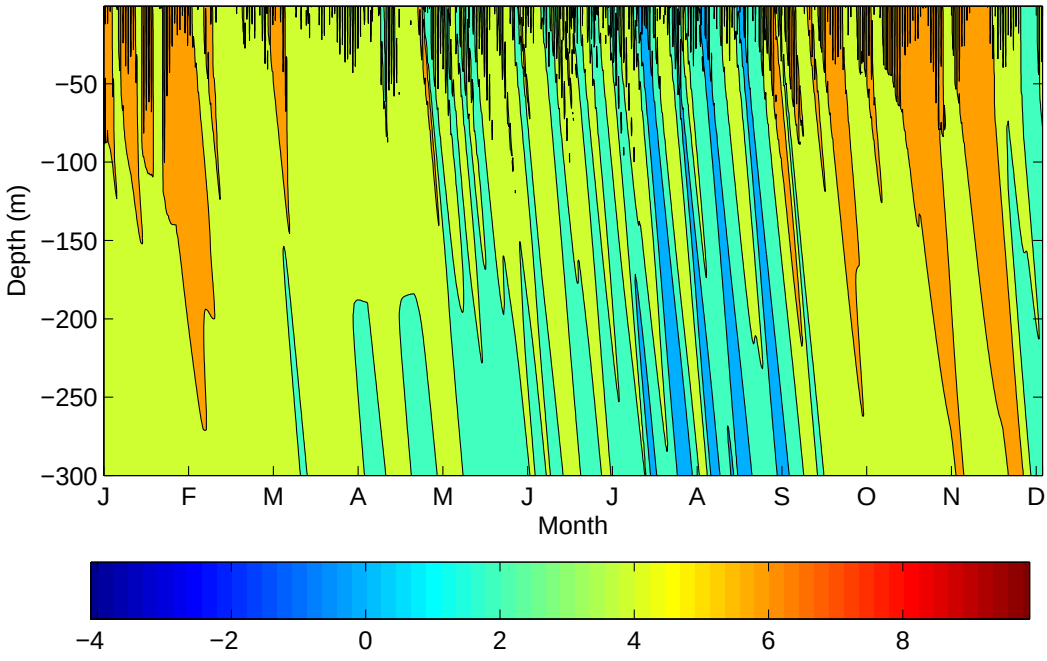

Figure 4.9: *Contour plot of the residence-time (in years) of dFe in the upper 300 m. Note the log-scale.*

parameters unchanged (Table 2.2, 1d). Two sensitivity runs per parameter were conducted, one with a 50% lower and one with a 100% higher value. For purposes of comparison, the same sensitivity study was done with the zero-dimensional model. The main effects of these parameter changes on dissolved iron concentrations are summarised in Table 4.3.

4.5.1 Comparison of parameter sensitivity between the 0d and the 1d model

Comparing the one-dimensional model results of the sensitivity study with model results of the same sensitivity study using the zero-dimensional model (Table 4.3) reveals that the one-dimensional model is much more sensitive to parameter changes of the main sources and sinks (solubility of atmospheric iron, colloidal aggregation and uptake by phytoplankton).

Model results of the zero-dimensional model indicate an important role of the vertical flux of iron due to the entrainment and detrainment of water during the annual cycle of mixed layer deepening and shoaling. This flux is dominant in the sense that it balances the other fluxes in such a way that the total dissolved iron concentration in the mixed layer does not depend strongly on the size of dust input, colloidal aggregation or uptake (Table 4.3), but remains tightly coupled to the concentration below the mixed layer, which is prescribed. In the one-dimensional model iron profiles below the mixed layer have to be generated by the model itself (see also Section 4.3.1). This leads to bidirectional feedbacks. Changes in the surface fluxes are not necessarily compensated by the exchange with deeper water anymore and need to be balanced in other ways. However, the vertical exchange in the one-dimensional model can buffer the sensitivity of certain fluxes as well. The most distinct example of this is the solubility of atmospheric iron. One would expect that doubling k_{sol} would increase [dFe] in the mixed layer by more than 13%, bearing in mind that dust deposition is a major source of iron in the model. Here, the higher solubility of iron is

Table 4.3: *Change in modelled dFe concentration [%] of the parameter sensitivity study with the one-dimensional model of the present study (1d) and the zero-dimensional model (0d). Zero values correspond to changes smaller than 0.5 %. Surf = upper 100m. 250 = 250 m depth. Bold values correspond to changes in concentration larger than 5%.*

	Surf Mean		Surf Max		Surf Min		250 Mean	
Parameter	double	half	double	half	double	half	double	half
1d								
k_{sol}	**13**	**-6**	**36**	**-18**	**10**	**-6**	3	-2
$r_{Fe:N}$	**-7**	3	**-7**	4	**-9**	**5**	2	-1
k_{ag}	**-5**	2	**-5**	3	**-7**	4	**-7**	4
k_{col}	-1	1	-1	1	-2	2	-2	2
k_{fel}	1	-1	1	0	1	-1	0	-1
k_{ld}	1	-1	1	-1	1	-2	1	-2
k_{sca}	0	0	0	0	0	0	0	0
k_{ox1}	0	0	0	0	0	0	0	0
k_{ox2}	0	0	0	0	0	0	0	0
k_{ox3}	0	0	0	0	0	0	0	0
k_{ph1}	1	-1	1	0	1	-1	0	0
k_{ph2}	1	-1	0	-1	1	-1	0	0
k_{ph3}	0	0	0	0	0	0	0	0
k_{ph4}	0	0	0	-1	1	-1	0	0
k_{red}	0	0	0	0	0	0	0	0
0d								
k_{sol}	2	-1	**7**	-3	1	0	-	-
$r_{Fe:N}$	-2	1	-1	0	**-8**	4	-	-
k_{ag}	-3	2	0	0	**-17**	**11**	-	-
k_{col}	-1	1	0	0	-4	5	-	-
k_{fel}	0	0	0	0	1	-3	-	-
k_{ld}	0	0	0	0	0	0	-	-
k_{sca}	0	0	0	0	0	0	-	-
k_{ox1}	0	0	0	0	0	0	-	-
k_{ox2}	0	0	0	0	0	0	-	-
k_{ox3}	0	0	0	0	0	0	-	-
k_{ph1}	1	-1	0	0	5	-4	-	-
k_{ph2}	0	0	0	0	0	0	-	-
k_{ph3}	0	0	0	0	0	0	-	-
k_{ph4}	1	-1	0	0	**8**	**-8**	-	-
k_{red}	0	0	0	0	0	0	-	-

buffered by changes in vertical iron fluxes in the same way than the interannual variability of dust deposition hardly influence the interannual consistency of [dFe] (see Section 4.4.2).

The one-dimensional model confirms therefore the results of the zero-dimensional model, that the concentration of dFe in the mixed layer is strongly regulated by the concentration below the mixed layer.

4.5.2 Atmospheric iron

Estimates of the solubility of iron from dust vary between 0.1% and 50%, (Zhuang et al., 1990; Duce and Tindale, 1991; Spokes and Jickells, 1996; Jickells and Spokes, 2001; Baker et al., 2006).

Changing the solubility of dust-deposited iron (k_{sol}) in the model has the strongest effect on [dFe] in surface waters of all parameters. In contrast, changes due to changes in k_{sol} are rather small at depth.

The main deposition of atmospheric iron occurs in summer when the mixed layer is shallow and the mixed layer prevents exchange with deeper water. A higher solubility leads therefore to a higher accumulation of iron in the upper water column. The solubility of atmospheric iron influences the annual mean profile of [dFe] down to 200 m with the strongest effect at the surface and a decreasing effect with depth. Almost all atmospheric iron which dissolves forms FeL, since the formation of organic complexes is a faster process than the formation of colloids (see Section 4.4.1). Hence an increase in solubility leads to an increase in [FeL] and the additional iron is kept in solution. Winter mixing brings it down to 200 m.

Increasing the solubility leads to an increase in both maximum and minimum dFe concentrations at the surface. As the spring minimum in dissolved iron is already quite high compared to observations, a solubility higher than about 2% seems unlikely.

4.5.3 Iron uptake

Changes in the maximum Fe:N-ratio in phytoplankton ($r_{Fe:N}$) affect the uptake of iron by phytoplankton and the amount of iron released during remineralisation of detritus. At the parameter values used (Table 2.2, 1d), iron is never limiting to phytoplankton so that the actual Fe:N ratio in phytoplankton, zooplankton and detritus is always close to the maximum.

An increased uptake due to doubling of $r_{Fe:N}$, decreases the mean concentration of dFe in the surface by 6% on average. During the phytoplankton bloom in spring [dFe] can be up to 9% lower. The increased uptake on the other hand leads to an increase in deep dissolved iron concentrations. The changes are strongest near the depth of maximum remineralisation (near 100m depth), but at 250m depth the increase in dFe concentration is still 2%.

This leads to a profile of [dFe] with a more pronounced difference between minimum concentrations at 50 m depth in the annual average and a local maximum below. Consequently, a smaller value of $r_{Fe:N}$ leads to less uptake, less remineralisation and a more uniform dFe profile with less difference between minimum and maximum concentrations. A profile like the one with higher $r_{Fe:N}$ comes closer to observed profile characteristics (Section 4.4.1). Sedwick et al. (2005) observed even higher differences between minimum and maximum concentrations, both more extreme. Hence, the model results suggest a higher maximum Fe:N-ratio than initially allowed. Bergquist and Boyle (2006) estimate an Fe:C ratio for the North Atlantic which is approximately twice the Fe:C-ratio used in the zero-dimensional model to calculate the Fe:N-ratio. The North Atlantic may have elevated Fe:C ratios compared with most of the ocean owing to the higher surface dFe and luxury Fe uptake by organisms (Sunda and Huntsman, 1995).

4.5.4 Colloids and ligands

The parameters relating to organic complexes and colloids were discussed in Section 4.3.2. One has to bear in mind that the uncertainty in the rates of colloidal aggregation and in the strength of organic complexes is orders of magnitude higher than the 50% to 100% range used in the sensitivity experiments here, for consistency, for all parameters.

Changes in the colloidal aggregation rate k_{ag} have the largest effect, as they change the concentration of dFe almost uniformly throughout the profile with a slightly greater effect below the mixed layer. Doubling the value of k_{ag} leads to a 5% decrease of [dFe] in the upper 100m and a 7% decrease below the mixed layer (250 m). The effect is stronger in deeper water because the photochemistry, which leads to redissolution of colloids in surface waters, vanishes with depth (see Section 4.4.1). In the sensitivity experiments, the effect of changes in colloid formation, the scavenging rate or the strength of ligands on [dFe] is much smaller (maximal 2%) than that of changes in k_{ag}. However, the speciation of iron is affected in different ways: Changing the colloid formation rate k_{col} leads to a shift between Fe_{col} and FeL throughout the whole profile, where, e.g. doubling the value of k_{col} leads to higher Fe_{col} concentration (around 0.08 nM) and consequently to higher export fluxes through colloidal aggregation (approximately 88% higher).

Changing the ligand formation rate k_{fel} leads to a shift between $[Fe_{col}]$ and [FeL] (around 0.05 nM), but mainly in the upper 200m, where higher k_{fel} leads to higher [FeL] at the expense of $[Fe_{col}]$. The model is more sensitive to this value in the upper water column due to higher production of inorganic redox forms by photochemical processes at the expense of both $[Fe_{col}]$ and [FeL] during the day, but mainly subsequently through complexation by free organic ligands in the nightime (see Section 4.4.1). This effect decreases with depth but reaches down as far as 200 m because of the deep winter mixing.

In contrast, changing the ligand stability k_{ld} leads to a shift between Fe_{col} and FeL only below the photic zone. A higher value of k_{ld} leads to higher Fe_{col} concentrations at the expense of [FeL] (up to around 0.08 nM). Below 50 m, no photochemical processes support organic complexation.

Overall, the impact of changes of the parameters k_{col}, k_{fel} and k_{ld} is small compared to that of changes in other parameters. A more detailed discussion of these processes has to await a significant reduction in the still substantial conceptual uncertainties, such as the parameterisation of colloidal aggregation.

4.5.5 Photochemical processes

Model results (Table 4.3) suggest that iron chemistry below the mixed layer is relatively insensitive to most parameter changes of this order of magnitude. This is especially true for all photochemically influenced processes since these have no immediate impact at this depth. However, even in the upper 100 m, oxidations processes are also insensitive to their parameter changes. While these processes are important in determining iron speciation and concentration in the upper water column (Section 4.4.1), their relatively insensitivity to dFe concentration arises through the fast photochemical reactions occuring during the day, making these two species important "reloading points". Reducing these rates by 50% slows down the cycle between Fe(III) and Fe(II)' but does not take away the dominance of these processes, which are still up to two orders of magnitude faster than all other processes of the iron cycle during the day.

In contrast to the insensitivity to photoreduction of Fe(III)' and Fe_{part} (k_{ph3} and k_{ph4}), the small (1%) but finite sensitivity due to doubling or halving the photoreduction rates of Fe_{col} and FeL (k_{ph1} and k_{ph_2}) is due to the difference in the respective iron concentrations. Fe_{col} and FeL are the dominant forms of iron in the mixed layer. Hence, doubling or halving their photoreduction rates has a greater impact.

The concentration difference of dFe is caused by a shift in the speciation of iron by changing k_{ph1} or k_{ph_2}. Doubling k_{ph1} leads to an increase of [FeL] at the expence of $[Fe_{col}]$ and vice versa. This allows iron to remain in solution longer by increasing FeL, or increasing Fe_{col} allowing higher export fluxes due to increased colloidal aggregation by increased Fe_{col}. This effect reaches down to 200 m, where the concentration of the species equalize with the concentrations from the standard model run.

This is especially interesting for k_{ph1}, since the importance of photoreduction has been revealed in field studies using ferrihydrite as a model solid but there is a lack of data on naturally occurring colloids (Moffet, 2001). There is a need to quantify these parameters through laboratory and field studies to validate the model.

The model still has a relatively simplistic representation of photochemical reactions which are assumed to vary with irradiance over the visible band.

Recent deck-incubation experiments with open ocean water showed, that the UV part of the solar spectrum plays a major role in the photoreduction of iron, suggesting that any increases in UV (e.g. stratospheric ozone depletion) could increase the formation of Fe(II) and therefore the residence time and bioavailability of iron in the euphotic zone (Rijkenberg et al., 2005). However, in seawater UV is much more attenuated with depth than the visible band. In moderatly productive water UV-B does not reach 10 m depth whereas visible light penetrates down to 50 m (Smith and Baker, 1979). Taking into consideration that doubling the photoreduction rates hardly influences the dFe concentration, an explicit consideration of UV in the model is of less relevance to the total iron concentration, than to the speciation of iron in the upper water column.

4.6 Introducing redissolution of particulate and colloidal iron

The low colloid aggregation rate required to reproduce observed iron concentrations (Section 4.3.2) has a strong influence on the temporal behaviour of iron concentrations within the mixed layer. In particular, the model now lacks the observed rapid decrease of [dFe] after pulsed iron additions (Nishioka et al., 2005).

The reduction in the aggregation rate is a consequence of the model setup in which there is no way back from particulate and/or colloidal iron to truly dissolved forms, other than photochemistry, which vanishes completely in the deep ocean.

One could therefore argue that an alternative to reducing the aggregation rate could be to introduce leaching of particulate iron and/or colloidal iron back into dissolved form, as in Parekh et al. (2004). Desorption of iron bound to particle surfaces as well as dissagregation processes and break-up of colloids are not unlikely but the processes driving them and their rates are still not very well understood (Moffet, 2001).

To investigate the effect of redissolution on deep iron concentrations, two additional source terms of iron are added in the equation for Fe(III)' and the corresponding sinks in the equation for particulate iron (Fe_p) and colloidal iron (Fe_{col}). The processes are parameterised as linearly dependent on the concentrations as,

$$\psi_p = k_{pd}[Fe_p] \tag{4.8}$$

$$\psi_c = k_{cd}[Fe_{col}] \tag{4.9}$$

with ψ_p indicating the flux from Fe_p to Fe(III)' and ψ_c the flux from Fe_{col} to Fe(III)'.

Table 4.4: *Annually averaged concentration of dFe [nM] of model runs with varying redissolution processes. surf= upper 100m, 250 = 250 m depth, 0.000 = values smaller than 0.001*

		dFe			
Run	Parameter	surf mean	surf max	surf min	250m mean
I	initial	0.015	0.198	0.000	0.000
A	standard	0.610	0.852	0.562	0.582
r1	with k_{pd}	0.161	0.833	0.027	0.050
r2	with k_{cd}	0.185	0.911	0.015	0.001
r3	with k_{pd} and k_{cd}	0.263	0.962	0.087	0.122

In the absence of information regarding rates for these processes, rates were chosen, which are of the same order of magnitude as photochemical dissolution rates in the mixed layer, $k_{pd} = k_{cd} = 0.2\ d^{-1}$. Both are probably at the very upper end of possible rates, and are also significantly higher than estimates by Parekh et al. (2004) (20-100 y^{-1}). However, the slow redissolution rate in Parekh et al. (2004) complements an equally slow scavenging rate, while the present study also attempts to represent faster processes.

Three additional experiments with redissolution were performed, one including ψ_p (Run r1), one with ψ_c (Run r2), and one with both processes (Run r3). For these experiments, the initial colloidal aggregation rate is used, while the conditional stability constant of iron binding ligands is taken from the present study (Run A). This allows comparison of the results of this experiment with results from Run A.

A summary of [dFe] in these experiments is shown in Table 4.4. In all experiments, dissolved iron concentrations are increased with respect to the case of the initial model run (Run I).

Results of the model runs with either ψ_p (Run r1) or ψ_c (Run r2) show that introducing these relatively high rates does not solve the problem entirely and that the high aggregation rate of colloidal iron leads still to iron depletion at depth. However, the concentration of dFe below the mixed

layer is around 50 pM in Run r1 and 1 pM in Run r2, which is up to more than two order of magnitude higher than in Run I (Table 4.4). The concentration in the mixed layer is likewise three times higher than in the initial model run. The maximum concentrations in the mixed layer are of a similar order of magnitude to observations by Wu et al. (2001); Sedwick et al. (2005). The minimum concentrations are one order of magnitude lower than observations. The annual minimum of [dFe] in the mixed layer remains relatively low, even in the run with k_{pd} and k_{cd} together (Run r3). The same holds for the [dFe] concentration below the mixed layer, although it is interesting to note that the increase in [dFe] with respect to Run I is larger than the sum of the increases in Runs r1 and r2.

Compared to the standard model run (Run A) with reduced colloidal aggregation rate, the amplitude of the annual cycle of [dFe] (difference between maximum and minimum value in Table 4.4) in the mixed layer is increased in all of these experiments. The annual pattern, with a minimum in early spring and a maximum in summer remains the same.

In summary, the model runs in this Section show that redissolution can lead to deep water and mixed layer concentrations of [dFe] that are closer to observed values, even with high colloid aggregation rates. However, the resulting [dFe] remains systematically too low even for probably unrealistically high redissolution rates. This further confirms that the colloid aggregation rate has to be lower than the value used in the zero-dimensional model. It is probable that by varying the colloid aggregation and redissolution rates simultaneously over the range of values considered here, a solution can be found that reproduces both the observed deep iron concentrations and the rapid removal of iron from the dissolved phase in iron fertilisation experiments. However, such a systematic parameter study is outside the scope of the present study. Introducing k_{pd} and/or k_{cd} might be especially interesting for future model studies with pulsed events, such as iron fertilisation experiments. However, such an improvement of the model will need further input from laboratory and field

experiments with regards to the processes and rates in which redissolution of colloids and inorganic particles take place.

4.7 Summary and conclusions of Chapter 4

Using parameter values guided by laboratory and field studies, the 1d-model is able to simulate the temporal patterns and the vertical profile of dissolved iron in the upper ocean for the Bermuda Atlantic Time series Study site reasonably well. However, the model solution still strongly depends on the choice of some biogeochemical parameters. The main outcome of this study is as follows:

1. High colloidal aggregation rates of iron, observed in particle-rich coastal waters (Wen et al., 1997) and during iron fertilisation experiments (Nishioka et al., 2005) can not be applied to reproduce iron profiles at the BATS site with the current model. To prevent unrealistic depletion of dissolved iron at depth, the model requires aggregation rates 3 orders of magnitude lower than those observed, even when scaled with the concentration of sinking particles. Introducing a hypothetical redissolution of colloids or of iron bound to sinking particle surfaces also leads to less depletion of dissolved iron at depth in the model, but not enough to overcome the need to reduce aggregation rates.

2. A relatively strong iron binding ligand is required in the model, especially at depth, to prevent dissolved iron from aggregation and scavenging and to maintain a realistic iron profile. The required value for the conditional stability constant depends on the rate chosen for colloidal formation and is at the higher end of observed values.

3. The solubility of atmospherically deposited iron has a strong influence on the surface dFe concentration, especially in summer. Solubilities of

more than 2% lead to modelled dFe concentrations that are higher than observations.

4. The Fe:N ratio in phytoplankton that corresponds to the 'typical' Fe:C ratio of $5 \cdot 10^{-6}$ (Sunda and Huntsman, 1995) leads to spring dissolved iron concentrations that are somewhat higher than observations, and to a not very pronounced vertical structure in the profiles with a weak minimum directly under the summer mixed layer and a maximum around 100 m depth. The agreement with observations by (Sedwick et al., 2005) is improved in those two respects when the Fe:N ratio is increased.

5. In the upper water column, the dominant processes affecting iron speciation are the photochemically driven redox-reactions of inorganic Fe and organic complexation. These manifest themselves as a strong daily cycle of iron and reactive oxygen speciation in the mixed layer. These processes act on such short timescales that vertical gradients within the mixed layer are produced that are strongest for the very short-lived species such as superoxide and ferrous iron and somewhat weaker for longer-lived species, such as hydrogen peroxide. Both determine the residence time of dissolved iron in the euphotic zone by keeping iron in solution and therefore preventing it from scavenging. This is manifested as a dissolved iron profile with higher concentration at the surface and a strong decrease in the upper 50 m following the decreasing light availability.

The conclusions are based on a still very limited data set. Further measurements, especially time series of dissolved iron and its speciation, would be extremely helpful to validate the model. The sensitivity of the model to slight changes in the parametrisation of still unclear processes indicates that we are far away from understanding the influence of iron in the marine ecosystem and to predict it with confidence in global climate models.

Chapter 5

Outlook

5.1 Contribution to laboratory and field experiments

The model used in the present study has demonstrated the capabilities and sensitivities of current estimates of iron speciation parameterisations. These are still very simplistic, in part constrained by the lack of observational data due to the difficulty of making appropriate measurements. The model is a tool to aid in understanding the key processes of the iron cycle and its sensitivities rather than as a numerically accurate reproduction of reality. To further improve the model and to make realistic, quantitative predictions about iron fluxes, export rates and iron bioavailability, it is now important to link modelling directly with laboratory and field measurements. Vice versa, established linkages can help to optimise iron measurements by identifying key processes of the iron cycle.

For example, model results suggest that colloidal pumping (the transfer of dissolved species to large aggregates via colloidal intermediates) is a key mechanism in the iron cycle, responsible for large variations in scavenging rates. Additionally, desorption from both particulate and colloidal iron may be an important counteracting process. However, the detail of processes

leading to such changes in particle size are not fully understood (Wells, 2002). This makes it difficult to represent colloidal processes in a model adequately. The analytical approaches used to study colloid reaction rates are mainly with respect to their transfer into particles (Wells, 2002). Improved modelling methods for the colloidal system now account for the direct adsorption to particles and desorption from both particulate and colloidal matter (e.g. microbial degradation). Measurements which lead to a more complete picture of these colloidal processes could be supplemented with model runs.

Running the model for other regions of the ocean would allow a comparison of the sensitivities studied under different environmental and biogeochemical conditions. This can lead to a better quantification of the mechanisms that control fluxes of iron in the ocean, the extent of iron limitation and an assessment of sensitivity to climate variation. For example, one should expect that modelling oceanic regions that are more stratified than the BATS site will yield modelled iron concentrations that are much more sensitive to parameters such as the solubility of iron in dust or the colloid aggregation rate.

The simple NPZD-type model as well as GOTM are easily adaptable to other regions of the ocean. However, using the model at other locations than BATS, one has to be aware of other sources of iron in addition to atmospheric dust deposition. Depending on the region, iron might also be sourced from resuspended shelf sediments, upwelling and lateral transport (Martin et al., 1989; Lam et al., 2006), ice melt (Sedwick and Ditullio, 1997; Sedwick et al., 2000), volcanic eruptions (Watson, 1997; Boyd et al., 1998), riverine sources or even extra-terrestrial dust (Johnson, 2001). Additional sources would need to be included and paramerterised in the model code where required.

The model could also be used to simulate iron fertilisation experiments. In iron limited regions, the growth rate of phytoplankton needs to be dependent on the iron quota of the cells or the external iron concentration.

Equations for this are already included in the model code but not considered herein (Section 2.3).

One particularly interesting region for applying the model of the present study could be the subarctic North Pacific. It is one of the major HNLC regions. Three mesoscale iron-enrichment experiments have been performed in the western and the Alaska gyres (SEEDS, SEEDS II and SERIES) to test the iron-limitation hypothesis at ecosystem scales (Tsuda et al., 2003; Boyd et al., 1998, 2004). From these, a range of iron data are available which could help to validate the model. Additionally, Ocean Station Papa (OSP) is also located in the HNLC region of the subarctic North Pacific. Here, time series of key biogeochemical parameters, including iron, were seasonally sampled during previous decades.

The General Ocean Turbulence Model (GOTM), used in the present study as the physical part of the 1d model, has already been successfully employed by Steiner et al. (2006) to investigate the coupling between atmosphere-ocean exchanges and the planktonic ecosystem during the SERIES field study. They embedded a seven-component ecosystem model, which includes nitrogen, organic and inorganic carbon, silica and oxygen cycling. However, iron limitation was only given by a constant parameter. The model of Steiner et al. (2006) could therefore provide a good initial base for embedding the chemical iron model of the present study, to investigate the biogeochemistry and speciation of iron under iron limiting conditions. In terms of iron sources, the north Pacific is more ambitious than the area around BATS. While iron enrichment experiments have demonstrated iron limitation in summer (Boyd et al., 1998, 2004), the degree of iron limitation in the subarctic Pacific is not constant through the year and productivity can be boosted by different natural sources of iron in different seasons. Recent observations of biomass stimulation in the subarctic Pacific by an Asian dust storm in April have confirmed that dust can relieve Fe limitation at OSP in spring (Bishop et al., 2002). Lam et al. (2006) suggested subsurface delivery of bioavailable iron from continental

shelves and deep wintertime mixing.

5.2 Contribution to 3d global modelling

In global biogeochemical models of the ocean, iron is typically treated as a dissolved nutrient with simplified or no chemistry (Section 1.3). However, this study has shown that colloidal pumping involving the aggregation of colloids plays a significant role, especially in the upper ocean. The formation of colloids depends on the speciation of iron. A full model of iron speciation requires very short timesteps to model fast chemical reactions such as complexation, photochemical and redox reactions, and is thus too costly to be used within global models. One solution for this problem could be the separation of timescales between these fast reactions and the other much slower processes, such as colloid formation, biological processes, scavenging and dust deposition. The prognostic part of the model could be reduced to the slow variables, while the speciation of truly dissolved iron is calculated diagnostically. This saves memory space and allows larger timesteps. Producing a model of intermediate complexity that is capable of describing colloidal pumping may also be used in large-scale models.

A first impression of such an intermediate model is given in the following experiment, comparing three models which differ in the complexity of their representation of iron biogeochemistry but are otherwise identical. All models are zero-dimensional, i.e. they assume homogeneity within the surface mixed layer of the ocean. They are coupled to the NPD-type ecosystem model of the present study (Section 2.2.1).

Figure 5.1 illustrates the difference between the three models:
(i) A simple model: This model is similar to the models by Christian et al. (2002a), ignoring iron speciation alltogether. Scavenging of iron is assumed to be proportional to the concentrations of iron and of sinking particles.

(ii) A complex model: This model is the zero-dimensional model of the

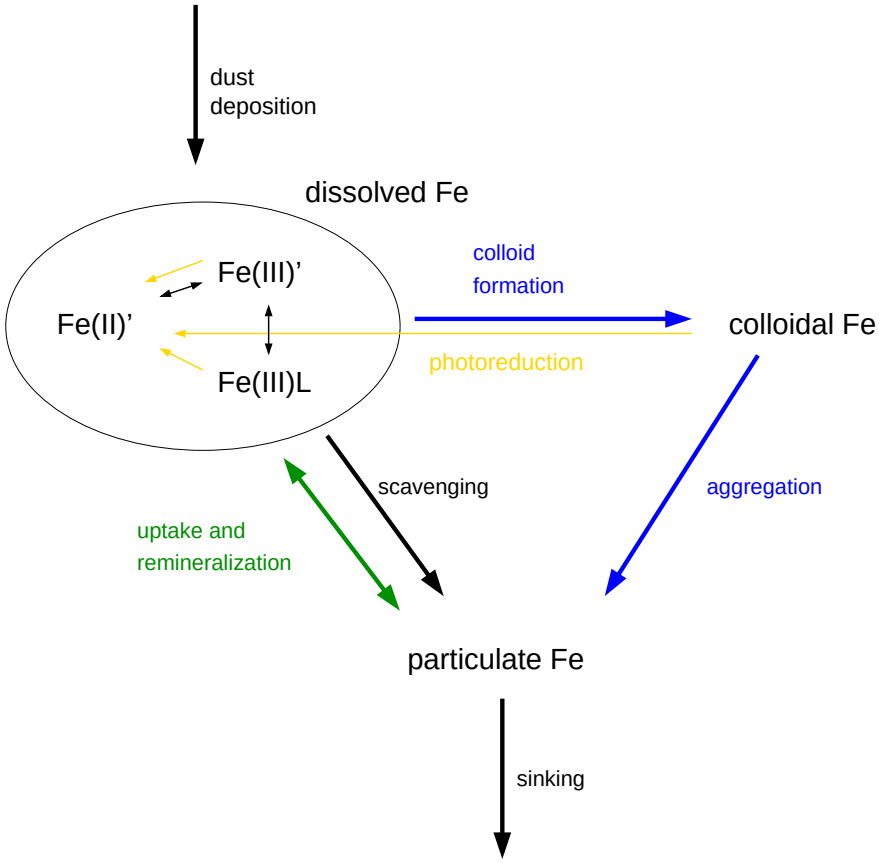

Figure 5.1: *Schematic illustration of the iron cycle in the mixed layer of the ocean. Typically, iron biogeochemistry models include only the black and green arrows, while the colloidal pumping mechanism (blue arrows) is not included. The thinner arrows represent fast conversion reactions between iron species, mostly driven by photochemical processes (yellow arrows).*

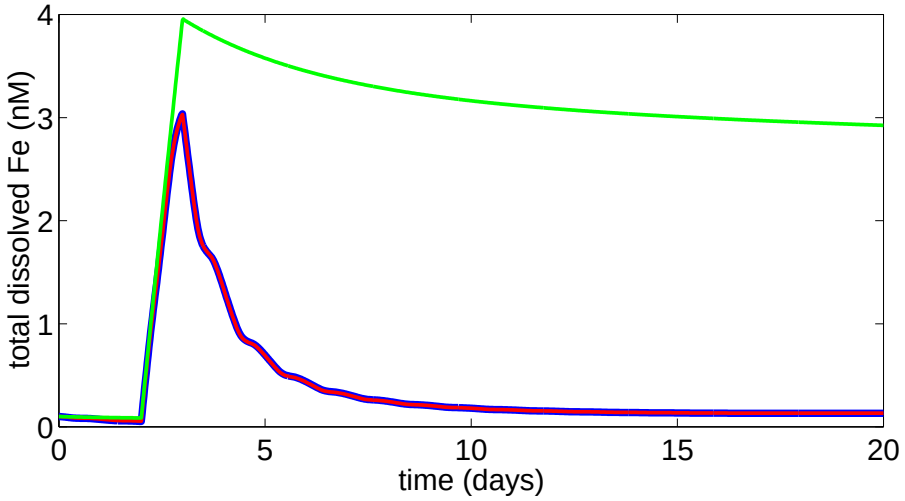

Figure 5.2: *Comparison of model results from three 0d models differing in the complexity of the iron chemistry: complex (red), intermediate(blue) and simple (green). In the experiment the iron concentration in the mixed layer is increased over the course of one day.*

present study (Section 2.2.2). The explicit modelling of shortlived chemical species such as Fe(II)' and of the superoxide radical make integration of this model costly.

(iii) An intermediate model: This model uses the time scale separation between the fast complexation, photochemical, and redox processes and the other much slower processes, such as colloid formation, biological processes, scavenging and dust deposition. This allows reduction of the prognostic part of the model to the slow variables, and the calculation of the speciation of truly dissolved iron diagnostically, saving memory space and allowing larger timesteps.

In the experiment, the iron concentration in the mixed layer is increased over the course of one day by applying a constant flux of iron sufficient to raise the iron concentration in the mixed layer by 4 nM. The mixed layer stays constant and a daily cycle of irradiance is prescribed.

Figure 5.2 shows the concentration of dissolved iron. Iron concentrations in the mixed layer decrease considerably faster in the 'complex' and 'intermediate' models (blue and red lines) than in the 'simple' model (green line), due to colloid formation and aggregation. The model results from the intermediate model do not differ significantly from a full prognostic model of iron speciation.

Using such an intermediate model could therefore allow to reconciliation between slow iron loss processes at depth and short reaction timescales in the mixed layer in models, which reproduce deep ocean Fe distribution with scavenging residence times between years and centuries (e.g. Archer and Johnson (2000); Parekh et al. (2004)). It could improve the prediction of such models in respect of bioavailable iron.

Chapter 6

Summary

A model was constructed that describes the cycling of iron between its various physical (dissolved, colloidal, particulate) and chemical (redox state and organic complexation) forms in the oceanic mixed layer. The model was coupled to a simple ecosystem model and was driven by observed or modelled values of dust deposition, mixed layer depth, temperature, and solar irradiation from the Bermuda Atlantic Timeseries Study (BATS).

Using parameter values suggested by laboratory and field studies, the model is able to simulate the temporal patterns and the vertical profile of dissolved iron in the upper ocean for the Bermuda Atlantic Time series Study site reasonably well (Wu and Luther III, 1995; Wu and Boyle, 2002; Sedwick et al., 2005). Modeled annual average fluxes of iron are also within the (still broad) limits of data-based estimates (Jickells, 1999). The primary aim of the present study was to achieve a better qualitative understanding of the role of iron speciation and the processes influencing it as part of the biogeochemical cycling of iron.

In the first part of the thesis, a zero-dimensional (0d) approach of the model was set up. The model results showed that the entrainment and detrainment of water during the annual cycle of mixed layer deepening and shoaling plays an important role in the vertical flux of iron. This flux is

dominant in the sense that it balances the other fluxes in such a way that the total dissolved iron concentration in the mixed layer at the BATS site does not depend strongly on the size of e.g. inputs by dust deposition, but remains tightly coupled to the concentration below the mixed layer. This result clearly depends on the strength of the annual mixed layer cycle and cannot be generalised to other more quiescent oceanic regions.

The original questions posed in the introduction (Section 1.4) are re-stated and answered below:

1. How strong is the daily photochemical redox-cycling of iron at the BATS site? How important is the direct photoreduction of iron species compared to the reduction by photoproduced superoxide? Is there an influence of other transition metals on the strength of the redox cycle?

   Regardless of the details of the chemical model, the daily irradiance cycle drives a strong cycle of iron speciation. This cycle is characterised by concentrations of Fe(II)′ that closely follow the irradiance cycle (with maximum values attained soon after noon). During the night, speciation is dominated by ferric iron species. The increase of [Fe(II)′] during the day is primarily driven by the reduction of Fe(III)′ by photoproduced superoxide, with direct photoreduction of organically complexed Fe(III) or other ferric iron species being much weaker. A strong diurnal cycling of Fe between its different dissolved forms was found in all model experiments. The maximum value of [Fe(II)′] reached during the day depends strongly on the chemical environment (mainly on the concentration and degree of organic complexation of copper, and on the rate of photochemical production of superoxide, less on the presence of organic ligands for iron). The model results therefore suggest that daylight concentrations of Fe(II)′ in the surface ocean will depend on local conditions such as presence of copper and coloured dissolved organic

matter. Nevertheless, the photochemically driven cycling of iron between its various chemical forms is generally rapid. The photochemical reactivity of organic complexes of iron seems to be of little importance for this cycling.

2. Under which conditions can colloid aggregation lead to a significant loss of iron from the surface layer of the ocean?

   This study does not include a full model of colloid formation and aggregation, but implies the formation of inorganic iron-containing colloids and their aggregation onto larger sinking particles. Bearing that in mind, and that the aggregation rate has been extrapolated from measurements made at much higher particle concentrations, the model results suggest that aggregation of colloids is an important process even in the open ocean, which can lead to significant iron removal from the mixed layer. Whether the iron that adsorbs on sinking particles by aggregation of colloids is exported out of the mixed layer, however, also depends on the photochemical lability of the adsorbed iron, which is not analysed in field or laboratory yet.

3. How strong is the influence of the solubility and the chemical form of dust-deposited iron?

   Model results show that increasing the percentage of dissolvable iron in dust increases the concentration of iron in the mixed layer mainly in summer, when the mixed layer is shallow. The annual mean concentration of iron is much less sensitive to the solubility. In an annual average the variation of iron input by variation of the solubility of iron in dust is compensated by the the iron flux via exchange with deeper waters, especially during the strong vertical mixing in winter. However, solubilities of atmospheric iron greater than 2.5% lead to dissolved iron concentrations in summer that are incompatible with most observations. The small sensitivity of the average dissolved iron concentration at the BATS site to the value of

the solubility is caused by the very strong vertical exchange associated with the mixed layer cycle at the BATS site and cannot be generalised to more stratified oceanic regimes. There has been some debate over which chemical species of iron is prevalent in dust deposition, especially in wet deposition. However, the speciation of deposited iron makes no significant difference to the model results. Whatever form of iron is deposited, the rapid daily cycling of iron between its different forms assures that neither the concentration and speciation of iron nor the iron fluxes are significantly affected.

4. Does it make a difference to the iron cycle, which chemical form of iron is taken up by phytoplankton? How sensitive are model results to changes in the Fe:N or Fe:C-ratio of phytoplankton uptake?

   Changes in the Fe:N ratio in organic matter do not strongly affect modelled total dissolved Fe concentrations. They lead to corresponding changes in the vertical biologically mediated flux of iron, but these changes are compensated by the same mechanism as changes in dust iron solubility, namely by exchange with water masses from below the mixed layer. Only Fe:N ratios above 150 μmol mol^{-1} lead to iron concentrations during the phytoplankton bloom that would limit phytoplankton growth. This is generally not assumed to happen at the BATS site. The insensitivity of modelled iron concentrations to the Fe:N ratio is again not valid for the ocean generally, but due to the strong vertical exchange at the BATS site. However, a more general conclusion is that from the point of view of the dissolved iron chemistry, it makes no significant difference whether phytoplankton cells take up Fe(III)$'$, Fe(II)$'$ or FeL. The rapid cycling of iron between its different dissolved forms ensures that any pool that is depleted by biological uptake gets replenished quickly. This is mainly due to the redox-reactivity of iron with respect to superoxide and on the daily concentration cycle of superoxide. It does not mean, on the other hand, that the preference

of phytoplankton for the one or the other form of dissolved iron cannot have biogeochemical consequences: it is assumed here that phytoplankton growth is unlimited by iron availability, but in reality, the uptake rate of any chemical species depends on its concentration in the medium, which would be different for individual iron species. This is likely to be of importance in iron-limited ocean regimes.

Some processes of the iron biogeochemistry (e.g. photochemistry) can lead to vertical concentration gradients within the mixed layer. Therefore, in the second part of the thesis, a one-dimensional (1d) extension of the zero-dimensional model was utilised. Compared to the zero-dimensional model (which treats the surface mixed layer as a homogeneous box), the one-dimensional approach permits analysis of the iron processes and behaviour with depth.

The aims of this part were to investigate: (i) the concentration and fluxes of dissolved iron below the annual mixed layer and how the concentration is affected by the parameterisation of loss processes that transfer dissolved iron to sinking particles either through scavenging or through a colloid intermediate. (ii) the vertical scale of the fast redox cycling within the mixed layer.

The main results of this part is as follows:

1. High colloidal aggregation rates of iron, observed in particle-rich coastal waters (Wen et al., 1997) and during iron fertilisation experiments (Nishioka et al., 2005) can not be applied to reproduce iron profiles at the BATS site with the current model. To prevent unrealistic depletion of dissolved iron at depth, the model requires aggregation rates 3 orders of magnitude lower than those observed, even when scaled with the concentration of sinking particles. Introducing a hypothetical redissolution of colloids or of iron bound to sinking particle surfaces also leads to less depletion of dissolved

iron at depth in the model, but not enough to overcome the need to reduce aggregation rates.

2. A relatively strong iron binding ligand is required in the model, especially at depth, to prevent dissolved iron from aggregation and scavenging and to maintain a realistic iron profile. The required value for the conditional stability constant depends on the rate chosen for colloidal formation and is at the higher end of observed values.

3. The solubility of atmospherically deposited iron has a strong influence on the surface dFe concentration, especially in summer. Solubilities of more than 2% lead to modelled dFe concentrations that are higher than observations.

4. The Fe:N ratio in phytoplankton that corresponds to the 'typical' Fe:C ratio of $5 \cdot 10^{-6}$ (Sunda and Huntsman, 1995) leads to spring dissolved iron concentrations that are somewhat higher than observations, and to a not very pronounced vertical structure in the profiles with a weak minimum directly under the summer mixed layer and a maximum around 100 m depth. The agreement with observations by (Sedwick et al., 2005) is improved in those two respects when the Fe:N ratio is increased.

5. In the upper water column, the dominant processes affecting iron speciation are the photochemically driven redox-reactions of inorganic Fe and organic complexation. These manifest themselves as a strong daily cycle of iron and reactive oxygen speciation in the mixed layer. These processes act on such short timescales that vertical gradients within the mixed layer are produced that are strongest for the very short-lived species such as superoxide and ferrous iron and somewhat weaker for longer-lived species, such as hydrogen peroxide. Both determine the residence time of dissolved iron in the euphotic zone by keeping iron in solution and therefore preventing it from scavenging.

This is manifested as a dissolved iron profile with higher concentration at the surface and a strong decrease in the upper 50 m following the decreasing light availability.

The complexity of iron biogeochemistry in seawater and the difficulty of direct measurement of chemical iron species require that a number of assumptions be made. Consequently, several of the processes modelled in this study involve parameters that are either not very well constrained or that have been measured under conditions different from open-ocean conditions. Therefore the model is a tool to aid understanding the key processes of the iron cycle and their sensitivities rather than a numerically accurate reproduction of reality. However, the high sensitivity of the model to slight changes in the parametrisation of still poorly constrained processes indicate that we are far away from understanding the influence of iron in the complex ecosystem.

Many of the still qualitative statements above could be made more quantitative if more data to validate the model predictions would become available. A dataset of time-resolved iron speciation, including measurements of Fe(II)′, H_2O_2, detailed colloidal chemistry and also some information on the concentration and organic complexation of copper would be useful in this respect.

Bibliography

Anderson, M. and Morel, F. (1982). The influence of aqueous iron chemistry on the uptake of iron by the coastal diatom *Thalassiosira weissflogii*. *Limnology and Oceanography*, 27:789–831.

Archer, D. and Johnson, K. (2000). A model of the iron cycle in the ocean. *Global Biogeochemical Cycles*, 14:269–279.

Arimoto, R. (2001). Eolian dust and climate: relationships to sources, tropospheric chemistry, transport, and deposition. *Earth-Science Reviews*, 54:29–42.

Armstrong, E., Granger, J., Mann, E. L., and Price, N. M. (2004). Outer-membrane siderophore receptors of heterotrophic oceanic bacteria. *Limnology and Oceanography*, 49(2):579–587.

Aumont, O., Maier-Reimer, E., Blain, S., and Monfray, P. (2003). An ecosystem model of the global ocean including Fe, Si, P colimitations. *Global Biogeochemical Cycles*, 17(2).

Baker, A. and Jickells, T. (2006). Mineral particle size as a control on aerosol iron solubility. *Geophysical Research Letters*, 33(17).

Baker, A., Jickells, T., Witt, M., and Linge, K. (2006). Trends in the solubility of iron, aluminium, manganese and phosphorus in aerosol collected over the Atlantic Ocean. *Marine Chemistry*, 98:43–58.

Balistieri, L., Brewer, P., and Murray, J. (1981). Scavenging residence times of trace metals and surface chemistry of sinking particles in the deep ocean. *Deep Sea Research*, 28A:101–121.

Barbeau, K. and Moffett, J. (1998). Dissolution of iron oxides by phagotrophic protists: Using a novel method to quantify reaction rates. *Environmental Science and Technology*, 32(19):2969–2975.

Barbeau, K. and Moffett, J. (2000). Laboratory and field studies of colloidal iron oxide dissolution as mediated by phagotrophy and photolysis. *Limnology and Oceanography*, 45(4):827–835.

Barbeau, K., Moffett, J., Caron, D., Croot, P., and Erdner, D. (1996). Role of protozoan grazing in relieving iron limitation of phytoplankton. *Nature*, 380(6569):61–64.

Barbeau, K., Rue, E., Bruland, K., and Butler, A. (2001). Photochemical cycling of iron in the surface ocean mediated by microbial iron(III)-binding ligands. *Nature*, 413:409–413.

Barbeau, K., Rue, E., Trick, C., Bruland, K., and Butler, A. (2003). Photochemical reactivity of siderophores produced by marine heterotrophic bacteria and cyanobacteria based on characteristic Fe(III) binding groups. *Limnology and Oceanography*, 48(3):1069–1078.

Baskaran, M., Santschi, P., Benoit, G., and Honeyman, B. (1992). Scavenging of thorium isotopes by colloids in seawater of the Gulf of Mexico. *Geochimica et Cosmochimica Acta*, 56(9):3375–3388.

Benner, R., Biddanda, B., Black, B., and McCarthy, M. (1997). Abundance, size distribution, and stable carbon and nitrogen isotopic compositions of marine organic matter isolated by tangential-flow ultrafiltration. *Marine Chemistry*, 57(3-4):243–263.

Bergquist, B. and Boyle, E. (2006). Dissolved iron in the tropical and subtropical Atlantic Ocean. *Global Biogeochemical Cycles*, 20:doi:10.1029/2005GB002505.

Bishop, J. K. B., Davis, R. E., and Sherman, J. T. (2002). Robotic observations of dust storm enhancement of carbon biomass in the north pacific. *Science*, 298(5594):817–821.

Bissett, W. P., Walsh, J. J., Dieterle, D. A., and Carder, K. L. (1999). Carbon cycling in the upper waters of the Sargasso Sea: I. numerical simulation of differential carbon and nitrogen fluxes. *Deep Sea Research Part I: Oceanographic Research Papers*, 46(2):205–269.

Boyd, P., Berges, J., and Harrison, P. (1998). In vitro iron enrichment experiments at iron-rich and -poor sites in the ne subarctic pacific. *Journal of Experimental Marine Biology and Ecology*, 227(1):133–151.

Boyd, P., Watson, A., Law, C.S.and Abraham, E., Trull, T., Murdoch, R., Bakker, D.C.E.and Bowie, A., Buesseler, K., Chang, H., Charette, M., Croot, P., Downing, K., Frew, R., Gall, M., Hadfield, M., Hall, J., Harvey, M., Jameson, G., LaRoche, J., Liddicoat, M., Ling, R., M.T., M., McKay, R., Nodder, S., Pickmere, S., Pridmore, R., Rintoul, S., Safi, K., Sutton, P., Strzepek, R., Tanneberger, K., Turner, S., Waite, A., and Zeldis, J. (2000). A mesoscale phytoplankton bloom in the polar southern ocean stimulated by iron fertilization. *Nature*, 407(doi:10.1038/35037500):695–702.

Boyd, P. W., McTainsh, G., Sherlock, V., Richardson, K., Nichol, S., Ellwood, M., and Frew, R. (2004). Episodic enhancement of phytoplankton stocks in New Zealand subantarctic waters: Contribution of atmospheric and oceanic iron supply. *Global Biogeochem. Cycles*, 18(1):1–23.

Boye, M., Aldrich, A., van den Berg, C., de Jong, J., Veldhuis, M., and de Baar, H. (2003). Horizontal gradient of the chemical speciation of iron in surface waters of the northeast atlantic ocean. *Marine Chemistry*, 80:129–143.

Brock (1981). Calculating solar radiation for ecological studies. *Ecological Modelling*, 14:1–19.

Bruland, K., Donat, J., and Hutchins, D. (1991). Interactive influences of bioactive trace metals on biological production in natural waters. *Limnology and Oceanography*, 36:1555–1577.

Bruland, K. and Rue, E. (2001). Analytical methods for the determination of concentrations and speciation of iron. In Hunter, K. and Turner, D., editors, *Biogeochemistry of Iron in Seawater*. John Wiley and Sons Ltd.

Buesseler, K. O. and Boyd, P. (2003). Will ocean fertilization work? *Science*, 300(5616):67–68.

Burchard, H., Bolding, K., Kuehn, W., Meister, A., Neumann, T., and Umlauf, L. (2006). Description of a flexible and extendable physical-biogeochemical model system for the water column. *Journal of Marine Systems*, 61(3-4 Spec. Iss.):180–211.

Burchard, H., Deleersnijder, E., and Meister, A. (2005). Application of Modified Patankar schemes to stiff biogeochemical models for the water column. *Ocean Dynamics*, 55:326–337.

Byers, B. R. and Arceneaux, J. E. L. (1998). Microbial iron transport: Iron acquisition by pathogenic microorganisms. *Metal ions in biological systems*, 35:37–66.

Byrne, R. and Kester, D. (1976). Solubility of hydrous ferric oxide and iron speciation in seawater. *Marine Chemistry*, 4:255–274.

Byrne, R., Kump, L., and Cantrell, K. (1988). The influence of temperature and pH on trace metal speciation in seawater. *Marine Chemistry*, 25:163–181.

Carlson, C., H.W.Ducklow, and A.F.Michaels (1994). Annual flux of dissolved organic-carbon from the euphotic zone in the northwestern Sargasso Sea. *Nature*, 371:405–408.

Carpenter, E. (1983). *Nitrogen fixation by marine Oscillatoria (Trichodesmium) in the world's ocean*. Academic Press, New York.

Carroll, D. (1996). Chemical laser modeling with genetic algorithms. *Amer. Inst. Aeor. Astro.*, 34:338–346.

Chen, M., Dei, R., Wang, W.-X., and Guo, L. (2003). Marine diatom uptake of iron bound with natural colloids of different orgins. *Marine Chemistry*, 81:177–189.

Chen, M. and Wang, W.-X. (2001). Bioavailability of natural colloid-bound iron to marine plankton:influence of colloidal size and aging. *Limnology and Oceanography*, 46:1956–1967.

Chin, W., Orellana, M., and Verdugo, P. (1998). Spontaneous assembley of marine dissolved organic matter into polymer gels. *Nature*, 391:568–572.

Chisholm, S., Falkowski, P., and Cullen, J. (2001). Oceans: Dis-crediting ocean fertilization. *Science*, 294(5541):309–310.

Christian, J., Verschell, M., Murtigudde, R., Busalacchi, A., and McClain, C. (2002a). Biogeochemical modelling of the tropical Pacific Ocean. I: Seasonal and interannual variability. *Deep Sea Research*, II 49:509–543.

Christian, J., Verschell, M., Murtigudde, R., Busalacchi, A., and McClain, C. (2002b). Biogeochemical modelling of the tropical Pacific Ocean. II: Iron biogeochemistry. *Deep Sea Research*, II 49:509–543.

Cloern, J., Grenz, C., and VidergarLucas, L. (1995). An empirical model of the phytoplankton chlorophyll:carbon ratio – the conversion factor between productivity and growth rate. *Limnology and Oceanography*, 40(7):1313–1321.

Coale, K. (1991). Effects of iron, manganese, copper, and zinc enrichments on productivity and biomass in the subarctic Pacific. *Limnology and Oceanography*, 36 (8):1851–1864.

Coale, K., Johnson, K., Fitzwater, S., Gordon, R., Tanner, S., Chavez, F., Ferioli, L., Sakamoto, C., Rogers, P., Millero, F., Steinberg, P., Nightingale, P., Cooper, D., Cochlan, W., Landry, M., Constantinou, J., Rollwagen, G., Trasvina, A., and Kudela, R. (1996). A massive phytoplankton bloom induced by an ecosystem-scale iron fertilization experiment in the equatorial Pacific Ocean. *Nature*, 383:495–501.

Coale, K. H., Johnson, K. S., Chavez, F. P., Buesseler, K. O., Barber, R. T., Brzezinski, M. A., Cochlan, W. P., Millero, F. J., Falkowski, P. G., Bauer, J. E., Wanninkhof, R. H., Kudela, R. M., Altabet, M. A., Hales, B. E., Takahashi, T., Landry, M. R., Bidigare, R. R., Wang, X., Chase, Z., Strutton, P. G., Friederich, G. E., Gorbunov, M. Y., Lance, V. P., Hilting, A. K., Hiscock, M. R., Demarest, M., Hiscock, W. T., Sullivan, K. F., Tanner, S. J., Gordon, R. M., Hunter, C. N., Elrod, V. A., Fitzwater, S. E., Jones, J. L., Tozzi, S., Koblizek, M., Roberts, A. E., Herndon, J., Brewster, J., Ladizinsky, N., Smith, G., Cooper, D., Timothy, D., Brown, S. L., Selph, K. E., Sheridan, C. C., Twining, B. S., and Johnson, Z. I. (2004). Southern ocean iron enrichment experiment: Carbon cycling in high- and low-si waters. *Science*, 304(5669):408–414.

Cooper, W., Zika, R., Petasne, R., and Plane, J. (1988). Photochemical formation of H_2O_2 in natural waters exposed to sunlight. *Environmental Science & Technology*, 22:1156–1160.

Croot, P., Bowie, A., Frew, R., Maldonado, M., Hall, J., Safi, K., Roche, J. L., Boyd, P., and Law, C. (2001). Retention of dissolved iron and Fe^{II} in an iron induced Southern Ocean phytoplankton bloom. *Geophysical Research Letters*, 28:3425–3428.

Cullen, J., Berquist, B., and Moffett, J. (2006). Thermodynamic characterization of partitioning of iron between soluble and colloidal species in the Atlantic Ocean. *Marine Chemistry*, 98:295–303.

de Baar, H. and la Roche, J. (2003). Trace metals in the ocean: evolution, biology and global change. In Wefer, G. and F.Lamy and F. Montoura, editor, *Marine Science Frontiers for Europe*, pages 79–105. Springer-Verlag.

de Baar, H. J. W., De Jong, J., Nolting, R., Timmermans, K., Van Leeuwe, M., Bathmann, U., and Loeff, R. V. D. (1999). Low dissolved fe and the absence of diatom blooms in remote pacific waters of the southern ocean. *Marine Chemistry*, 66(1-2):1–34.

Doney, S. (1996). A synoptic atmospheric surface forcing data set and physical upper ocean model for the U.S. JGOFS Bermuda Atlantic Time-Series Study site. *Journal of Geophysical Research*, 101 C:25615–25634.

Doney, S., Najjar, R., and Stewart, S. (1995). Photochemistry, mixing and diurnal cycles in the upper ocean. *Journal of Marine Research*, 53:341–369.

Duce, R. (1986). The impact of atmospheric nitrogen, phosphorus, and iron species on marine biological productivity. In Buat-Menard, P., editor, *The role of air-sea exchange in geochemical cycling*, pages 497–529. Reidel.

Duce, R. and Tindale, N. (1991). Atmospheric transport of iron and its deposition in the ocean. *Limnology and Oceanography*, 36:1715–1726.

Dugdale, R. and Wilkerson, F. (1998). Silicate regulation of new production in the equatorial pacific. *Nature*, 391:270–273.

Dutkiewicz, S., Follows, M. J., and Parekh, P. (2005). Interactions of the iron and phosphorus cycles: A three-dimensional model study. *Global Biogeochemical Cycles*, 19(1):1–22.

Emmenegger, L., Schönberger, R., Sigg, L., and Sulzberger, B. (2001). Light-induced redox cycling of iron in circumneutral lakes. *Limnology and Oceanography*, 46:49–61.

Evans, A. (1980). *An introduction to ore geology*. Elsevier North Holland Inc., New York.

Evans, G. and Parslow, J. (1985). A model of annual plankton cycles. *Biological Oceanography*, 3:327–347.

Falkowski, P. (1997). Evolution of the nitrogen cycle and its influence on the biological sequestration of CO_2 in the ocean. *Nature*, 387:272–275.

Falkowski, P. and Wilson, C. (1992). Phytoplankton productivity in the North Pacific ocean since 1900 and implications for absorption of anthropogenic CO_2. *Nature*, 385:741 – 743.

Farley, K. and Morel, F. (1986). Role of coagulation in the kinetics of sedimentation. *Environmental Science & Technology*, 20:187–195.

Fasham, M. (1993). Modelling the marine biota. In Heimann, M., editor, *The Global Carbon Cycle*, pages 457–504. Springer-Verlag, Berlin.

Fennel, K., Losch, M., Schroedter, J., and Wenzel, M. (2001). Testing a marine ecosystem model: sensitivity analysis and parameter optimization. *Journal of Marine Systems*, 28:45–63.

Fung, I., Meyn, S., Tegen, I., Doney, S., John, J., and Bishop, J. (2000). Iron supply and demand in the upper ocean. *Global Biogeochemical Cycles*, 14:281–301.

Geider, R. and La Roche, J. (1994). The role of iron in phytoplankton photosynthesis and the potential for iron-limitation of primary productivity in the sea. *Photosynthesis Research*, 39:275–301.

Geider, R., La Roche, J., Greene, R., and Olaizola, M. (1993). Response of the photosynthetic apparatus of *Phaeodactylum tricornutum (Bacillariophyceae)* to nitrate, phosphate, or iron starvation. *Journal of Phycology*, 29:755–766.

Geider, R., MacIntyre, H., and Kana, T. (1998). A dynamic regulatory model of phytoplankton acclimation to light, nutrients and temperature. *Limnology and Oceanography*, 43:679–694.

Gervais, F., Riebesell, U., and Gorbunov, M. (2002). Changes in primary productivity and chlorophyll a in response to iron fertilization in the Southern Polar Frontal Zone . *Limnology and Oceanography*, 47(5):1324–1335.

Gledhill, M. and van den Berg, C. (1994). Determination of complexation of iron(III) with natural organic complexing ligands in seawater using cathodic stripping voltammetry. *Marine Chemistry*, 47:41–54.

Graham, T. (1861). Liquid diffusion applied to analysis. *Phil. Trans. R. Soc. London*, 151:183.

Gran, H. (1931). On the conditions for the production of plankton in the sea. *Rapp. Proc. Verb. Cons. Int. Explor. Mer.*, 75:37–46.

Granger, J. and Price, N. M. (1999). The importance of siderophores in iron nutrition of heterotrophic marine bacteria. *Limnology and Oceanography*, 44(3):541–555.

Gruber, N., N.Bates, and Keeling, C. (2002). Interannual variability in the North Atlantic Ocean carbon sink. *Science*, 298:2374–2378.

Gunz, D. and Hoffmann, M. (1990). Atmospheric chemistry of peroxides: A review. *Atmospheric Environment - Part A General Topics*, 24A(7):1601–1633.

Guo, L., Santschi, P. H., and Warnken, K. W. (2000). Trace metal composition of colloidal organic material in marine environments. *Marine Chemistry*, 70(4):257–275.

Haygood, M., Holt, P., and Butler, A. (1993). Aerobactin production by a planktonic marine *Vibrio sp. Limnology and Oceanography*, 38:1091–1097.

Holland, H. (1984). *The chemical evolution of the atmosphere and oceans*. Princton University Press, Princton, NJ.

Honeyman, B. and Santschi, P. (1989). A brownian-pumping model for trace metal scavenging: evidence from Th isotopes. *Journal of Marine Research*, 47:951–992.

Hopkins, B. and Barbeau, K. (2006). Organic and redox speciation of iron in the eastern tropical north pacific suboxic zone. *Marine Chemistry*, in press:doi:10.1016/j.marchem.2006.02.008.

Hudson, R., Covault, D., and Morel, F. (1992). Investigations of iron coordination and redox reactions in seawater using ^{59}Fe radiometry and ion-pair solvent extraction of amphiphilic iron complexes. *Marine Chemistry*, 38:209–235.

Hudson, R. and Morel, F. (1990). Iron transport in marine phytoplankton: Kinetics of cellular and medium coordination reactions. *Limnology and Oceanography*, 35:1002–1020.

Hudson, R. and Morel, F. (1993). Trace metal transport by marine microorganisms: implications of metal coordination kinetics. *Deep-Sea Research*, 40:129–150.

Hurtt, G. C. and Armstrong, R. A. (1996). A pelagic ecosystem model calibrated with BATS data. *Deep Sea Research Part II: Topical Studies in Oceanography*, 43(2-3):653–683.

Hutchins, D. and Bruland, K. (1998). Iron-limited diatom growth and si:n uptake ratios in a coastal upwelling regime. *Nature*, 393:561–564.

Hutchins, D., Witter, A., Butler, A., and Luther III, G. (1999). Competition among marine phytoplankton for different chelated iron species. *Nature*, 400:858–861.

Jenkins, W. J. and Doney, S. C. (2003). The subtropical nutrient spiral. *Global Biogeochemical Cycles*, 17(4):1110.

Jerlov, N. (1968). *Optical oceanography*. Elsevier.

Jickells, T. (1995). Atmospheric input of metals and nutrients to the oceans: their magnitude and effects. *Marine Chemistry*, 48:199–214.

Jickells, T. (1999). The input of dust-derived elements to the Sargasso Sea: a synthesis. *Marine Chemistry*, 68:5–14.

Jickells, T., Deuser, W., and Belastock, R. (1990). Temporal variations in the concentrations of some particulate elements in the surface waters of the sargasso sea and their relationship to deep-sea fluxes. *Marine Chemistry*, 29:203–219.

Jickells, T., Dorling, S., Deuser, W., Church, T., Arimoto, R., and Prospero, J. (1998). Air-borne dust fluxes to a deep water sediment trap in the sargasso sea. *Global Biogeochemical Cycles*, 12:311–320.

Jickells, T. and Spokes, L. (2001). Atmospheric iron inputs to the oceans. In Turner, D. and Hunter, K., editors, *The Biogeochemistry of Iron in Seawater*, SCOR/IUPAC Series, pages 85–121. J. Wiley.

Johnson, K. (2001). Iron supply and demand in the upper ocean: Is extraterrestrial dust a significant source of bioavailable iron? *Global Biogeochemical Cycles*, 15(1):61–63.

Johnson, K., Chavez, F., and Friederich, G. (1999). Continental-shelf sediment as a primary source of iron for coastal phytoplankton. *Nature*, 398(6729):697–700.

Johnson, K., Coale, K., Elrod, V., and Tindale, N. (1994). Iron photochemistry in seawater from the equatorial Pacific. *Marine Chemistry*, 46:319–334.

Johnson, K., Gordon, R., and Coale, K. (1997). What controls dissolved iron concentrations in the world ocean? *Marine Chemistry*, 57:137–161.

Kieber, R., Cooper, W., Wiley, J., and Jr., G. A. (2001). Hydrogen peroxide at the Bermauda Atlantic Timeseries Station. part 1: Temporal variability of atmospheric hydrogen peroxide and its influence on seawater concentrations. *Journal of Atmospheric Chemistry*, 39:1–13.

Kim, G., Alleman, L., and Church, T. (1999). Atmospheric depositional fluxes of trace elements, ^{210}Pb, and ^{7}Be to the Sargasso Sea. *Global Biogeochemical Cycles*, 13:1183–1192.

Kim, G. and Church, T. (2001). Seasonal biogeochemical fluxes of ^{234}Th, and ^{210}Po in the upper Sargasso Sea: influence from atmospheric iron deposition. *Global Biogeochemical Cycles*, 15:651–661.

King, D., Aldrich, R., and Charniecki, S. (1993). Photochemical redox cycling of iron in NaCl solutions. *Marine Chemistry*, 44:105–120.

King, D., Lounsbury, H., and Millero, F. (1995). Rates and mechanism of Fe(II) oxidation at nanomolar total iron concentrations. *Environmental Science & Technology*, 29:818–824.

Kuma, K.and Katsumoto, A., Kawakami, H., Takatori, F., and Matsunaga, K. (1998). Spatial variability of Fe(III) hydroxide solubility in the water column of the northern North Pacific Ocean. *Deep-Sea Research Part I: Oceanographic Research Papers*, 45(1):99–113.

Kuma, K., Isoda, Y., and Nakabayashi, S. (2003). Control on dissolved iron concentrations in deep waters in the western North Pacific: Iron(III) hydroxide solubility. *J. Geophys. Res.*, 108(C9):5–1 – 5–10.

Kuma, K. and Matsunaga, K. (1995). Availability of colloidal ferric oxides to coastal marine phytoplankton . *Marine Biology*, 122(1-2):1–11.

Kuma, K., Nakabayashi, S., Suzuki, Y., Kudo, I., and Matsunaga, K. (1992). Photo-reduction of Fe(III) by dissolved organic substances and existence of Fe(II) in seawater during spring blooms. *Marine Chemistry*, 37:15–27.

Kumar, N., Anderson, R., Mortlock, R., Froelich, P., Kubik, P., Dittrich-Hannen, B., and Suter, M. (1995). Increased biological productivity and export production in the glacial Southern Ocean. *Nature*, 378(6558):675–680.

Lam, P.J.and Bishop, J., Henning, C., Marcus, M., Waychunas, G., and Fung, I. (2006). Wintertime phytoplankton bloom in the subarctic Pacific supported by continental margin iron . *Global Biogeochemical Cycles*, 20(1):doi: 10.1029/2005GB002557.

Lancelot, C., Hannon, E., Becquevort, S., Veth, C., and De Baar, H. (2000). Modeling phytoplankton blooms and carbon export production in the Southern Ocean: dominant controls by light and iron in the Atlantic sector in Austral spring 1992. *Deep Sea Research*, I 47:1621–1662.

Lefevre, N. and Watson, A. (1999). Modelling the geochemical cycle of iron in the oceans and its impact on atmospheric CO_2 concentrations. *Global Biogeochemical Cycles*, 13:727–736.

Macrellis, H., Trick, C., Rue, E., Smith, G., and Bruland, K. (2001). Collection and detection of natural iron-binding ligands from seawater. *Marine Chemistry*, 76:175–187.

Mahowald, N., Kohfeld, K., Hansson, M., Balkanski, Y., Harrison, S., Prentice, I., Schulz, M., and Rodhe, H. (1999). Dust sources and deposition during the last glacial maximum and current climate: A comparison of model results with paleodata from ice cores and marine sediments. *Journal of Geophysical Research. D. Atmospheres*, 104:15895–15916.

Maldonado, M. and Price, N. (1999). Utilization of iron bound to strong organic ligands by plankton communities in the subarctic North Pacific. *Deep Sea Research*, II 46:2447–2473.

Maldonado, M. and Price, N. (2001). Reduction and transport of organically bound iron by *Thalassiosira oceanica* (Bacillariophyceae). *Journal of Phycology*, 37:298–309.

Maldonado, M., Strzepek, R., Sander, S., and Boyd, P. (2005). Acquisition of iron bound to strong organic complexes, with different fe binding groups and photochemical reactivities, by plankton communities in fe-limited subantarctic waters. *Global Biogeochemical Cycles*, 19(GB4S23):doi:10.1029/2005GB002481.

Markels Jr., M. and Barber, R. (2001). Sequestration of carbon dioxide by ocean fertilization. *ACS Division of Fuel Chemistry, Preprints*, 46(1):45–48.

Martin, J., Coale, K., Johnson, K., Fitzwater, S., Gordon, R., Tanner, S., Hunter, C., Elrod, V., Nowicki, J., Coley, T., Barber, R., Lindley, S., Watson, A., Scoy, K. V., Law, C., Liddicoat, M., Ling, R., Stanton, T., Stockel, J., Collins, C., Anderson, A., Bidigare, R., Ondrusek, M., Latasa, M., Millero, F., Lee, K., Yao, W., Zhang, J., Friedrich, G., Sakamoto, C., Chavez, F., Buck, K., Kolber, Z., Greene, R., Falkowski, P., Chisholm, S., Hoge, F., Swift, R., Yungel, J., Turner, S., Nightingale, P., Hatton, A., Liss, P., and Tindale, N. (1994). Testing the iron hypothesis in ecosystems of the equatorial Pacific Ocean. *Nature*, 371:123–129.

Martin, J. and Fitzwater, S. (1988). Iron deficiency limits phytoplankton growth in the northeast Pacific subarctic. *Nature*, 331:341–343.

Martin, J., Gordon, R., Fitzwater, S., and Broenkow, W. (1989). VERTEX: phytoplankton/iron studies in the Gulf of Alaska. *Deep-Sea Research*, 36:649–680.

McClain, C. and Firestone, J. (1993). An investigation of Ekman upwelling in the North Atlantic. *Journal of Geophysical Research*, 98:12,327–12,339.

Michaels, A. and Knap, A. (1996). Overview of the U.S. JGOFS Bermuda Atlantic Timeseries Study and Hydrostation S program. *Deep Sea Research*, II 43:157–198.

Miller, W., King, D., Lin, J., and Kester, D. (1995). Photochemical redox cycling of iron in coastal seawater. *Marine Chemistry*, 50:63–77.

Millero, F. and Hawke, D. (1992). Ionic interactions of divalent metals in natural waters. *Marine Chemistry*, 40:19–48.

Millero, F. and Sotolongo, S. (1989). The oxidation of Fe(II) with H_2O_2 in seawater. *Geochimica et Cosmochimica Acta*, 53:1867–1873.

Millero, F., Sotolongo, S., and Izaguirre, M. (1987). The oxidation kinetics of Fe(II) in seawater. *Geochimica et Cosmochimica Acta*, 51:793–801.

Mills, M., Ridame, C., Davey, M., Roche, J. L., and Geider, R. (2004). Iron and phosphorus co-limit nitrogen fixation in the eastern tropical North Atlantic. *Nature*, 429(6989):292–294.

Moffet, J. (2001). Transformations among different forms of iron in the ocean. In Turner, D. and Hunter, K., editors, *The Biogeochemistry of Iron in Seawater*, SCOR/IUPAC Series, pages 1–7. J. Wiley.

Moffett, J. W. (1995). Temporal and spatial variability of copper complexation by strong chelators in the sargasso sea. *Deep Sea Research Part I: Oceanographic Research Papers*, 42(8):1273–1295.

Mongin, M., Nelson, D. M., Pondaven, P., Brzezinski, M. A., and Tréguer, P. (2003). Simulation of upper-ocean biogeochemistry with a flexible-composition phytoplankton model: C, N and Si cycling in the western Sargasso Sea. *Deep Sea Research Part I: Oceanographic Research Papers*, 50(12):1445–1480.

Moore, J., Doney, S., Kleypas, J., Glover, D., and Fung, I. (2002). An intermediate complexity marine ecosystem model for the global domain. *Deep Sea Research Part*, II 49(1-3):403–462.

Mopper, K., Zhou, J., Ramana, K., Passow, U., Dam, H., and Drapeau, D. (1995). The role of surface-active carbohydrates in the flocculation of a diatom bloom in a mesocosm. *Deep-Sea Research, Part II*, 42(1):47–73.

Moran, S. B. and Buesseler, K. O. (1992). Short residence time of colloids in the upper ocean off Bermuda. *Nature*, 359:221–223.

Morel, F., Reinfelder, J., Roberts, S., Chamberlain, C., Lee, J., and Yee, D. (1994). Zinc and carbon co-limitation of marine phytoplankton. *Nature*, 369(6483):740–742.

Muggli, D., Lecourt, M., and Harrison, P. (1996). Effects of iron and nitrogen source on the sinking rate, physiology and elemental composition of an oceanic diatom from the subarctic Pacific. *Marine Ecology Progress Series*, 132:215–227.

Musgrave, D., Chow, J., and Jenkins, W. (1988). Application of a model of upper-ocean physics for studying seasonal cycles of oxygen. *Journal of Geophysical Research*, 93:15679–15700.

Nakabayashi, S., Kusakabe, M., Kuma, K., and Kudo, I. (2001). Vertical distributions of iron(iii) hydroxide solubility and dissolved iron in the northwestern north pacific ocean. *Geophysical Research Letters*, 28:4611–4614.

Nishioka, J., Takeda, S., de Baar, H. J., Croot, P. L., Boye, M., Laan, P., and Timmermans, K. R. (2005). Changes in the concentration of iron in different size fractions during an iron enrichment experiment in the open Southern Ocean. *Marine Chemistry*, 95(1-2):51–63.

Nodwell, L. and Price, N. (2001). Direct use of inorganic colloidal iron by marine mixotrophic phytoplankton. *Limnology and Oceanography*, 46:765–777.

Nyffeler, U., Li, Y.-H., and Santschi, P. (1984). A kinetic approach to describe trace-element distribution between particles and solution in natural aquatic systems. *Geochimica et Cosmochimica Acta*, 48:1513–1522.

Obernosterer, I., Ruardij, P., and Herndl, G. (2001). Spatial and diurnal dynamics of dissolved organic matter (DOM) fluorescence and H_2O_2 and the photochemical demand of surface water DOM across the subtropical Atlantic Ocean. *Limnology and Oceanography*, 46(3):632–643.

Olson, R., Chisholm, S.W.and Zettler, E., Altabet, M., and Dusenberry, J. (1990a). Spatial and temporal distributions of prochlorophyte picoplankton in the north atlantic ocean. *Deep-Sea Research*, 37(6A):1033–1051.

Olson, R., Chisholm, S.W.and Zettler, E., and Armbrust, E. (1990b). Pigments, size, and distribution of synechococcus in the north atlantic and pacific oceans. *Limnology and Oceanography*, 35(1):45–58.

Ono, S., amd R.G. Najjar, A. E., and Bates, N. (2001). Shallow remineralization in the Sargasso Sea estimated from seasonal variations in oxygen, dissolved inorganic carbon and nitrate. *Deep-Sea Research Part II*, 48(8-9):1567–1582.

Oschlies, A. and Schartau, M. (2005). Basin-scale performance of a locally optimized marine ecosystem model. *Journal of Marine Research*, 63:335–358.

O'Sullivan, D., Hanson, A., Miller, W., and Kester, D. (1991). Measurement of Fe(II) in surface water of the equatorial Pacific. *Limnology and Oceanography*, 36:1727–1741.

Palter, J. B., Lozier, M. S., and Barber, R. T. (2005). The effect of advection on the nutrient reservoir in the North Atlantic subtropical gyre. *Nature*, 437:687–692.

Parekh, P., Follows, M., and Boyle, E. (2004). Modelling the global ocean iron cycle. *Global Biogeochemical Cycles*, 18.

Passow, U. and Alldredge, A. (1995). Aggregation of a diatom bloom in a mesocosm: the role of transparent exopolymer particles (tep). *Deep-Sea Research, Part II*, 42(1):99–109.

Petit, J., Jouzel, J., Raynaud, D., Barkov, N., Barnola, J., Basile, I., Bender, M., Chappellaz, J., Davis, M., Delaygue, G., Delmotte, M., Kotlyakov, V., Legrand, M., Lipenkov, V., Lorius, C., Pepin, L., Ritz, C., Saltzman, E., and Stievenard, M. (1999). Climate and atmospheric history of the past 420,000 years from the Vostok ice core, Antarctica. *Nature*, 399(6735):429–436.

Piketh, S., Tyson, P., and Steffen, W. (2000). Aeolian transport from southern Africa and iron fertilization of marine biota in the South Indian Ocean. *South African Journal of Science*, 96(5):244–246.

Raven, J. (1990). Predictions of Mn and Fe use efficiencies of phototrophic growth as a function of light availability for growth and C assimilation pathway. *New Phytologist*, 116:1–18.

Raven, J. and Falkowski, P. (1999). Oceanic sinks for atmospheric CO2. *Plant, Cell and Environment*, 22(6):741–755.

Raymond, K., Müller, G., and Matzanke, B. (1984). Complexation of iron by siderophores. A review of their solution and structural chemistry and biological function. *Topics in Current Chemistry*, 123:49–102.

Reid, R., Live, D., Faulkner, D., and Butler, A. (1993). A siderophore from a marine bacterium with an exceptional ferric ion affinity constant. *Nature*, 366:455–458.

Rich, H. and Morel, F. (1990). Availability of well-defined iron colloids to the marine diatom *Thalassiosira Weissdlogii*. *Limnology and Oceanography*, 35:652–662.

Rijkenberg, M., Fischer, A., Kroon, J., Gerringa, L., Timmermans, K., Wolterbeek, H., and de Baar, H. (2005). The influence of UV irradiation on the photoreduction of iron in the Southern Ocean. *Marine Chemistry*, 93(2-4):119–129.

Rijkenberg, M., Gerringa, L., Carolus, V., Velzeboer, I., and de Baar, H. (2006). Enhancement and inhibition of iron photoreduction by individual ligands in open ocean seawater. *Geochimica et Cosmochimica Acta*, 70:2790–2850.

Rose, A. and Waite, T. (2003a). Kinetics of hydrolysis and precipitation of ferric iron in seawater. *Environmental Science & Technology*, 37:3897–3903.

Rose, A. and Waite, T. (2003b). Kinetics of iron complexation by dissolved natural organic matter in coastal waters. *Marine Chemistry*, 84:85–103.

Rose, A. and Waite, T. (2003c). Predicting iron speciation in coastal waters from the kinetics of sunlight-mediated iron redox cycling. *Aquatic Sciences*, 65:375–383.

Rue, E. and Bruland, K. (1995). Complexation of iron(III) by natural organic ligands in the Central North Pacific as determined by a new competitive ligand equilibration / adsorptive cathodic stripping voltammetric method. *Marine Chemistry*, 50:117–138.

Sakugawa, H.and Kaplan, I., Tsai, W., and Cohen, Y. (1990). Atmospheric hydrogen peroxide. does it share a role with ozone in degrading air quality? *Environmental Science and Technology*, 24(10):1452–1462.

Sarmiento, J. and Gruber, N. (2002). Sinks for Anthropogenic Carbon. *Physics Today*, 55(8):30–36.

Schartau, M. and Oschlies, A. (2003a). Simultaneous data-based optimization of a 1D-ecosystem model at three locations in the North Atlantic Ocean. part I: Method and parameter estimates. *Journal of Marine Research*.

Schartau, M. and Oschlies, A. (2003b). Simultaneous data-based optimization of a 1D-ecosystem model at three locations in the North Atlantic Ocean. part II: Standing stocks and nitrogen fluxes. *Journal of Marine Research*.

Schartau, M., Oschlies, A., and Willebrand, J. (2001). Parameter estimates of a zero-dimensional ecosystem model applying the adjoint method. *Deep Sea Research*, II 48:1769–1800.

Sedwick, P., Church, T., Bowie, A., Marsay, C., Ussher, S., Achilles, K., Lethaby, P., Johnson, R., Sarin, M., and McGillicuddy, D. (2005). Iron in the Sargasso Sea (BATS region) during summer: Eolian imprint, spatiotemporal variability, and ecological implications. *Global Biogeochemical Cycles*, 19:doi:10.1029/2004GB002445.

Sedwick, P. and Ditullio, G. (1997). Regulation of algal blooms in Antarctic shelf waters by the release of iron from melting sea ice. *Geophysical Research Letters*, 24(20):2515–2518.

Sedwick, P., DiTullio, G., and Mackey, D. (2000). Iron and manganese in the Ross Sea, Antarctica: Seasonal iron limitation in Antarctic shelf waters. *Journal of Geophysical Research*, 105(C5):11321–11336.

Siegel, D. (1990). Meridional variations of the springtime phytoplankton community in the sargasso sea. *Journal of Marine Research*, 48(2):379–412.

Siegel, D. and Deuser, W. (1997). Trajectories of sinking particles in the sargasso sea: Modeling of statistical funnels above deep-ocean sediment traps. *Deep-Sea Research Part I*, 44(9-10):1519–1541.

Smith, R. and Baker, K. (1979). Penetration of UV-B and biologically effective dose-rates in natural waters. *Photochemistry and Photobiology*, 29:311–323.

Soria-Dengg, S. and Horstmann, U. (1995). Ferrioxamines B and E as iron sources for the marine diatom *Phaeodactylum tricornutum*. *Marine Ecology Progress Series*, 127:269–277.

Spitz, Y. H., Moisan, J. R., and Abbott, M. R. (2001). Configuring an ecosystem model using data from the Bermuda Atlantic Time Series (BATS). *Deep Sea Research Part II: Topical Studies in Oceanography*, 48(8-9):1733–1768.

Spokes, L. and Jickells, T. (1996). Factors controlling the solubility of aerosol trace metals in the atmosphere and on mixing into seawater. *Aquatic Geochemistry*, 1:355–374.

Steinberg, D., Carlson, C., Bates, N., and Johnson, R.J.and Michaels, A. A. K. (2001). Overview of the US JGOFS Bermuda Atlantic Time-series Study (BATS): A decade-scale look at ocean biology and biogeochemistry. *Deep-Sea Research Part II*, 48(8-9):1405–1447.

Steiner, N., Denman, K., McFarlane, N., and Solheim, L. (2006). Simulating the coupling between atmosphereocean processes and the planktonic ecosystem during SERIES. *Deep-Sea Research Part II*, in press(doi:10.1016/j.dsr2.2006.05.030).

Stumm, W. (1992). *Chemistry of the solid-water interface*. Wiley-Interscience.

Stumm, W. and Morgan, J. (1981). *Aquatic Chemistry*. Wiley, New York.

Sulzberger, B. and Laubscher, H. (1995). Reactivity of various types of iron(III) (hydr)oxides towards light-induced dissolution. *Marine Chemistry*, 50:103–115.

Sunda, W. (1989). Trace metal interactions with marine phytoplankton. *Biological Oceanography*, 6:411–442.

Sunda, W. (2001). Bioavailability and bioaccumulation of iron in the sea. In Hunter, K. and Turner, D., editors, *Biogeochemistry of Iron in Seawater*. John Wiley and SOns Ltd.

Sunda, W. and Guillard, R. (1976). The relationship between cupricion activity and the toxicity of copper to phytoplankton. *Journal of Marine Research*, 34:511–529.

Sunda, W. and Huntsman, S. (1995). Iron uptake and growth limitation in oceanic and coastal phytoplankton. *Marine Chemistry*, 50:189–206.

Sunda, W. and Huntsman, S. (1997). Interrelated influence of iron, light and cell size on marine phytoplankton growth. *Nature*, 390:389– 392.

Takeda, S. (1998). Influence of iron availability on nutrient consumption ratio of diatoms in oceanic waters. *Nature*, 393(6687):774–777.

Talley, L. (1982). Eighteen degree water variability. *Journal of Marine Research*, 40:757–775.

Taylor, S. (1964). Abundance of chemical elements in the continental crust: a new table. *Geochimica et Cosmochimica Acta*, 28:1273–1285.

Timmermans, K., Stolte, W., and de Baar, H. (1994). Iron-mediated effects on nitrate reductase in marine phytoplankton. *Marine Biology*, 121(2):389–396.

Trick, C., Andersen, R., Price, N., Gillam, A., and Harrison, P. (1983). Examination of hydroxamate-siderophore production by neritic eukariotic marine phytoplankton. *Marine Biology*, 75:9–17.

Trick, C. and Wilhelm, S. W. (1995). Physiological changes in the coastal marine cyanobacterium *Synechococcus sp.* pcc 7002 exposed to low ferric ion levels. *Marine Chemistry*, 50:207–217.

Tsuda, A., Takeda, S., Saito, H., Nishioka, J., Nojiri, Y., Kudo, I., Kiyosawa, H., Shiomoto, A., Imai, K., Ono, T., Shimamoto, A., Tsumune, D., Yoshimura, T., Aono, T., Hinuma, A., Kinugasa, M., Suzuki, K., Sohrin, Y., Noiri, Y., Tani, H., Deguchi, Y., Tsurushima, N., Ogawa, H., Fukami, K., Kuma, K., and Saino, T. (2003). A mesoscale iron enrichment in the western subarctic pacific induces a large centric diatom bloom. *Science*, 300(5621):958–961.

Turner, D., K.A.Hunter, and de Baar, H. (2001). Introduction. In Turner, D. and Hunter, K., editors, *The Biogeochemistry of Iron in Seawater*, SCOR/IUPAC Series, pages 1–7. J. Wiley.

Turner, S. M., Harvey, M. J., Law, C. S., Nightingale, P. D., and Liss, P. S. (2004). Iron-induced changes in oceanic sulfur biogeochemistry. *Geophys. Res. Lett.*, 31(14):1–4.

Uppala, S., Kallberg, P., Simmons, A., Andrae, U., da Costa Bechtold, V., Fiorino, M., Gibson, J., Haseler, J., Hernandez, A., Kelly, G., Li, X., Onogi, K., Saarinen, S., Sokka, N., Allan, R., Andersson, E., Arpe, K., Balmaseda, M., Beljaars, A., van de Berg, L., Bidlot, J., Bormann, N., Caires, S., Chevallier, F., Dethof, A., Dragosavac, M., Fisher, M., Fuentes, M., Hagemann, S., Holm, E., Hoskins, B., Isaksen, L., Janssen, P., Jenne, R., McNally, A., Mahfouf, J.-F., Morcrette, J.-J., Rayner, N., Saunders, R., Simon, P., Sterl, A., Trenberth, K., Untch, A., Vasiljevic,

D., Viterbo, P., and Woollen, J. (2005). The ERA-40 re-analysis. *Quarterly Journal of the Royal Meteorological Society*, 131:2961–3012.

Ussher, S., Achterberg, E., and Worsfold, P. (2004). Marine biogeochemistry of iron. *Environmental Chemistry*, 1:67–80. doi:10.1071/EN04053.

Van den Berg, C. (1995). Evidence for organic complexation of iron in seawater. *Marine Chemistry*, 50:139–157.

van Leeuwe, Scharek, R., De Baar, H., De Jong, J., and Goeyens, L. (1997). Iron enrichment experiments in the southern ocean: Physiological responses of plankton communities. *Deep Sea Research Part II*, 44(1-2):189–207.

Voelker, B. and Sedlak, D. (1995). Iron reduction by photoproduced superoxide in seawater. *Marine Chemistry*, 50:93–102.

Vold, R. and Vold, M. (1983). *Colloid and interface chenistry.* Addison-Wesley, Reading, MA.

Völker, C. and Wolf-Gladrow, D. (1999). Physical limits on iron uptake mediated by siderophores or surface reductases. *Marine Chemistry*, 65:227–244.

Waite, T. and Morel, F. (1984). Photoreductive dissolution of colloidal iron oxides in natural waters. *Environmental Science & Technology*, 18:860–868.

Waite, T., Szymczak, R., Espey, Q., and Furnas, M. (1995). Diel variations in iron speciation in northern Australian shelf waters. *Marine Chemistry*, 50:79–91.

Watson, A. (1997). Volcanic iron, CO2, ocean productivity and climate. *Nature*, 385(6617):587–588.

Watson, A. (2001). Iron limitation in the ocean. In Turner, D. and Hunter, K., editors, *The Biogeochemistry of Iron in Seawater*, SCOR/IUPAC Series, pages 9–39. J. Wiley, Chichester.

Webb, E. A., Moffett, J. W., and Waterbury, J. B. (2001). Iron stress in open-ocean cyanobacteria (*Synechococcus, Trichodesmium* and *Crocosphaera spp.*): Identification of the i*di*a protein. *Applied Environmental Microbiology*, 67:5444–5452.

Weber, L., Völker, C., Schartau, M., and Wolf-Gladrow, D. (2005). Modeling the speciation and biogeochemistry of iron an the Bermuda Atlantic Timeseries Study site. *Global Biogeochemical Cycles*, 19:doi:10.1029/2004GB002340.

Wells, M. (2002). Marine Colloids and Trace Metals. In Hansell, D.A. and C.A. Carlson, editor, *Marine Dissolved Organic Matter*, pages 367–404. Academic Press, Elsevier.

Wells, M. and Goldberg, E. (1992). Marine submicron particles. *Marine Chemistry*, 40:5–18.

Wells, M. and Goldberg, E. (1993). Colloid aggregation in seawater. *Marine Chemistry*, 41:353–358.

Wells, M. and Goldberg, E. (1994). The distribution of colloids in the North Atlantic and Southern Oceans. *Limnology and Oceanography*, 39:286–302.

Wells, M. and Mayer, L. (1991). The photoconversion of colloidal iron oxyhydroxides in seawater. *Deep-Sea-Research*, 38:1379–1395.

Wells, M., Price, N., and Bruland, K. (1995). Iron chemistry in seawater and its relationship to phytoplankton: A workshop report. *Marine Chemistry*, 48:157–182.

Wells, M., Smith, G., and Bruland, K. (2000). The distribution of colloidal and particulate bioactive metals in narragansett bay. *Marine Chemistry*, 71:143–163.

Wen, L.-S., Santschi, P., and Tang, D. (1997). Interactions between radioactively labeled colloids and natural particles: Evidence for colloidal pumping. *Geochimica et Cosmochimica Acta*, 61:2867–2878.

Wilhelm, S. and Trick, C. (1994). Iron-limited growth of cyanobacteria: Multiple siderophore production is a common response. *Limnology and Oceanography*, 39:1979–1984.

Witter, A., Hutchins, D., Butler, A., and Luther III, G. (2000). Determination of conditional stability constants and kinetic constants for strong model Fe-binding ligands in seawater. *Marine Chemistry*, 69:1–17.

Witter, A. and Luther III, G. (1998). Variation in Fe-organic complexation with depth in the northwestern Atlantic Ocean as determined using a kinetic approach. *Marine Chemistry*, 62:241–258.

Wu, J. and Boyle, E. (1998). Determination of iron in seawater by high-resolution isotope dilution inductively coupled plasma mass spectrometry after $Mg(OH)_2$ coprecipitation. *Analytica Chimica Acta*, 367:183–191.

Wu, J. and Boyle, E. (2002). Iron in the Sargasso Sea: Implications for the processes controlling dissolved Fe distribution in the ocean. *Global Biogeochemical Cycles*, 16.

Wu, J., Boyle, E., Sunda, W., and Wen, L.-S. (2001). Soluble and colloidal iron in the oligotrophic North Atlantic and North Pacific. *Science*, 293:847–849.

Wu, J. and Luther III, G. (1994). Size-fractionated iron concentrations in the water column of the western North Atlantic Ocean. *Limnology and Oceanography*, 39:1119–1129.

Wu, J. and Luther III, G. (1995). Complexation of Fe(III) by natural organic ligands in the Northwest Atlantic Ocean by a competitive ligand equilibration method and a kinetic approach. *Marine Chemistry*, 50:159–177.

Yuan, J. and Shiller, A. (2001). The distribution of hydrogen peroxide in the southern and central Atlantic ocean. *Deep Sea Research*, II 48:2947–2970.

Zafiriou, O. and True, M. (1980). Interconversion of iron(III) hydroxy complexes in seawater. *Marine Chemistry*, 8:281–288.

Zhong, M. S. G., Holt, P., Jung, H.-T., Haygood, C. C. M. G., and Butler, A. (2000). Self-assembling amphiphilic siderophores from marine bacteria. *Science*, 287:245–247.

Zhu, X., Prospero, J., and Millero, F. (1997). Diel variability of soluble Fe(II) and soluble total Fe in North African dust in the trade winds at Barbados. *Journal of Geophysical Research-Atmospheres*, D17:21297–21305.

Zhuang, G., Duce, R., and Kester, D. (1990). The dissolution of atmospheric iron in the surface seawater of the open ocean. *Journal of Geophysical Research*, 95:16207–16216.

Zhuang, G., Yi, Z., Duce, R., and Brown, P. (1992). Chemistry of iron in marine aerosols. *Global Biogeochemical Cycles*, 6:161–173.

Zuo, Y. and Holgne, J. (1992). Formation of hydrogen peroxide and depletion of oxalic acid in atmospheric water by photolysis of iron(iii)-oxalato complexes. *Environmental Science and Technology*, 26(5):1014–1022.